2005

Thermal management of the LSU micro gas chromatograph

Praveen K. Pasupuleti
Louisiana State University and Agricultural and Mechanical College

THERMAL MANAGEMENT OF THE LSU MICRO GAS CHROMATOGRAPH

A Thesis

Submitted to the Graduate Faculty of the
Louisiana State University and
Agricultural and Mechanical College
in partial fulfillment of the
requirements for the degree of
Master of Science in Mechanical Engineering

in

The Department of Mechanical Engineering

by
Praveen Kumar Pasupuleti
B.E., Andhra University, 2000
May 2005

To

my mother *Smt*. *Subhashini Pasupuleti* , father *Sri. Bhaskara Rao Pasupuleti* ,

brother *Narashima Satish Babu Pasupuleti* , sweet niece *Meghana Gudamsetty,*

sister *Smt. Lakshmi Sulakshana Madhavi Gudamsetty*, Brother-in-Law *Sri. Hazarathaiah*

Gudamsetty, uncles *Late Sri.Audiseshaiah,* and *Sri.Premchand Naidu* and

Narendra KumarReddy Veduru.

ACKNOWLEDGMENTS

First and foremost, I thank God for having given me the strength and determination to face the challenges and handle the unpredictable course of this period of my life. Secondly, I am thankful to my family who has always has been the biggest inspiration on a personal and academic level, and has given me unconditional love and support.

Also, I would like to express my appreciation to Dr. Michael Murphy for giving me the opportunity to take part in this exciting research project and offering me his suggestions, support, and patience throughout the process. I am also grateful to have had Dr. Edward Overton, Dr. Jost Goettert and Dr. Srinath Ekkad as my committee members.

I am greatly indebted to Mr.Audiseshaiah and Mr.Premchand Naidu, who cleared major obstacle on my way to USA. I am thankful to Narendra, for his unconditional support, Dr.Sudha Malini, for teaching me simplicity in life, Raj Kumar Ethakota and Madhu Babu Ethakota, my childhood icons, my teachers at Nirmala School, for nurturing my interest towards science.

My sincere gratitude is given to the management and staff at the Center for Advanced Microstructures and Devices (CAMD), for having provided me with the facilities, and equipment necessary for this research. Likewise, my appreciation is extended Dr. Yohanness Desta, Abhinav Bhushan, Dawit Yemane, Tracy Morris, Shaloma Malveaux, Proyog Datta and Yoonyoung Jin for all of their great technical and administrative assistance without which this project would never have been possible.

I am thankful to my roommates, Venkata Chandra Krishnan Ramaswamy Chandrasekhakarapuram, Diwakar Surya Narayana Iyer, Sudheer Rani, Phani Surya Kiran Mylavarapu and Hari Prasad Rayapalyam, for their cooperation and support during my stay at Baton Rouge.

I am also thankful to my friends, Venugopal Jogi, Netaji Subhas Chandra Bose Ayirala, Ambica Pilli, Anoop Kumar Somanchi, Chandrasekhar Busireddy, Prasad Rao Veeram, Priya David, Shanti Pampana, Indrani Venkata Volety, Chandrika Janapala, Srilekha Sirigiri, Amit, Vatsalya Kunchakarra, Smt.Leela Varalakshmi, Madan Pichuka, Srinivas Tikkireddi, Vijayvardhan Reddy Kandi, Mythili Anumanchipalli, Raghuveer Chaudhary Karnati, Sriman Narayana Gavara, Srinivas Adusumalli, Rajesh Yedida, Sree Rama Murthy Gudadi, Srinivas Kummarasetti, Arvind Dwarapureddy, HimaBindu Desiraju, Srilekha Challa, Raji Aunty, Mani Uncle and Maami for their invaluable help.

I am also thankful to my colleagues at the Microsystems (μset) Lab, Dinakar Palaparthi, Catherine Oropeza, Michael Mitchell, Johns Williams, Adam Cygan, Michael guillet, Dhanamjaya Reddy Guda, Diwakar Iyer, Byonghi you, Dwhyte barret, for their support.

TABLE OF CONTENTS

ACKNOWLEDGEMENTS ii

ABSTRACT viii

CHAPTER 1. INTRODUCTION 1
1.1 Micro Gas Chromatography 3
1.2 Micro GC Column Temperature Control 4
1.2.1 Isothermal Analysis 4
1.2.2 Temperature Programming 4
1.2.3 Advantages and Limitations of Temperature Programming 6
1.2.4 Existing Approaches of Temperature Programming 8
1.2.5 Device Requirements for Temperature Programming 8
1.3 Thesis Outline 9

CHAPTER 2. BACKGROUND 10
2.1 Chromatography 10
2.1.1 Gas Chromatography 10
2.1.2 Mechanism of Chromatography 11
2.1.3 Basic Apparatus for Gas Chromatography 12
2.1.3.1 Column 12
2.1.3.2 Detectors 14
2.1.3.3 Carrier Gas 14
2.1.4 Nomenclature 15
2.1.4.1 Phase Ratio 15
2.1.4.2 Partition Coefficient *K* and Retention Factor *k* 15
2.1.4.3 Theoretical Plate Number 16
2.1.4.4 Theoretical Plate Height 17
2.2 Miniaturization of Gas Chromatograph 17
2.2.1 Gas Chromatography System on a Silicon Wafer 17
2.2.1.1 Limitations Micro Gas Chromatography on Silicon Wafer 19
2.2.2 Parylene Gas Chromatograph 19
2.2.3 Miniaturization of Gas Chromatograph at LSU 19
2.2.3.1 Advantages of LSU LIGA MicroGC over MicroGCs 20

CHAPTER 3.THERMAL SYSTEM 21
3.1 Introduction 21
3.2 Thermal System Design 22
3.2.1 Pseudo Bondgraph Modeling for Thermal Systems 22
3.2.2 Heat Distribution Model 23
3.2.3 Six Lump Model 23
3.2.4 Heat Distribution Model for Four Lumps 27

CHAPTER 4. HEATER DESIGN AND FABRICATION 31
4.1 Introduction 31
4.2 Device Requirements..... 31
4.3Advantages of In Situ Heaters over Commercial Heaters 31
4.4 Review of Heaters Used for Gas Chromatographs 32
4.5 In Situ Heaters 32
4.5.1 Material Selection 32
4.5.2 Advantages and Limitations of Electroplating over Physical Vapor Deposition 33
4.5.3 Electrodeposition of NiCr Alloys 34
4.5.3.1 Introduction 34
4.5.3.2 Experimental 34
4.5.3.2.1 Electrolytes Used 34
4.5.3.2.2 Experimental Setup 36
4.5.3.3 Plating Parameters 37
4.6 Design of Final Heaters 40
4.6.1 Composition of NiCr for Final Heaters..... 45
4.7 Fabrication 49
4.7.1 Optical Lithography 49
4.7.2 Optical Mask Design 49
4.7.3 Substrate Preparation 51
4.7.4 Spin Coating and Pre-Bake of Resist 52
4.7.5 UV Exposure and Development of Resist 52
4.7.6 Electroplating 52
4.7.7 Copper Etching 54
4.7.8 Titanium Etching 54
4.7.9 Electric Connections 54
4.7.10 Resistance of Electroplated NiCr Alloy 55
4.8 Summary 57

CHAPTER 5. CONTROL SYSTEM 58
5.1 Introduction 58
5.2 Controller 59
5.2.1 PID Control Parameters 59
5.2.2 Control Model of LSU MicroGC 60
5.3 MicroGC Assembly 63
5.3.1 Experimental Apparatus 63
5.3.2 Thermal Cycling 63
5.4 Conclusions 66

CHAPTER 6. CONCLUSIONS AND FUTURE WORK 67
6.1. Contributions to the MicroGC Project 67
6.2. Recommendations for the Future work..... 68

REFERENCES ……..…… 69
APPENDIX HEATER DESIGN……..…….……. 73
VITA ……..…… 87

ABSTRACT

Gas chromatography is a technique widely used for the separation and analysis of gas samples. Gas chromatographs are used for environmental maintenance, monitoring sophisticated biological analyses, and to separate components from a mixture of gases for mass spectrometer analysis. There has been a tremendous interest in miniaturization of gas chromatograph systems because of the potential for portability, faster response time, lower dead volume, lower power consumption, and lower cost of operation.

Conventional gas chromatography keeps the column at a constant temperature during separation, which is called isothermal analysis. Temperature programming is a mode of gas chromatography in which the column temperature is raised progressively during the course of analysis. Temperature programming facilitates separation of a wider range of components, when compared to isothermal analysis, in less time. No miniaturized gas chromatograph systems with temperature programming capability have been reported to date.

A temperature programming cycle was implemented for the LSU microGC. The thermal behavior of the device was modeled using an energy-based approach to determine the thermal power requirements. Two heaters were designed, one heater gave uniform temperature distribution over the LSU microGC column, and the other gave a linear temperature gradient along the length of microGC. The heaters were fabricated by electrodepositing Ni-Cr (97.5-2.5) alloy on silicon substrates. The heaters were integrated with test microGC. A commercial PID controller was integrated with the heater and fan to direct the temperature programming for the LSU microGC. Heating and cooling ramp rates of more than 2.46 ^{o}C/sec were obtained.

CHAPTER 1
INTRODUCTION

The Micro Electro Mechanical Systems (MEMS) technology revolution has had a profound impact on our society in such diverse fields as automobiles, computers, communications, medicine, and home entertainment over the past 15 years. MEMS are already used for tasks ranging from in-dwelling blood pressure monitoring to active suspension systems for automobiles [1]. The nature of MEMS technology and the diverse useful applications make it potentially a far more pervasive technology than integrated circuit microchips.

MEMS technology has introduced portability, speed, and reduction in both the capital, and operating costs of laboratory equipment. Examples of the benefits of reducing size can be seen in lab-on-chip systems. Shrinking a conventional chemistry laboratory down to the size of a credit card is the driving concept behind lab-on-a-chip technology. Complex reactions with many chemicals can take place on a lab-on-a-chip device; the products of these chemical reactions can be pumped into a different chamber for another reaction, or they can be separated and used for analysis. The possibilities for chemistry on a chip nearly match the macroscopic chemistry laboratory possibilities, and the gap is rapidly closing [1]. Examples of lab-on-chip devices are shown in Figures 1.1, and 1.2. There are many benefits to using a miniature laboratory over a conventional laboratory. Many reagents used in chemistry and biochemistry are very expensive, so the prospect of using very tiny amounts of chemical for an application is very appealing.

Another advantage of using very small amounts is that they will mix and react quickly. This will greatly reduce the time needed for some chemical analyses, such as DNA sequencing. Also, some reagents and reaction products can be very harmful. So another benefit of lab-on-a-chip devices is that they minimize human interaction with harmful reagents and reaction products.

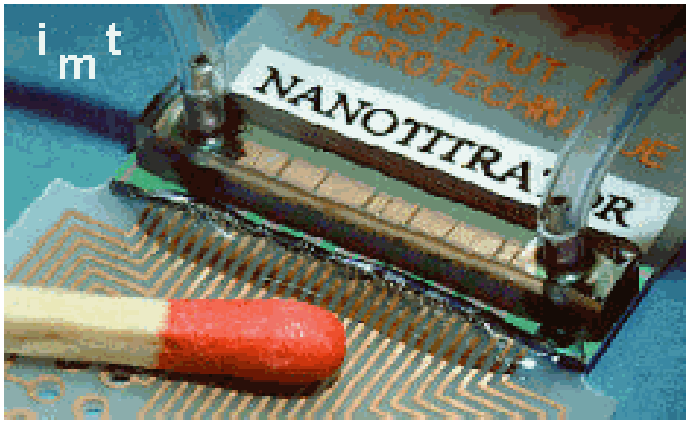

Figure 1.1: Nanotitrator is composed of a planar electrode and a micro channel [2].

MEMS, like many new technologies, are expensive to design and develop; however, once developed, the cost savings can be significant. Many MEMS units can be produced on one substrate, which, like computer chips produced on a single wafer, reduces costs significantly.

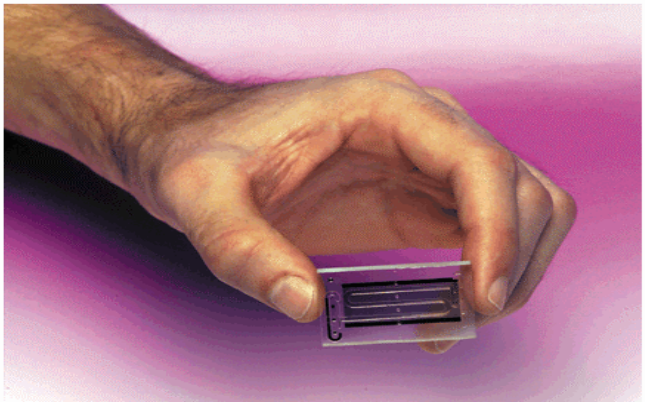

Figure 1.2: The integrated injection-separation-detection system being developed by a DARPA project team resides on 2.5 by 4-centimeter substrate [3].

1.1 Micro Gas Chromatography

Gas chromatography is a technique widely used for the separation and analysis of gas samples. Sample components are transported through a long capillary tube, typically called a column, by a mobile phase consisting of an inert gas, and are separated based on their boiling points and their relative affinity for the stationary phase lining the walls of the column. The separated chemicals are detected at the exit using a detector.

Gas chromatographs are used for environmental maintenance, monitoring sophisticated biological analyses, and to separate components from a mixture of gases for mass spectrometer analysis. Traditionally, they have been used in plant control for remote process testing, where samples had to be taken to a laboratory to be separated into the components and analyzed. This is due to size of typical macro scale analysis systems. In conventional GC systems capillary columns or tubes with internal diameters of 270 to 530 μm and lengths from 10 to 30 m are used as the separating component. The inside walls of the columns are coated with a thin uniform layer of an organic polymer, the GC liquid phase, to a thickness of less than one micrometer.

Separation of samples in these columns is determined by the column diameter and the stationary phase [5]. High resolution is achieved with narrow columns, while selectivity is achieved through appropriate use of the stationary phase and detector design. The separation efficiency of the column is determined by the height equivalent of theoretical plates (HETP), which represents that portion of the column in which the partition equilibrium is established at one time. To avoid use of a long column and separation time, the HETP should be as small as possible.

As the diameter of a column is reduced, peak widths become narrower, resulting in higher resolution between closely eluting compounds [5]. Most modern gas chromatograph systems, such as the HP 5890 series GC (Agilent Technologies, Inc., Palo Alto, CA) (26’’x20’’x18.5’’), are too bulky to be operated in remote, hostile environments. There has been significant interest in the miniaturization of GC systems because of the potential for portability, fast response time, low power consumption, and low cost. There have been several efforts to develop a miniature GC using silicon micromachining technology [6]. While conventional GC systems use a fused silica

capillary column, most of the previous efforts to develop miniature GC systems have used micromachined silicon channels, can be anodically bonded to glass plates, because this micromachined silicon/glass column can provide smaller size, lower power consumption for heating and an ability to integrate other components on a single chip. Researchers at the Georgia Institute of Technology used parylene micro columns, which has lower heat capacity than micromachined silicon/glass column [7].

Bhushan [4] successfully fabricated metal High Aspect Ratio (HAR) GC columns using the LIGA process. The main advantage of a metal column is its potential as a molding tool. The major component in the LSU micro-GC is a HAR (high aspect ratio), rectangular cross-section GC column made out of electroplated metal. The 1-3 m long, 25-50 μm wide, 250-1000 μm tall column, with integrated injector and detector can sit on a chip 2 cm x 3 cm [4].

1.2 Micro GC Column Temperature Control

1.2.1 Isothermal Analysis

Isothermal analysis is suitable for simple samples containing relatively few components. An appropriate column temperature to achieve the separation of components can be determined experimentally using isothermal analysis [5]. Isothermal operation is also preferred when accurate retention data are required for identification purposes, as it is easy to control and reproduce. The cycle time of a programmed run can take much longer than an isothermal separation because of the time required for cooling and re-equilibrating the oven at the completion of the cycle. Hence, isothermal operation has an advantage in some situations, such as process control and when sample throughput is important consideration [7].

1.2.2 Temperature Programming

Temperature is one of the two most important variables in GC, the other being the nature of the stationary phase.

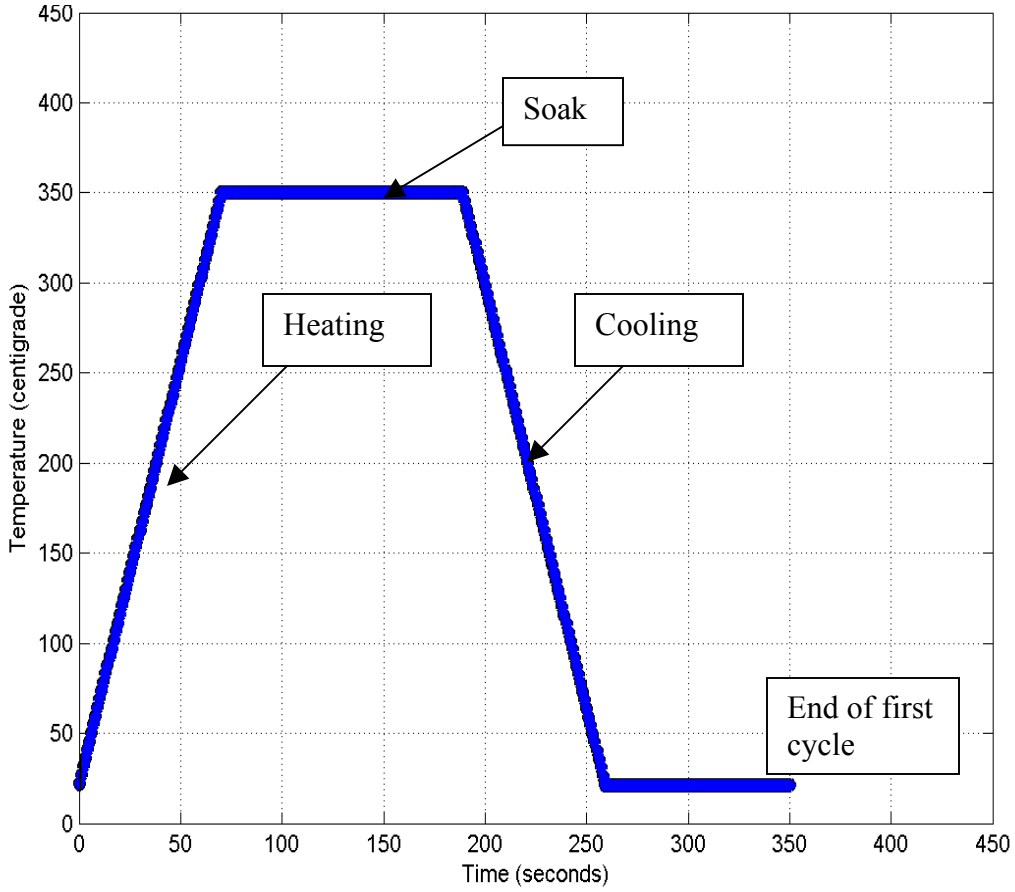

Figure 1.3: Typical temperature cycle for the temperature programming of the GC. The cycle will be repeated every 7 minutes.

Temperature programming is a mode of gas chromatography in which the column temperature is raised progressively during the course of the analysis. It is used to analyze complex mixtures containing compounds with wide range of vapor pressures [7]. Figure 1.3 shows the typical temperature programming cycle for the operation of the micro gas chromatograph column.

Typical temperature programming cycle is shown in Figure 1.3. The first part of the cycle is heating. The designed thermal system should have very fast response times, with heating rate of 5^{o}C/sec or more. The second part of the temperature programming is soaking. The temperature is held constant. The GC columns are cleaned in this part. The third part is cooling. The cooling is done to restore the GC system to initial state and start analysis of new sample. The ideal cooling rates is 5^{o}C/sec or more.

1.2.3 Advantages and Limitations of Temperature Programming

Many samples contain components with a wide range of vapor pressures (boiling points), making it impossible to determine a suitable temperature for an isothermal run. As an example, consider the separation of a wide range of homologs like the kerosene sample shown in Figure1.3a. An isothermal run at 150^{o}C prevents the lighter components ($<C_8$) from being totally separated and still takes over 90 minutes to elute the C_{15} paraffin. The separation can be significantly improved using temperature programming.

Figure 1.3(b) shows one such programmed temperature run in which the temperature started at 50^{o}C less than the isothermal temperature used in Figure 1.3(a), and was programmed at 8^{o}C/min up to 250^{o}C, a temperature higher than the isothermal temperature. Increasing the temperature during the run decreases the partition coefficients of the analytes still on the column, so that they move through the column faster, yielding decreased retention times. The temperature programming facilitated the separation of the low-boiling point paraffins, easily resolving several peaks before the C_8 peak while increasing the number of paraffins detected.

The C_{15} peak eluted much faster, in about 21 minutes and it was not the last peak, since six more hydrocarbons were observed by temperature programming. All the peak widths are about equal under the temperature program; in the isothermal run, some fronting* was evident in the higher boiling point compounds. Since the peak widths do not increase in temperature programming, the heights of late eluting analytes are increased, the peak areas are constant, providing better detectivity [7].

***** Fronting-Peak shape in which the front part of a peak (before the apex) in a chromatogram tapers in advance of the remainder of the peak.

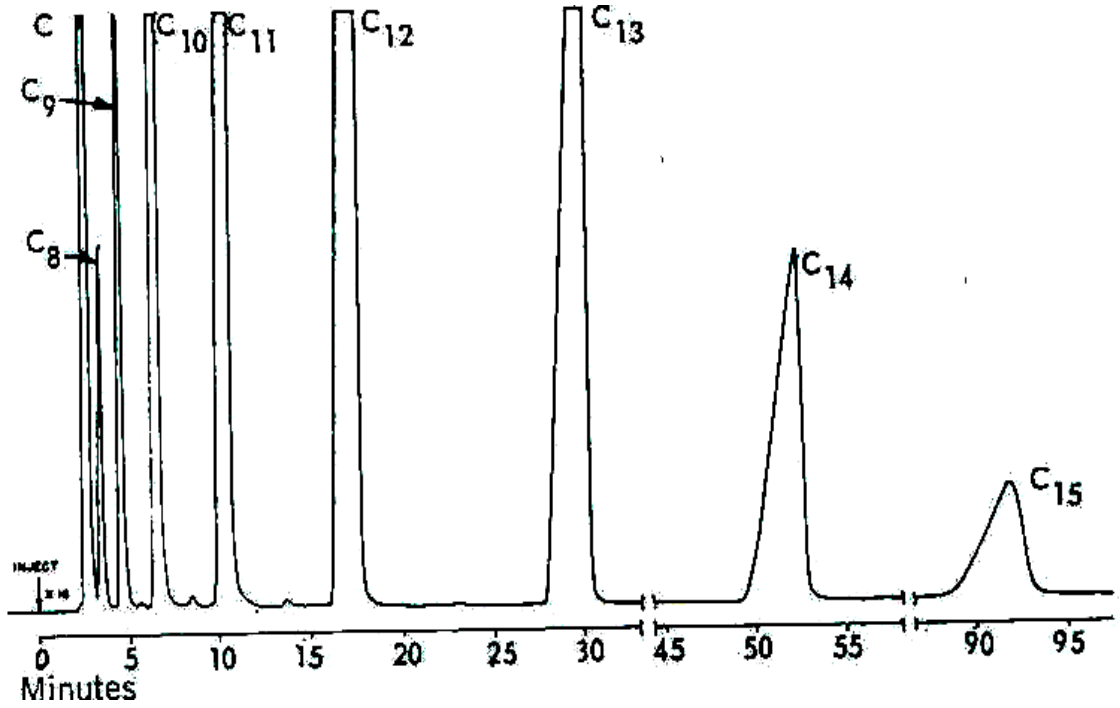

Figure1.3 (a): An Isothermal temperature separation of n-paraffins [7].

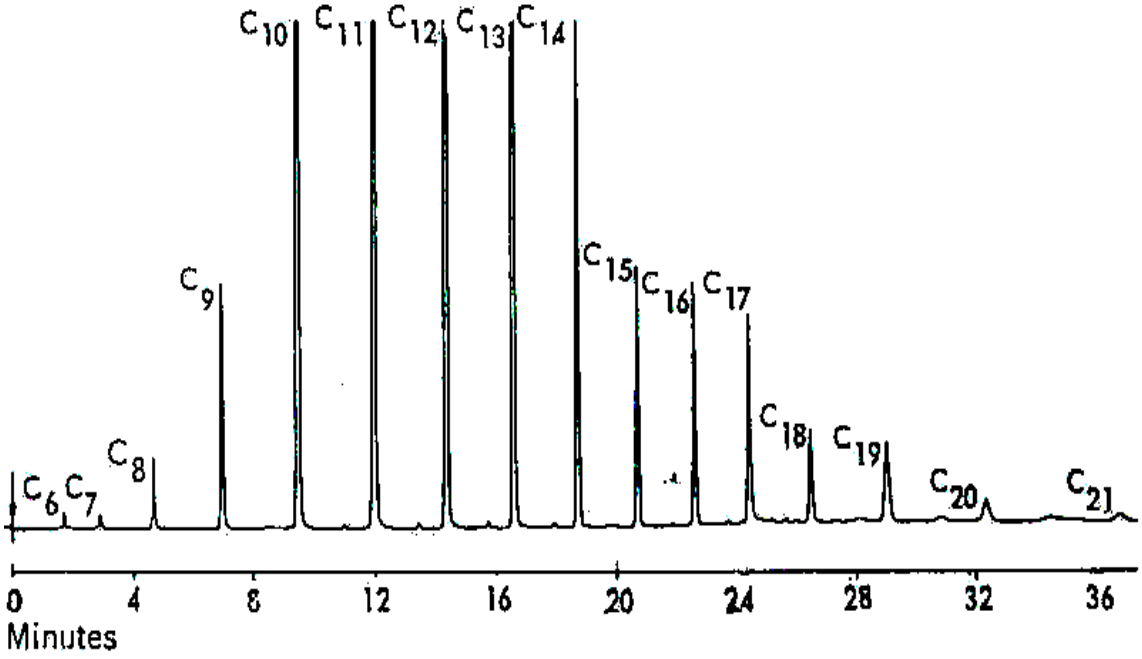

Figure1.3 (b): Programmed temperature separations of n-paraffins [7].

1.2.4 Existing Approaches to Temperature Programming

Gas chromatographs, which are commercially available, are equipped with ovens to perform temperature programming. A conventional oven has a heating rate of 40^{o}C/min or less depending on the model [9]. Cooling times are often not much faster. The Agilent GC (Model # HP5890 Agilent technologies Inc. Palo Alto, CA) uses an oven capable of programming at 10 ^{o}C/min. From a practical point of view, ovens are bulky, require large amounts of electrical power, and are not easily portable.

To enable the use of higher heating rates and acceptable cooling times, a number of systems based on resistive heating were recently developed. To adopt such a technique, a capillary column can be coated with a conductive material, or a coil can be wrapped around or run in parallel to the column, or the capillary column can be inserted into metal tubing.

Jain and Phillips [9] successfully applied a conductive coating onto the capillary column, and obtained a fast heating program with heating rates up to 20^{o}C/sec. By using aluminum-clad columns, Hail and Yost [11] achieved the separation of C_7-C_{10} in 2 seconds.

Ehrmann and coworkers [12] tested two concepts of resistive heating. One was based on the use of a metal tube as a heater and the second used a metal wire that was run parallel to the column as the heater, a collinear at-column heater.

It was found that a collinear at-column heater was more reliable than the coaxial heater and also enabled rates of 20^{o}C/sec. The latter suffered from differences in expansion coefficients of the metal and fused silica, causing damage to the fused-silica column.

1.2.5 Device Requirements for Temperature Programming

Temperature programming requires a more versatile instrument than an isothermal GC. Most important is the ability to control the temperature of the column while keeping the detector and injection port at constant temperature. An electronic temperature controller is needed along with a high heat flux heater and a high volume flow rate fan to carry out temperature programming of a micro-GC column.

1.3. Thesis Outline

The thesis is broken down into the following sections. The fundamentals of gas chromatography and the history of the gas chromatograph and miniaturization of the gas chromatograph are discussed in Chapter 2. The mathematical models of the thermal system, three dimensional thermal finite element analyses, power consumption calculations for different designs of the micro-GC and the experimental results of heating experiment are presented in Chapter 3. The process of heater design, heater fabrication and integration of the heater with the micro-GC are presented in Chapter 4. The analytical models of the open loop control systems and closed loop control systems, and the selection of the control loop are presented in Chapter 5. Conclusions and suggestions for minimizing heat loss are presented in Chapter 6.

CHAPTER 2

BACKGROUND

2.1 Chromatography

The Russian botanist Mikhail Tswett first developed the process of chromatography in 1903. He extracted a mixture of pigments from plant leaves and pushed a small sample of the mixture dissolved in petroleum ether (mobile phase) through a thin column coated with calcium carbonate [chalk] (stationary phase). The various plant pigments separated from each other based on their attraction for the calcium carbonate while being pushed through the column, resulting in a trail of colored bands. These colored bands signified the components of the mixture of plant pigments. The word chromatography is a combination of the two Greek words “khroma” (color) and “grafein” (written) [5]. Chromatography is essentially a process of separation utilizing the interaction between two phases of matter: a mobile phase and a stationary phase. The mobile phase is either a gas or a liquid and the stationary phase is a solid or liquid. The components of a sample mixture which is to be separated have varying affinities for the mobile and stationary phases. Those components which have a higher affinity for the mobile phase will move through the system much faster than those which have less affinity for the mobile phase and more affinity for the stationary phase. The components which have the highest affinity for the stationary phase will move through the system at the slowest rate. As the various components move across the stationary phase they emerge at the output of the chromatographic system in a process called elution. The various components of the sample mixture elute at differing times, called retention times, which result in separation and identification [7].

2.1.1 Gas Chromatography

The various chromatographic processes are named according to the physical state of the mobile phase. In gas chromatography, the mobile phase is a gas. A sub classification is made according to the state of the stationary phase.

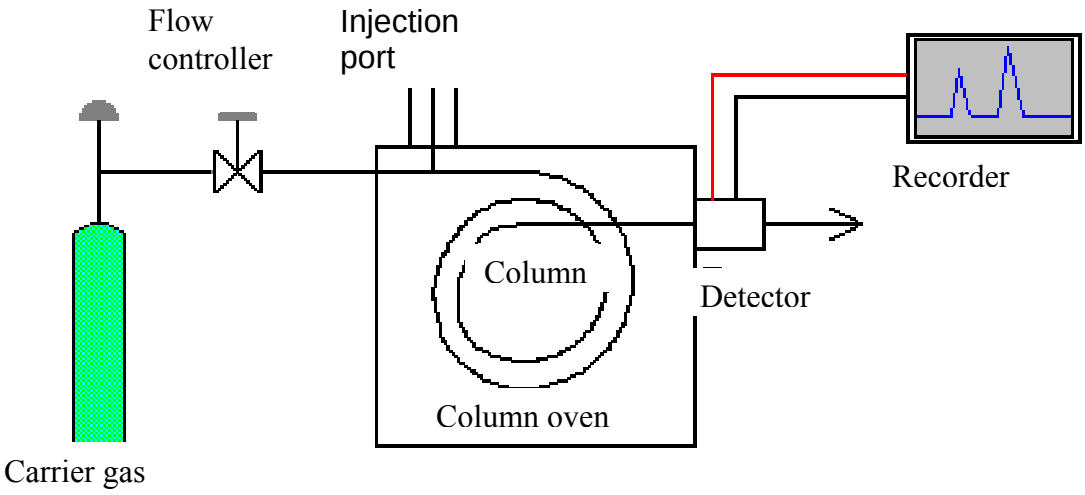

Figure 2.1 Schematic of the apparatus for GC analysis (not to scale).

If the stationary phase is solid, the gas chromatography technique is called gas solid chromatography, and if it is a liquid, gas-liquid chromatography.

Figure 2.1 shows a schematic of a typical gas chromatography analysis. A sample is introduced into one end of a long narrow tube called the chromatograph column. The stationary phase acts as a selective retardant to the passage of the chemicals through the column. At the end of the column the components in a gas mixture are detected using a detector and recorded using a data recording system.

2.1.2 Mechanism of Chromatography

The movement of substances during chromatography is the result of two opposing forces, the driving force of the mobile phase and the resistive action of the stationary phase (sorbent). The driving force acts to move the substances from the injection port in the direction of the mobile-phase flow. The resistive action impedes the movement of the substances by desorbing them out of the flowing phase back onto the stationary phase (sorbent). Each molecule alternates between an absorbed and unabsorbed condition, following a stop and go path through the column. Although the zone moves constantly forward, only a fraction of the molecules in the zone is moving at any one time. At the end of development, each zone has migrated a certain mean distance and has spread because of the fluctuations in the movement of individual molecules in the zone.

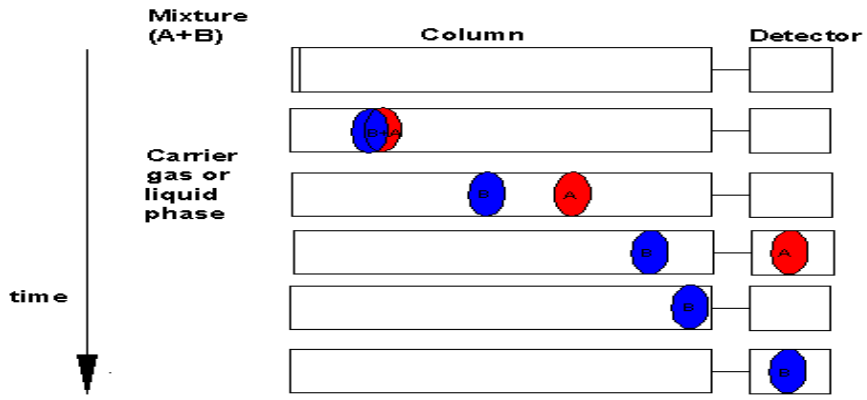

Figure 2.2: Mechanism of chromatography [9].

The distance traveled by each solute zone in a given time is a result of the difference between the driving and resistive forces. Figure 2.2 shows the mechanism of chromatography. The mixture of A and B is separated during passage through the column. A detector is placed at the end of the produces the signals representing passage of the mixtures [5].

2.1.3 Basic Apparatus for Gas Chromatography

2.1.3.1 Column

The column tubing is typically made from copper, stainless steel, aluminum, or glass in a straight, bent, or coiled form. Copper may be unsuitable in some cases when the sample contains amines and acetylenes, which react with copper. Straight columns are more efficient, but can be cumbersome. If coiled, the spiral diameter is at least ten times the column diameter in order to reduce diffusion. Column lengths vary from a few centimeters to more than 15 m in length. Common analytical packed columns are 1 to 3 m in length while capillary columns are generally 9 m to 28 m long. The carrier gas velocity changes during passage through the column; only a short section of the column operates at the optimum flow rate.

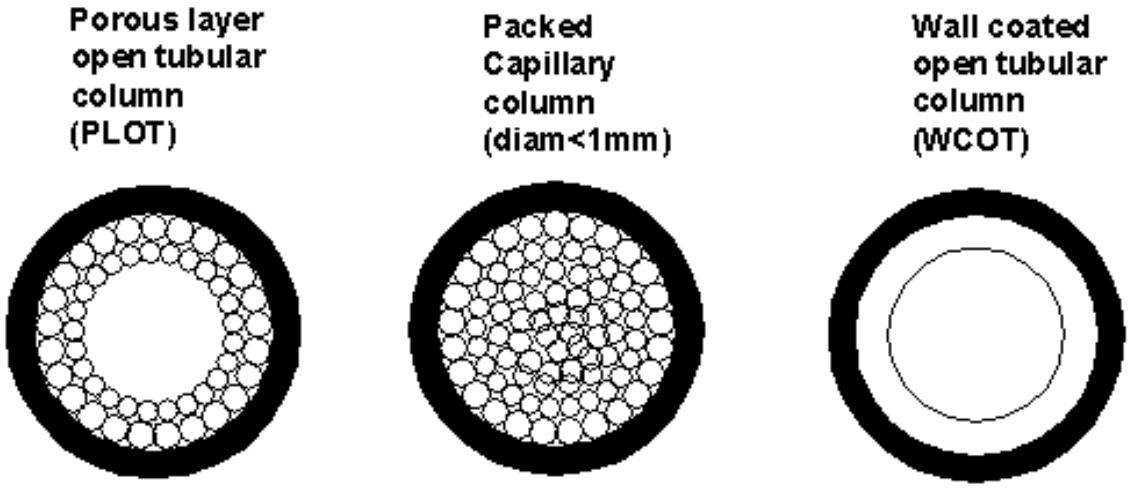

Figure 2.3 Types of capillary columns [10]

In addition, longer columns need higher injection pressures, introducing potential problems such as gas leakage. Packed column diameters may vary from 0.25 mm to 50 mm. The smaller the column diameter, the higher is the column efficiency [6]. There are three types of capillary columns in current use, including: porous layer open tubular columns (PLOT), packed capillary columns, and wall-coated open tubular columns (WCOT).

Figure 2.3 shows diagrammatical representations of the cross-sections of those three column types. In open tubular columns, the stationary phase is coated as an even layer over the inner wall of the tube.

This phase can be either liquid, sometimes highly cross-linked to be solid in appearance, or it can be a porous layer of solid absorbent material such as aluminum, or a molecular sieve. The latter columns are known as porous layer open tubular (PLOT) columns and make a very important contribution to modern capillary GC. Most open tubular columns are constructed either from fused silica or stainless steel. Packed capillary columns have similar tube geometry to open tubular columns except that they are filled with packing material. The packing is accomplished in a variety of ways, but usually the packing density is lower than in conventional packed columns, giving a higher permeability.

2.1.3.2 Detectors

The detector is used to indicate the presence of the solute components and to measure the amount of each component in the column effluent.

Desirable characteristics of the detector are:

1) High sensitivity to analytes;
2) Low noise level;
3) Response to all types of components;
4) Low sensitivity to changes in flow and temperature changes;
5) Rugged and inexpensive.

Thermal conductivity and flame ionization detectors are widely used [10]. Specific detectors, such as electron capture and nitrogen phosphorus detectors, have the advantage that they selectively detect only certain types of compounds. This makes them extremely useful for trace and quantitative analyses. The thermal conductivity detector typically employs a tungsten filament, which is heated by passing a constant current through it [10]. Carrier gas flows continuously over this heated filament and dissipates heat at a constant rate. When sample molecules mixed with the carrier gas pass over the hot filament, the rate of the heat loss is reduced and the resistance of the filament increases. This small change in resistance is measured by a Wheatstone bridge arrangement and the output is recorded.

In the Flame Ionization Detector, hydrogen and air are used to produce a flame. A collector electrode with a DC potential is placed above the flame and measures the conductivity of the flame. With pure hydrogen, the conductivity is low. However, as organic compounds are burnt, the conductivity increases and the current increases, which can be correlated with the compounds.

2.1.3.4 Carrier Gas

The sample is dissolved in the mobile phase, which may be a gas, a liquid, or a super critical fluid. In principle, any gas can be used as a carrier, but for practical and economic reasons the choice of the mobile phase is limited to hydrogen, helium, argon, nitrogen, carbon dioxide and air. Hydrogen has a very low viscosity, therefore high flow rates can be obtained with a relatively low pressure drop. Other gases including helium

have comparable, but slightly higher, viscosities. Helium is the most commonly used carrier gas.

2.1.4 Nomenclature

2.1.4.1 Phase Ratio

A fundamental property of the open tubular column is the phase ratio β, defined as follows:

$$phase\ \ ratio(\beta) = \frac{volume\ \ of\ \ carrier\ \ gas\ \ in\ \ column}{volume\ \ of\ \ stationary\ \ phase\ \ in\ \ column} \qquad (1)$$

From the known geometry of the column, the phase ratio can be calculated:

$$\beta = \left(\frac{d_i}{4d_f} \right) \qquad (2)$$

where d_i is the internal column diameter, and d_f is the thickness of the stationary phase film in the same units.

2.1.4.2 Partition Coefficient *K* and Retention Factor *k*

The retention properties of compounds depends critically on the phase ratio, and also on the affinity of compounds for the stationary phase, as measured by the partition coefficient *K*, defined as:

$$K = \frac{concentration\ \ in\ \ stationary\ \ phase}{concentration\ \ in\ \ carrier\ \ gas} \qquad (3)$$

Where, the concentrations are measured in terms of mass or volume percent. In practice it is more useful to convert this to the retention factor, *k*, defined as the ratio of the mass of each component in the stationary phase to its mass in the carrier gas at equilibrium.

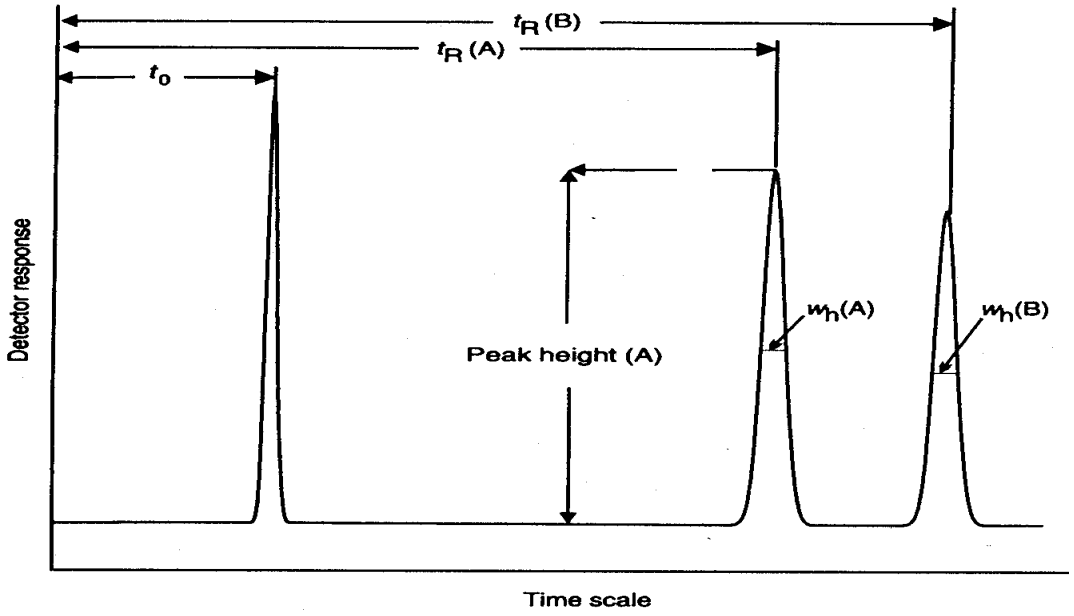

Figure 2.4 Basic chromatographic measurements.

Key: t_0 = column holdup time;

$t_R(A)$ = total retention time for *A*;

$t_R(B)$ = total retention time for B;

$w_h(A)$ = peak width at half height for *A*;

$w_h(B)$ = peak width at half height for *B*.

$$retention\ \ factor\ \ k = \frac{mass\ \ of\ \ solute\ \ in\ \ stationary\ \ phase}{mass\ \ of\ \ solute\ \ in\ \ carrier\ \ gas} \qquad (4)$$

The retention factor can be calculated from the measured retention times in the chromatogram.

2.1.4.3 Theoretical Plate Number

A theoretical plate is a peak in chromatogram. A typical method to characterize the column of a GC is the theoretical plate number, *N*, calculated from a chromatogram run under isothermal conditions from the following relationship:

$$N = 5.54 \times \left(\frac{t_R}{w_h} \right)^2 \qquad (6)$$

Where, w_h is the width of the peak at half height. The column efficiency defines the width of the chromatographic zone inside the column just before it emerges and enters the detector. Columns with high theoretical plate numbers produce a very narrow peak that increases the probability of separating all the components of complex mixtures.

2.1.4.4 Theoretical Plate Height

Plate height gives the extent of peak broadening for a solute as it passes through the column. The theoretical plate height is calculated by dividing the length of the column by its number of theoretical plates:

$$H = \frac{L}{N} \tag{7}$$

Although the theoretical plate height is a measure of column performance, it does not indicate the resolving power of the column.

2.2 Miniaturization of Gas Chromatograph

There has been a tremendous interest in miniaturization of GC systems because of potential capabilities such as portability, fast response time, low dead volume, low power consumption and low cost. Introduction of fast, portable GC systems would allow real time analysis of the composition and monitoring of gas mixtures in dangerous places, like coal mines, which may improve work safety and the quality of the resulting products.

2.2.1 Gas Chromatography System on a Silicon Wafer

A number of efforts have been mounted over the past 25 years to develop miniaturized GCs. The original idea of fabricating an integrated GC consisting of an injection valve, along column and a detector (TCD), fabricated on a silicon wafer was developed at Stanford in the 1970's [Terry, 1979]. This simple device has been reworked in the last 25 years, creating a new family of portable and fast chromatographs (Figure. 2.6).

Extending Terry's idea, researchers at Lawrence Livermore National Laboratory (LLNL), used the Bosch DRIE process to build a 40 μm wide, 250 μm deep and 1 m long separation columns (Figure 2.5). At Texas Christian University, Kolesar and Reston [6] fabricated a 0.9 m long and 300 μm wide and 10 μm high column in silicon, and integrated it with off-the shelf components.

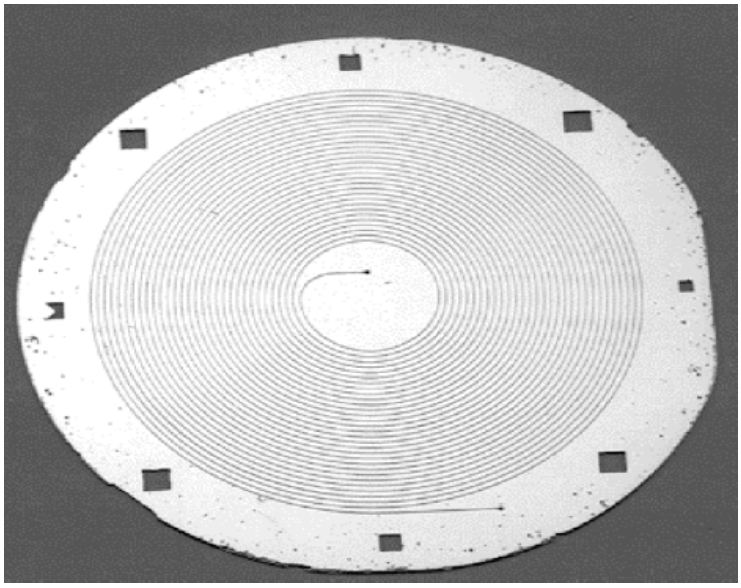

Figure 2.5: Gas chromatograph columns on silicon substrate produced at Lawrence Livermore National Laboratories [13].

A 10 μl sample volume of ammonia and nitrogen dioxide, introduced at a pressure of 40 psi, was separated in about 30 minutes at operating temperatures of 55-80^{o}C.

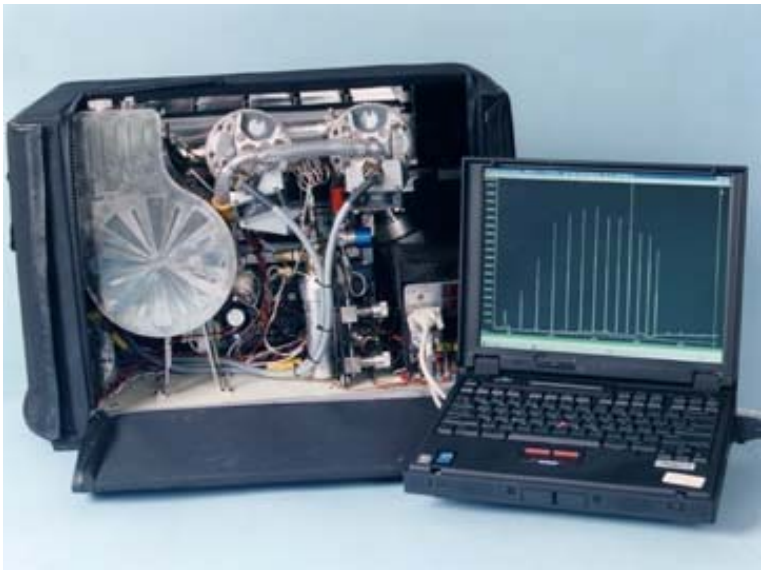

Figure 2.6: GS-MS Portable System produced by Lawrence Livermore National Laboratories [14].

2.2.1.1 Limitations of Micro Gas Chromatograph on Silicon Wafer

Microfabricated GC columns typically consist of a micromachined substrate (silicon) and a cover sheet (Pyrex glass), bonded together. These devices are suitable for isothermal runs, with long analysis times, leading to low separation resolution. The devices are also limited to separating compounds with high vapor pressures, very-volatile compounds such as carbon monoxide, carbon dioxide gases, and benzene only. If the selected isothermal temperature is low, the peaks will be spaced far apart, resulting in high retention times and eventual broadening of peaks for compounds eluted towards the end of the chromatogram. If the isothermal analysis is done at higher temperature, the peaks elute too close together, resulting in a loss in resolution for early eluting compounds [15]. A solution to this problem is temperature programming, where, the column temperature is increased at a linear rate during the analysis [15]. This temperature ramp decreases the retention time and improves detectability of the compounds but requires use of considerable power.

2.2.2 Parylene Gas Chromatograph

Researchers at the Georgia Institute of Technology fabricated a 1 m long Parylene micro column with a rectangular cross-section (100 μm wide, 350 μm high) for a miniature gas chromatograph. The Parylene column reached the steady state temperature of 100 ^{o}C in 30 seconds [16].

The main advantage of the Parylene micro-column was its lower heat capacity compared with the micromachined silicon column. The Parylene micro GC was the first miniature GC with an embedded heating element. The analysis time and power consumption of the miniature GC system were lower than for the microGC on a silicon wafer [16].

2.2.3 Miniaturization of Gas Chromatograph at LSU

The LIGA (German acronym for Lithographie, Galvanoformung, Abformtechnik) process was used for miniaturization of the gas chromatograph at LSU. Bhushan [4] fabricated 50 μm wide, 250-500 μm tall gas chromatograph columns using the LIGA process (Figure 2.9). The columns were made free standing to facilitate uniform coating of the stationary phase.

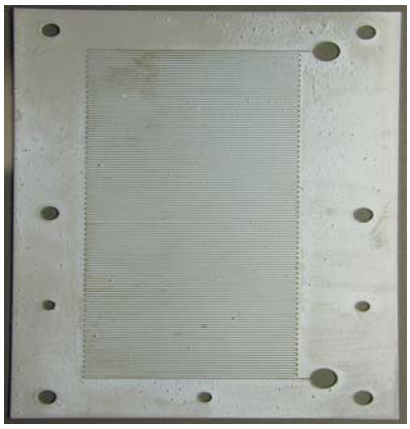

Figure 2.9: Nickel column [4].

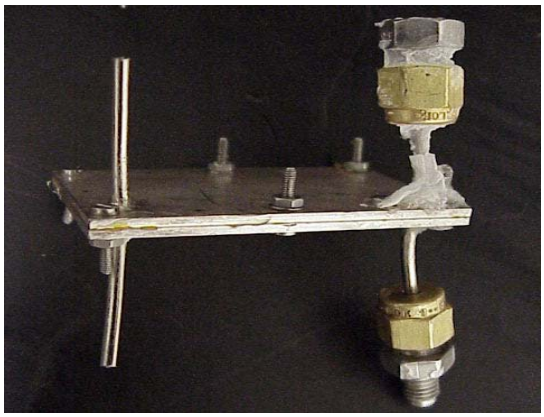

Figure 2.10: Test-bed for final µGC column [4].

Hydrogen and helium were used as carrier gases at flow rates of 3ml/min-10ml/min. Nickel plates were used to cover the open ends of the columns and were joined using mechanical fasteners [4]. Successful sealing was not obtained. In ongoing research, 2m long, 50µm wide, and 500 µm tall polymer (PMMA) GC columns were fabricated using deep X-ray lithography (DXRL). The open end of the columns was sealed with 810 tape (3M, St. Paul MN). After providing the input/output connections to the column assembly, very narrow methane sample plugs were passed through the column at different flow rates (ml/min) and detected with a flame ionization detector (FID). The results from the tests were encouraging because the leading edge had a vertical profile, indicating that the sample was traversing the column with little dispersion, and that the dispersion was relatively constant over a range of flow rates [4].

2.2.3.1 Advantages of LSU LIGA MicroGC over MicroGCs

Rectangular columns have lower HETPs, thus better performance, than the conventional capillary columns [6]. Using rectangular columns makes it possible to individually select the HETP and the carrier gas flow by independently adjusting the column height and width respectively. The ability to increase the performance without sacrificing resolution is the biggest advantage of rectangular columns over similar area, circular columns. The possibility of fabricating high aspect ratio structures with high quality sidewalls using LIGA was another advantage. Sloped sidewalls cause non-uniform absorption of the effluent in the stationary phase, leading to the peak broadening.

CHAPTER 3
THERMAL SYSTEM

3.1 Introduction

The main objective of studying the system dynamics of the micro GC was to determine the required thermal input for different designs of micro GCs for selection or design of the heater. Figure 1.3 shows the typical temperature programming cycle for the operation of the micro gas chromatograph column. The thermal system should have very fast response times, with a range of heating rate more than 5 ^{o}C/sec during the first part of the temperature cycle, and the cooling rate more than 5 ^{o}C/sec.

The initial proposed GC assembly is shown in Figure 3.2(a). The top plate, columns, and the bottom plate represent the microGC. The heater was placed in between two insulators, which in turn was supported by a metal plate as shown in Figure 3.2(a). Figure 3.2(b) shows the revised proposed GC assembly. The insulator is bonded to the micro GC using silver solder.

The heater was designed based on the dynamic performance estimated using thermal models of the gas chromatograph. The heat distribution models for an alternative assembly and analytical calculations of power consumption for different configurations of the gas chromatograph will be presented in Section 3.2.

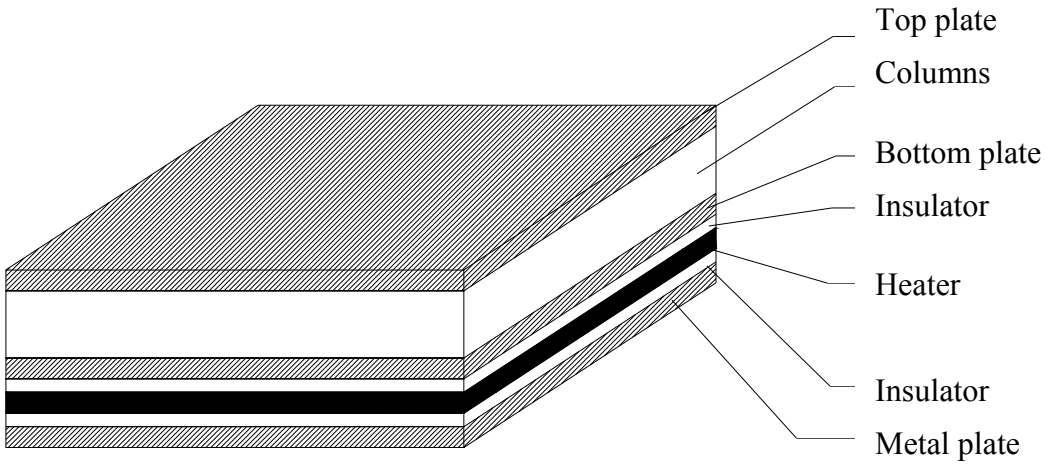

(a)

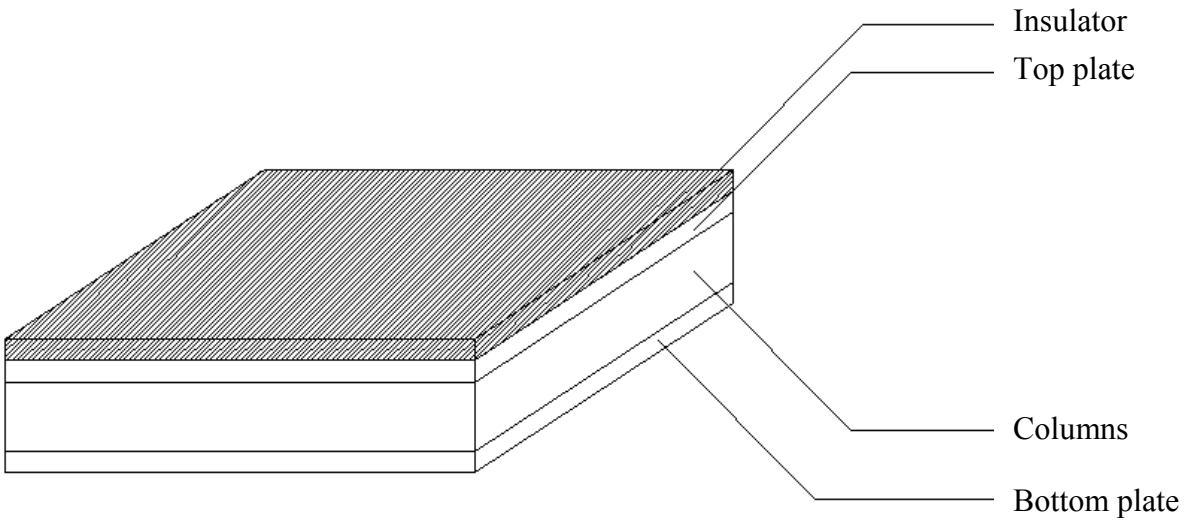

Figure 3.2 (a): Schematic diagram of initial proposed GC assembly.
(b): Schematic diagram of revised proposed GC assembly.

3.2 Thermal System Design

3.2.1 Pseudo Bond Graph Modeling for Thermal Systems

In order to study the dynamics of the system a lumped parameter thermal model of the micro GC was developed using the pseudo bond graph method [Karnopp, 2000]. Thermal systems have no inertial element so that the only one-port elements that were used in this system model were sources, resistors, and capacitors. In the case of thermal systems, the product of temperature and heat flow is not equal to power. For this reason, a thermal bond graph with temperature as the effort variable and heat flow as the flow variable is called a pseudo bond graph.

Power input was from the bottom side of the micro GC, and was modeled as a constant heat flux (flow source). The ambient condition was taken as a constant temperature, T_∞, which was represented by an effort source. Since the ratio of the thickness compared to the length and width of the device was less than 0.001, one dimensional heat transfer was assumed.

3.2.2 Heat Distribution Model

The dynamic thermal response of the gas chromatograph was modeled using lumped mechanical elements. The essence of the lumped capacitance method is the assumption that the temperature of the solid is partially uniform at any instant during the transient process. This assumption implies that temperature gradients within the solid are negligible. The top plate, column, bottom plate, two insulators and a nickel plate to hold the insulators were considered as different lumps.

The microGC was reticulated into six subsystems capable of storing energy; these represented three metal plates, two insulators, and a column. The capacities were evaluated using the Equation 3.1.

$$C=mc_p \qquad 3.1$$

Where c_p was the heat capacity at constant pressure, and m was the mass.

Equation 3.2 defines the resistance for heat transfer by conduction, R_{cond}.

$$R_{cond} = \frac{L_T}{k_{Th}A} \qquad 3.2$$

Where, L_T is the length of the block, A the cross sectional area, and k_{Th} the thermal conductivity of the material of the block. Equation 3.3 defines the resistance for convective heat transfer.

$$R_{conv} = \frac{1}{h_c A} \qquad 3.3$$

Where, h_c is the local convective heat transfer coefficient. Radiation loss was neglected, as it was 5% of the total heat loss.

3.2.3 Six Lump Model

The top plate, column bottom plate and two insulators were considered as different lumps. The dimensions of the lumps are presented in Table 3.1. Each of the lumps has resistance and capacitance. There was heat loss to the atmosphere.

Table 3.1: Dimensions of lumps.

	Length (m)	Breadth (m)	Height (μm)
Top plate (Nickel)	0.05	0.04	250
Columns (Nickel)	0.04	0.03	500
Bottom plate (Nickel)	0.05	0.04	250
Insulator (Alumina, (Al_2O_3))	0.05	0.04	640
Support plate (Nickel)	0.05	0.04	250

The schematic of heat loss is shown in the Figure 3.3 (a), with the equivalent pseudo bond graph in Figure 3.3 (b). There are sixteen principal components: the four conductive resistances (R_2, R_4, R_6, and R_9) representing the conductive heat loss from lump 1 to lump 2, from lump 2 to lump 3, from lump 3 to lump 4, and from lump 5 to lump 6, respectively, given by Equation 3.2; the six convective resistances (R_1, R_3, R_5, R_7, R_8, and R_{10}) accounting for the heat loss from lumps to the atmosphere, given by Equation 3.3; the thermal capacities (C_1, C_2, C_3, C_4, C_5, and C_6) which model the thermal capacities of the six lumps, given by Equation 3.1; the flow source (S_f) equivalent of the input heat flux; and the effort source (S_e) equivalent of the heat sink for the heat loss to the atmosphere.

Heat flux input to a node equals the sum of the heat flux transmitted, the heat flux lost due to convection, and the heat flux used to heat the lump. Balancing heat flux at the six zero junctions, the equations at the six nodes can be written (Equation 3.4). The convective heat transfer coefficient, h_c, for free convection of gases at a boundary typically ranges between 2 - 50 W/m^{2}K (Incropera, 1990). The coefficient depends on conditions in the boundary layer, which are influenced by surface geometry and the

nature of the fluid flow. A value of 50 W/m^{2}K was taken for h_c as the worst-case scenario for maximum heat transfer from the surface. Simulations were run with Matlab 6.5 (The Mathworks, Newton, MA). A partial differential equation (PDE) solver, ode45, was used to solve Equations 3.4 for a range of input heat fluxes. A wide range (10W-200W) of step inputs was applied to the system to observe the temperature response. It was observed that for a step input of 75W, the system reached 350^{o}C in 66 seconds, corresponding to a ramp rate of 5^{o}C/sec. The response from a step input of 75W is presented in Figure 3.4.

$$
\begin{aligned}
S_f &= C_1 \frac{dT_1}{dt} + \frac{1}{R_2}(T_1 - T_2) + \frac{1}{R_1}(T_1 - T_\infty) \\
\frac{1}{R_2}(T_1 - T_2) &= C_2 \frac{dT_2}{dt} + \frac{1}{R_4}(T_2 - T_3) + \frac{1}{R_3}(T_2 - T_\infty) \\
\frac{1}{R_4}(T_2 - T_3) &= C_3 \frac{dT_3}{dt} + \frac{1}{R_6}(T_3 - T_4) + \frac{1}{R_5}(T_3 - T_\infty) \\
\frac{1}{R_6}(T_3 - T_4) &= C_4 \frac{dT_4}{dt} + \frac{1}{R_7}(T_4 - T_\infty) \\
S_f &= C_5 \frac{dT_5}{dt} + \frac{1}{R_9}(T_5 - T_6) + \frac{1}{R_8}(T_5 - T_\infty) \\
\frac{1}{R_9}(T_5 - T_6) &= C_6 \frac{dT_6}{dt} + \frac{1}{R_{10}}(T_6 - T_\infty)
\end{aligned}
\qquad 3.4
$$

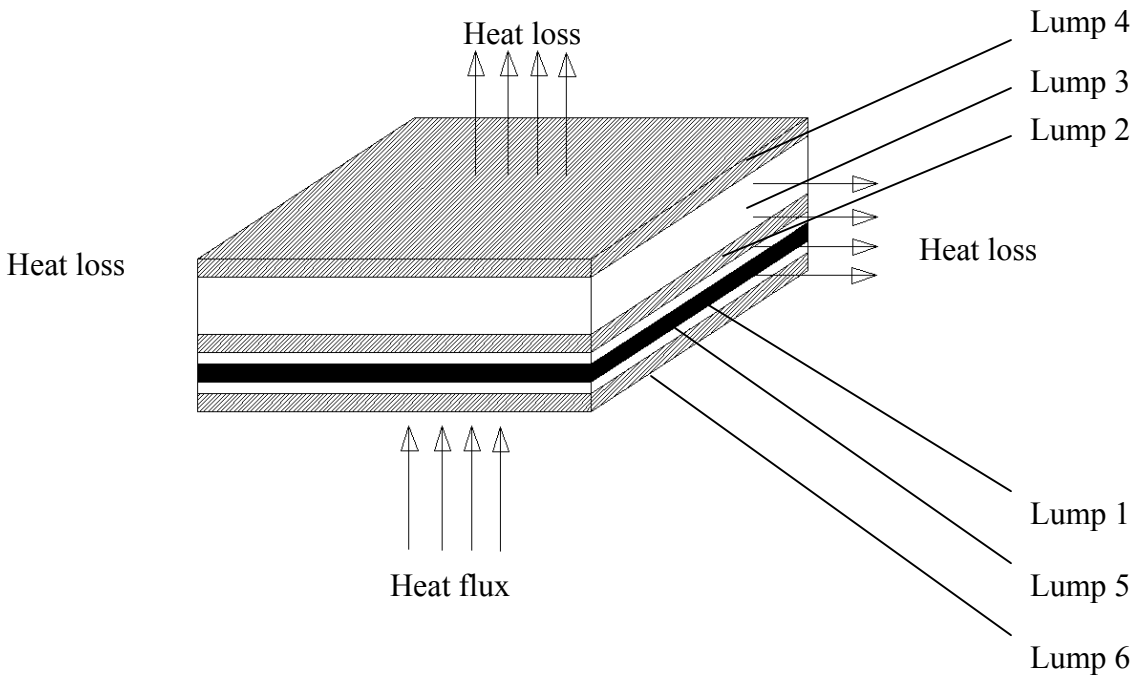

Figure 3.3 (a): Six Lump model.

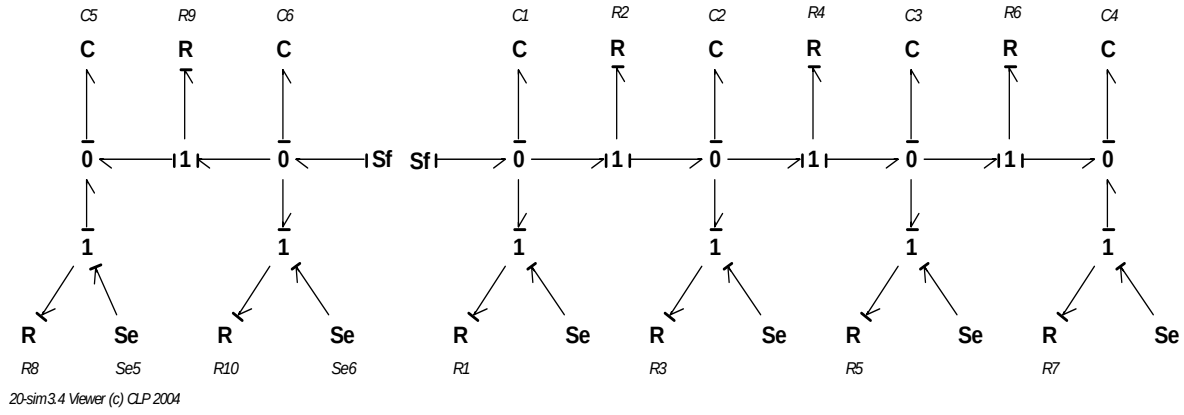

Figure 3.3 (b): Pseudo bond graph model for GC heat distribution. The flow source, S_f, represents the heat flux input from the heater. The effortsource, S_e, represents the thermal energy loss to the atmosphere.

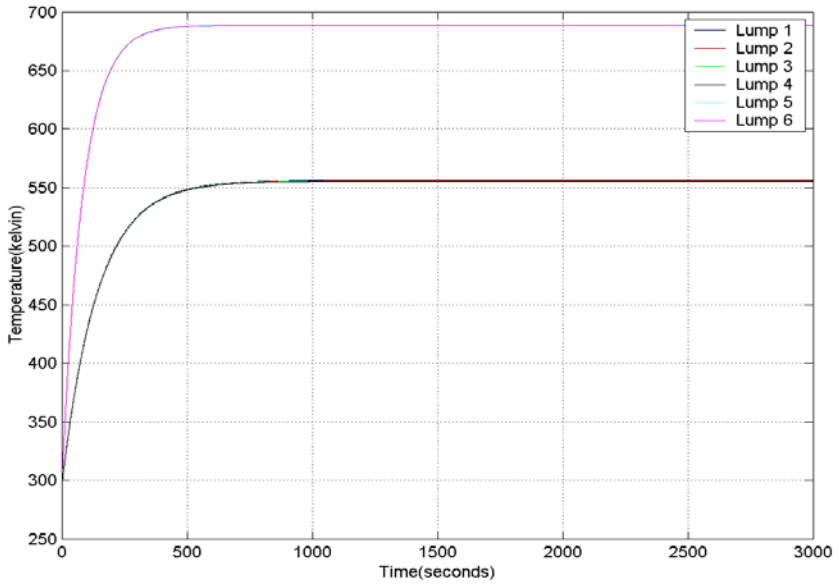

Figure: 3.4: Temperature response for a step input of 75W.

3.2.4. Heat Distribution for Four Lumps

The heat distribution model for four lumps was done to determine the temperature response of the revised GC assembly as shown in figure 3.2(b).

Table 3.2: Dimensions of the micro GC system.

	Length (m)	**Breadth (m)**	**Height (µm)**
Insulator (Alumina)	0.05	0.04	640
Top plate (Nickel)	0.05	0.04	250
Columns (Nickel)	0.04	0.03	500
Bottom plate (Nickel)	0.05	0.04	250

$$S_f = C_1 \frac{dT_1}{dt} + \frac{1}{R_2}(T_1 - T_2) + \frac{1}{R_1}(T_1 - T_\infty)$$

$$\frac{1}{R_2}(T_1 - T_2) = C_2 \frac{dT_2}{dt} + \frac{1}{R_4}(T_2 - T_3) + \frac{1}{R_3}(T_2 - T_\infty) \qquad 3.5$$

$$\frac{1}{R_4}(T_2 - T_3) = C_3 \frac{dT_3}{dt} + \frac{1}{R_6}(T_3 - T_4) + \frac{1}{R_5}(T_3 - T_\infty)$$

$$\frac{1}{R_6}(T_3 - T_4) = C_4 \frac{dT_4}{dt} + \frac{1}{R_7}(T_4 - T_\infty)$$

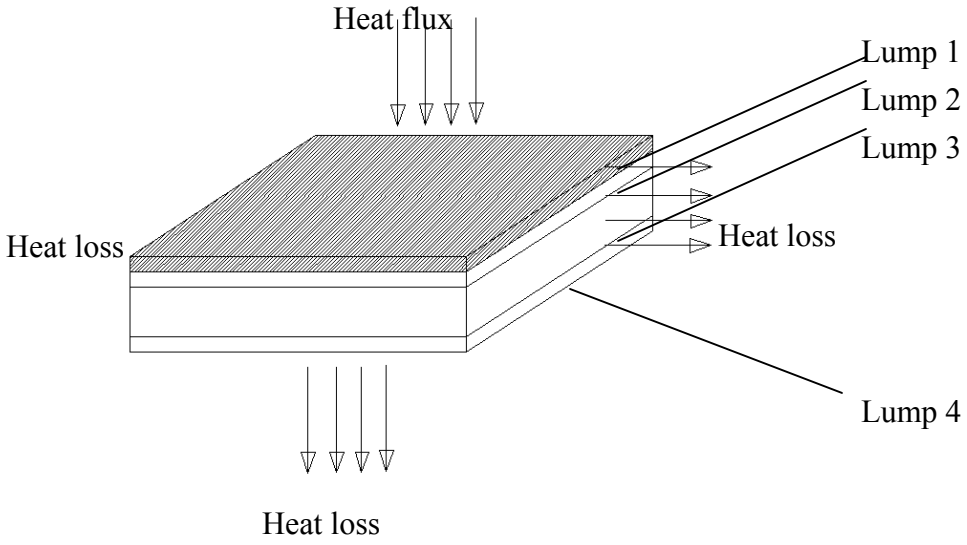

Figure: 3.5 (a) Heat distribution model for four lumps.

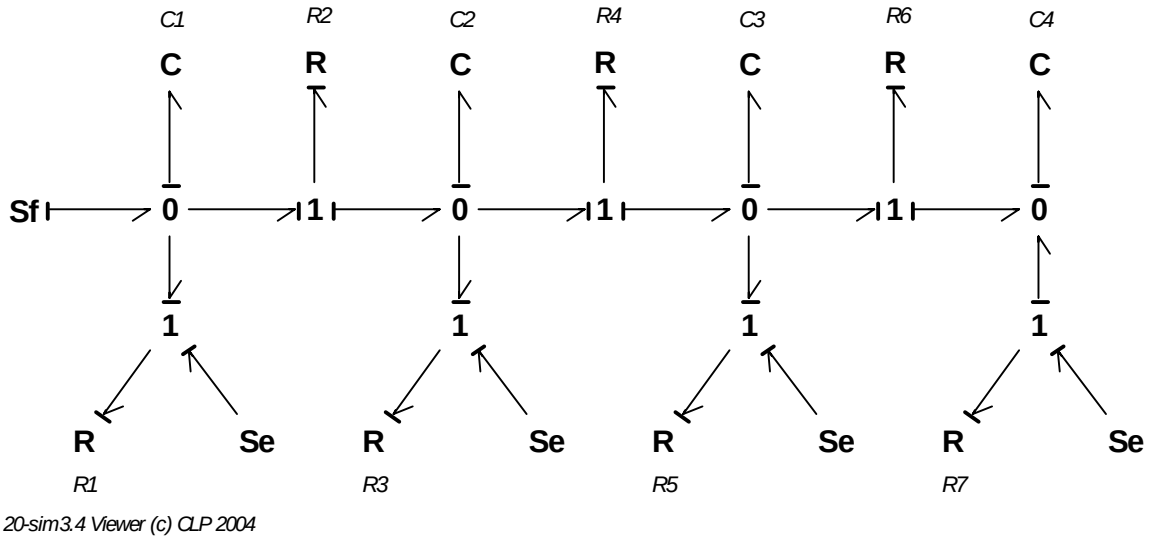

Figure. 3.5 (b): Pseudo bond graph model for the four lump heat distribution model.

The top plate, column, bottom plate, and an insulator were considered as different lumps. The dimensions of the lumps are shown in Table 3.2. The heat flux was applied on the top of the system. There was a heat loss to the atmosphere. Each of the lumps has resistance and capacitance. It is shown in schematic in the Figure 3.5 (a), with the equivalent bond graph in Figure 3.5 (b).

Table 3.3: Power input for different designs of micro GCs to achieve the ramp 25^{o}C/sec.

Chip size (cm^2)	Power Input (W)
1	23
1.5	34
2	45.5
4	90.5
8	180
12	270

Balancing heat flux at the four zero junctions, the equations at the four nodes can be written (Equation 3.5). A wide range of step inputs was applied to the four-lump model to find the power input that provides a ramp rate of 5^{o}C/sec, and 25^{o}C/sec. The power required to achieve a ramp of 5^{o}C/sec on microGC assembly (0.04 cm x 0.03 cm x 1890 μm) was calculated to be 100 W. Table 3.3 shows the modeling results, which indicate that to achieve the desired ramp rate (25^{o}C/sec), with a power input of less than 100W, the size of the GC should be around 4 cm^2 or smaller.

CHAPTER 4
HEATER DESIGN AND FABRICATION

4.1 Introduction

Temperature is one of the major parameters determining the time required for separation, sorbent selectivity, and spreading of chromatographic zones. By changing the temperature of a chromatographic column, it is possible to dramatically change the retention of the substances both in time and space on the sorbent layer [8].

Though commercially available gas chromatographs are equipped with reliable ovens, they still have some practical limitations. A conventional oven is relatively large and can be heated only. The Agilent GC (Model # HP5890 Agilent technologies Inc. Palo Alto, CA) uses an oven capable of programming at 10^{o}C/min. Cooling times are often not much faster. From a practical point of view, ovens are bulky, require large amounts of electrical power, and are not easily portable [17]. These limitations in temperature control can be reduced by the direct resistive heating of the column. Much less electrical power is required because only the column itself is heated. Cooling is fast when compared to the commercial gas chromatograph, because the column has a smaller thermal capacitance with a large surface area. The direct resistive heating of microGC columns offers additional advantages such as fast heating of the column [17]. It could also facilitate temperature control for thermal focusing, multidimensional gas chromatography, and the miniaturization of the gas chromatograph [17].

4.2 Device Requirements

The heater used for the micro gas chromatograph should follow the heating cycle of temperature programming shown in Figure 1.3. It should ramp the temperature of the gas chromatograph column to 350^{o}C in 66 seconds or less. The power required to achieve such a ramp was shown to be 100 W over an area of 12 cm^2, a power density of 8.33 W/cm^2, in the previous chapter.

4.3 Advantages of In Situ Heaters over Commercial Heaters

An extensive search was carried out for commercially available heaters that could provide the required power density (8.33 W/cm^2). “Thick Film on Quartz” from Watlow

Heaters (Hannibal, MO) provided a power density of 7.7 W/cm^2. Mica heaters from Minco (MINCO HM6800 R4.5L12T2, Minneapolis, MN) can provide a power density up to 17 W/cm^2, but they were made only in larger sizes than needed. The smallest size of mica heater was 38 mm x 77 mm, which was about four times the area (20 mm x 40 mm) of the microGC. Commercial heaters are expensive and typically have a thick electrical insulating layer, about 750μm (MINCO HM6800 R4.5L12T2, Minneapolis, MN), around the heater coil. Proposed in situ heaters for GC columns use a 500μm thick insulator around the heater coil, but have a potential of reducing thickness to 10 μm (polyimide), reducing the heat loss to the insulator, when compared to commercial heaters.

4.4 Review of Heaters Used for Gas Chromatographs

Jain and Phillips [17] showed that the fused–silica open tubular capillary columns can be heated by passing an electric current through a thin conductive film applied to the outer surface. Noh *et al* [16] used an embedded heating element in a parylene gas chromatograph. The heating element was a thin gold film evaporated on the corrugated surface of the parylene column, having a rectangular geometry. The silicon gas chromatograph from Sandia National Laboratories used tungsten, which was sputtered on the rear of the gas chromatograph, as a heating element [20].

4.5 In Situ Heaters

4.5.1 Material Selection

Different materials are used as resistance heaters. Nickel-chromium alloys are predominantly used as the heater material for commercial heaters, due to high resistivity and oxidation resistance. Gold, platinum and tungsten are also used as heaters. The comparison of thermal material properties is shown in Table 4.1. The Ni-Cr alloy was selected for its properties such as high resistivity, stability at high temperature, and the relative ease of electroplating, when compared to electroplating of other potential metals like platinum, and tungsten

Table4.1: Properties of metals for potential heaters [19]

	Ni-Cr (80-20)	Gold	Platinum	Tungsten
Electrical Resistivity (Ω-m*e-06)	1.08	0.022	0.106	0.0565
Heat Capacity (J/kg-K)	450	132.3	134	134
Thermal Conductivity (W/m-K)	13.4	301	69.1	163.3
Melting point (^{o}C)	1400	1064.43	1769	3370
Coefficient of Thermal Expansion (CTE) (µm/m-°C)	14	15.2	9.1	4.4
Density (kg/m^3)	8400	19320	21450	1930

4.5.2 Advantages and Limitations of Electroplating over Physical Vapor Deposition

Electroplating is a technology for depositing metals and alloys on conducting substrates. Compared to competing technologies, especially physical vapor deposition (PVD), it requires only relatively simple equipment, although some high throughput plating processes use highly sophisticated installations. Electroplating is well-suited for mass production such as high speed plating of steel sheets or barrel plating of small objects. Substrates of complex shape can be plated uniformly with electrolytes having a high throwing power. Contrary to coatings produced from the vapor phase, which are often porous, electrodeposits can be made dense, permitting their use for corrosion protection. A serious drawback of electroplating compared to PVD techniques is the need for careful and costly effluent treatment in order to abide with environmental regulations. Furthermore, process control in electroplating is sometimes delicate because of the use of

additives and/ or proprietary baths of unknown composition to the user. Even today, practical electroplating still relies much on empiricism, and there remains a gap between fundamental electrochemical research on metal deposition kinetics and industrial plating practice [18].

4.5.3 Electrodeposition of NiCr Alloys

4.5.3.1 Introduction

The major interest in developing electroplated nickel chromium alloys was based on the expectation that the electrodeposited alloys would display the same physical and mechanical properties as the metallurgically produced counterparts, as well as the excellent corrosion resistance of the thermally-prepared alloys, like 80-20 Ni-Cr. The early work suggested that significant quantities of nickel and iron are unlikely to be co-deposited with chromium from chromic acid based solutions. Better results were obtained with trivalent chromium solutions [28]. For example, nickel-chromium with compositions comparable to thermally prepared commercial alloys has been deposited from trivalent chromium–dimethylformamide electrolytes. Lashmore [21] described a pulse plating process for electrodepositing smooth, dense nickel alloys containing up to 20% chromium from aqueous trivalent solutions containing formic acid, sodium citrate, sodium bromide and ammonium chloride.

4.5.3.2 Experimental

4.5.3.2.1 Electrolytes Used

Three types of electrolytes, two aqueous baths and an amide bath were studied. The aqueous bath in Table 4.2 was adopted from Lin and Ho [22]. The chromium and sodium citrate concentration was increased by 0.1 moles in modified aqueous bath as shown in Table 4.3. The amide bath was adopted from Lashmore [21], is shown in Table 4.4.

Table. 4.2: Recipe for aqueous NiCr electroplating bath [20].

Chemical Name	Chemical Formulae	g/l
Chromium Chloride	$CrCl_3.6H_2O$	100
Nickel Chloride	$NiCl_2.6H_2O$	30
Ammonium Chloride	NH_4Cl	50
Boric Acid	H_3BO_3	30
Sodium Citrate	$C_3H_4(OH)(COONa)_3.2H_2O$	80
Formic Acid	HCOOH, 98%	35

Solvent: DI water.

Table.4.3: Recipe for modified aqueous Ni-Cr electroplating bath [20].

Chemical Name	Chemical Formulae	g/l
Chromium Chloride	$CrCl_3.6H_2O$	126.6
Nickel Chloride	$NiCl_2.6H_2O$	30
Ammonium Chloride	NH_4Cl	50
Boric Acid	H_3BO_3	30
Sodium Citrate	$C_3H_4(OH)(COONa)_3.2H_2O$	109.4
Formic Acid	HCOOH, 98%	35

Solvent: DI water.

Table.4.4: Recipe for amide Ni-Cr electroplating bath [21].

Chemical Name	Chemical Formulae	g/l
Chromium Chloride	$CrCl_3.6H_2O$	126.6
Nickel Chloride	$NiCl_2.6H_2O$	30
Ammonium Chloride	NH_4Cl	50
Boric Acid	H_3BO_3	30
Sodium Citrate	$C_3H_4(OH)(COONa)_3.2H_2O$	109.4
Formic Acid	HCOOH, 98%	35

Solvent: H_2O: Dimethyl ether formamide: CH_3OH (2:1:1)

4.5.3.2.2 Experimental Setup

High conductivity copper plates (Kocour, Chicago, IL) were used as cathodes for test plating. High-density graphite (Poco Graphite Inc., Decatur, TX) was used as an anode. The size of the cathode area exposed for deposition was 2.5 cm x 2.5 cm. Non-working areas were insulated with a non-conducting tape (Model # MD4000M Q250/ROLL, Harman Corp., Rochester, MI). Copper cathodes were prepared, by degreasing in acetone, then cleaning with isopropanol and deionized water. After preparation all cathodes were immediately transferred while wet to the plating cell. Graphite anodes were also degreased in acetone and cleaned with isopropanol and deionized water. The electrodeposition apparatus is shown in Figure 4.3. This contained a square thin walled polyethylene cell (20 cm x 20 cm x 20 cm) (Nalge Nunc Inc, Rochester, NY). To circulate the electrolyte the cell was fitted with outlets leading to a peristaltic pump (Pump Pro, Cincinnati, OH). The flow was from anode to cathode. The electrolyte was agitated using a mechanical stirrer (Model LR-400, Yamato Scientific America, San Francisco, CA).

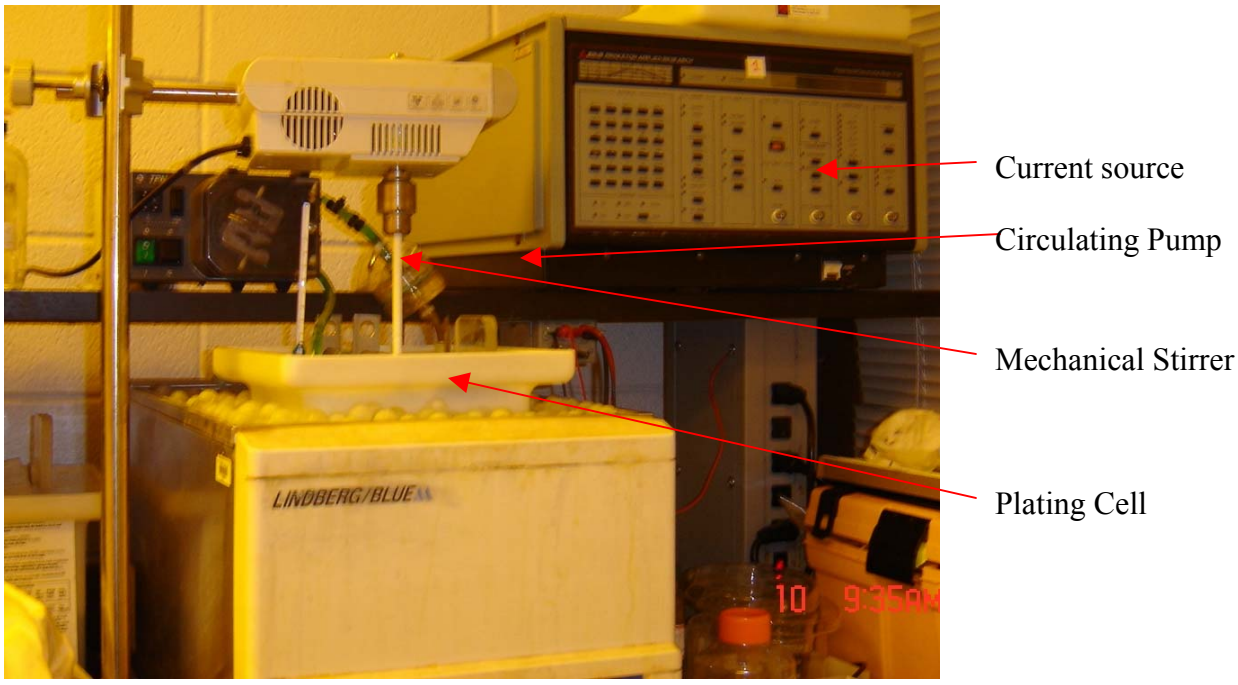

Figure 4.3: Electrodeposition apparatus.

A Princeton Applied Research 273A Potentiostat/Galvanostat (Princeton Applied Research, Oak Ridge, TN) was used as a current source for electrodeposition. Composition of the deposits on the cylinders was obtained using Kevex Omicron X-ray Fluorescence Spectroscope.

Kevex Omicron uses the energy-dispersive x-ray spectrometry (EDS) analytical method to analyze the elements. When an atom is bombarded with high energy X-rays, inner shell electrons may be removed from their atomic shell that results in the filling up of that vacancy by an electron from an outer shell. Each transformation results in the loss of a specific amount of energy, namely the difference in energy between the vacant shell and the shell contributing the electron. This energy, which uniquely identifies the element from which it came, is given up in the form of electromagnetic radiation X-rays. The X-rays are named after the type of the transition involved. The Omicron spectrometer uses an X-ray source to generate X-rays from the sample, which is detected by a detector. The X-ray source consists of an electron gun and a target sealed inside a vacuum envelope. X-rays are generated by bombarding a target with either charged particles (electrons or alpha particles) or high-energy photons (X-rays or gamma rays). These emitted X-rays are characteristic of the elements present because of the physical properties of atomic structure. The target is maintained at a high voltage with respect to the electron gun, such that the electron beam generated from the filament is accelerated toward it. The detector absorbs X-rays emitted from the sample and then acts as an energy to charge transducer quickly passing information to an amplifier and multichannel analyzer. The detected X-rays are digitized and sorted and presented as a spectrum, which is plotted from raw X-ray data in counts vs. energy format. These counts are calibrated with known standards so that the composition of the alloy can be determined.

4.5.3.3 Plating parameters

The major problems in nickel chromium electroplating were cracking and failure of sustained deposition. The reason for the failure of sustained deposition was the precipitation of basic chromium compounds caused by the slow build up of high pH in the vicinity of the cathode. To control cracking and to get uniform deposition, high stirring rates and continuous circulation of the electrolyte were required [21].

A series of experiments were conducted to determine the correct plating conditions for NiCr (80-20) on copper. These conditions were pH of the solution, the bath composition, operating procedure, plating temperature. The initial experiments were done using the aqueous bath shown in Table 4.2. The solvent was DI water and the pH of the solution was 2.2.

A Hull cell (Kocour Company, Chicago, IL) was used to see the effect of current distribution. The Hull cell gives varying current density on a single test piece. The highest current density applied in the Hull cell was 0.05 A/cm^2. The results from the Hull cell showed that a maximum chromium percentage of 1% was obtained at 0.02 A/cm^2 for the bath showed in Table 4.2. The temperature effects on chromium percentage were studied. The chromium percentage increased as the temperature was decreased. The temperature of the plating bath was decreased by placing ice around the Hull cell. The maximum percentage of chromium of 11.29% was obtained at around 6^oC for the bath showed in Table 4.2.

The chromium and sodium citrate salts were increased by 0.1 moles in the new bath as shown in Table 4.3. The temperature of the plating bath was kept at around 6^oC. Galvanostatic plating was carried out with a current density of 0.02 A/dm^2. The highest chromium percentage of 21.2% obtained.

Even though the desired chromium percentage (20%) was obtained the problem of cracking was not solved. For deposition times greater than 20 to 30 minutes a rapid deterioration of deposit quality was observed. The deposits became black in appearance with an eventual loss of metallic character and adhesion. In both cases the deposition was characterized by an initial rise in chromium content during first 20 min followed by a rapid fall. Conventional constant current technique yielded only thin coatings, in general suitable only for the decorative use. It was found that the potential of the working cathode with respect to a reference electrode drifted continuously to lower potentials. The decrease in potential after 20 to 30 minutes reached values at which high levels of Chromium-II are formed leading to a rapid detererioration of the deposit quality [21]. One of the solutions for this problem may be the pulsing of current.

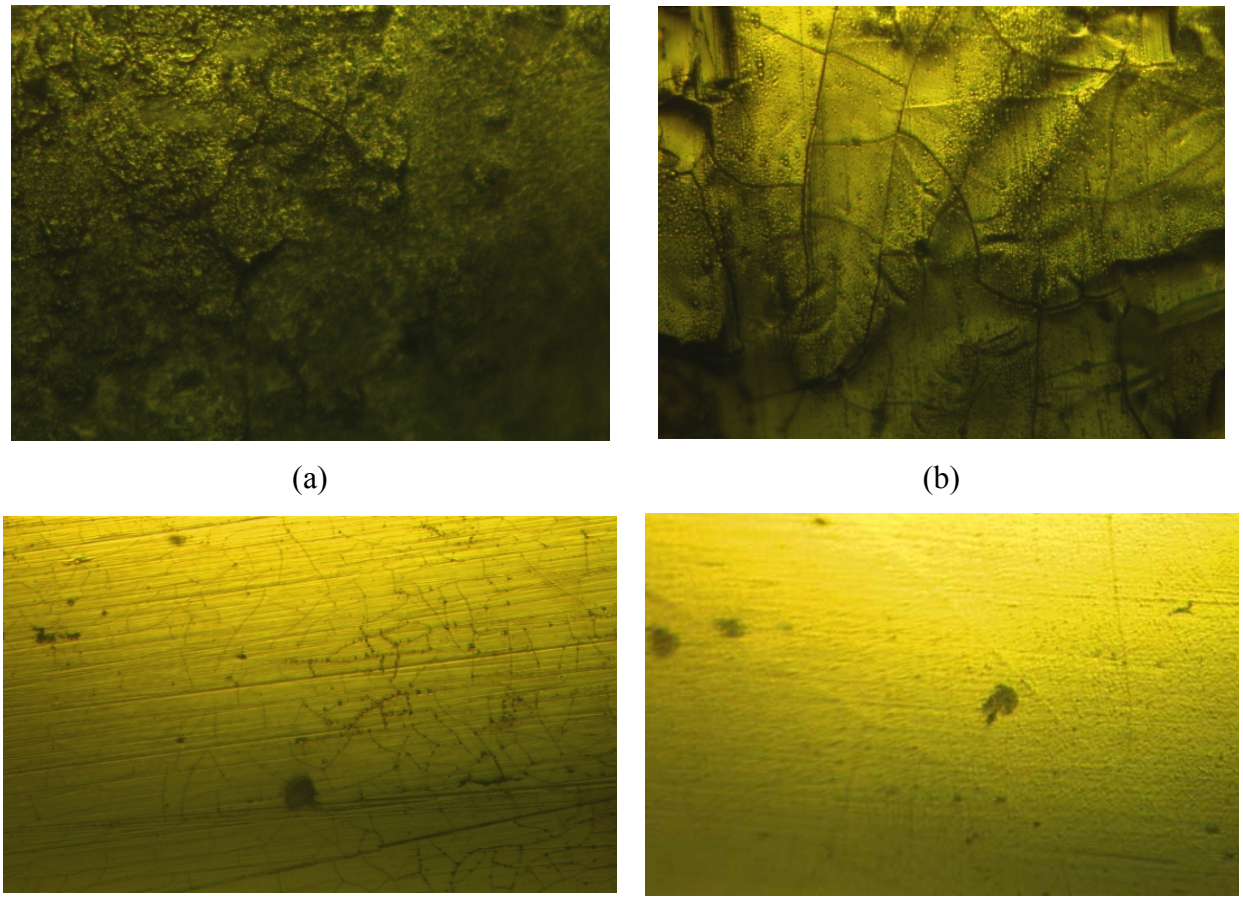

(a) (b)

(c) (d)

Figure 4.4(a): Optical picture of the NiCr (99-1) deposited from bath in Table 4.2 by galvanostatic plating with current density of 0.02 A/cm^2 (rough plating can be observed).

(b): Optical picture of the NiCr (80-20) deposited from bath in Table 4.3 by galvanostatic plating with current density of 0.05 A/cm^2.

(c): Optical picture of the NiCr (90-10) deposited from bath Table 4.4 by galvanostatic pulsing with pulse current density of 0.05 A/cm^2, 'on' time of 166 ms and 'off' time 100 ms.

(d): Optical picture of the NiCr (97.5-2.5) deposited from bath Table 4.4 by galvanostatic pulsing with pulse current density of 0.05 A/cm^2, 'on' time of 100 ms and off time 'off' 100 ms.

When there was a constant current supply there was decrease in potential, but the pulse shuts off current before the potential reaches a low value. During pulsing the hydrogen was liberated during off time, reducing the cracking of chromium. The plating was carried out at room temperature (22^{o}C). Lung and Ho suggested an amide bath with pulse plating (5ms 'on' and 3ms 'off') for smooth electroplating of a NiCr alloy without cracks. The recipe for the amide bath is shown in Table 4.4. The equipment used for pulsing, Princeton Applied Research 273A Potentiostat/Galvanostat (Princeton Applied Research, Oak Ridge, TN) was able to provide pulsing for times only greater than 100 ms. The same ratio of on and off times were used. The maximum chromium of 15.6% was achieved at a pulse of 166ms on and 100 ms off. The significant achievement in this process was the reduction of cracking as shown in Figure 4.4. There was much less cracking when compared to the constant current process and thick layers of 5 μm were deposited with minimal cracking. Even though the plating rate was low (1.0 μm/hr) there was much less cracking. The 'off' time in pulsing was increased to 50% so that there would be more time for hydrogen relief. Pulsing with 100 ms 'on' and 100 ms 'off' with current density 0.05 A/cm^2 yielded a chromium composition of 10% with minimal cracking. As shown in Figure 4.4 (d), pulsing with 100 ms on and 100 ms off with current density 0.02 A/cm^2 yielded a chromium composition of 2.5% without any cracking.

4.6 Design of Final Heaters

The objective of this work was two-fold:

1) To design a heater which produced uniform ($\pm$ 5^{o}C) temperature on the microGC;
2) To design a heater which produced a linear temperature gradient across the length of the microGC.

Different designs were simulated for temperature distribution, using a commercial finite element analysis package (ANSYS vs.8.0, Canonsburg, PA). The heater design shown in Figure 4.5 gave a nearly uniform temperature distribution on the microGC. As shown in Figure 4.5, the heater was placed on a 500 μm thick silicon substrate. Three nickel plates (0.04m x 0.03m x 1000 μm) thick were used to mimic the

microGC. A heat generation of 100 W was applied to heater coil. Natural convection boundary conditions were applied to all areas of the assembly.

The isometric view of the steady-state analysis is shown in Figures 4.6. The temperature profile and the paths on the bottom of microGC, opposite the heater side, are shown in Figure 4.7(a). The temperature profile along the length of the paths is shown in 4.7(b). The results show that there was a 5^{o}C range on the bottom of microGC.

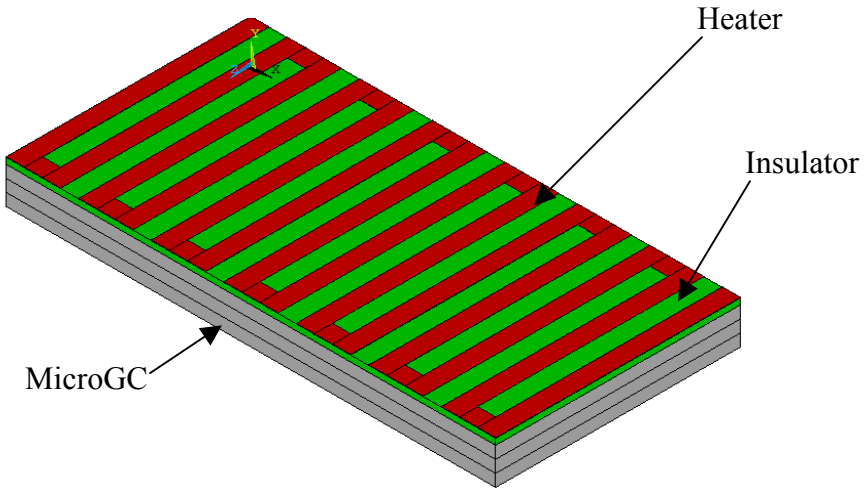

Figure 4.5: Schematic of final uniform heat flux heater assembly.

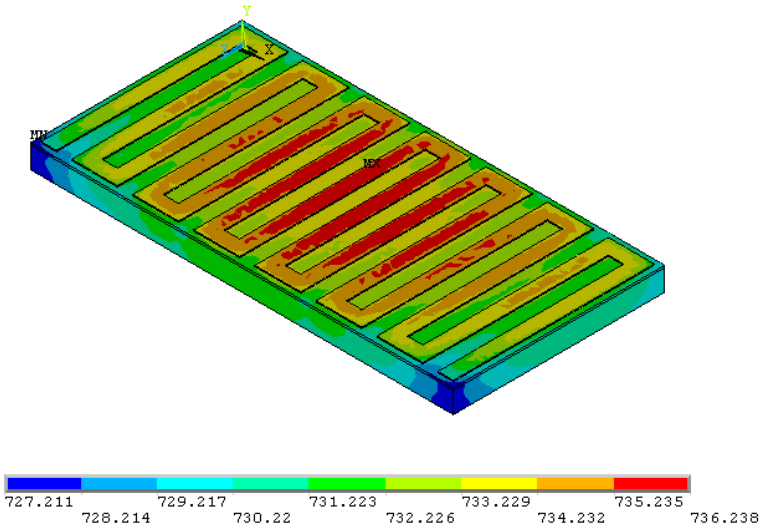

Figure 4.6: ANSYS simulated temperature contour plot showing the temperature distribution (in kelvin) on the microGC in an isometric view.

Alternative designs for heaters were simulated for the temperature distribution, to fulfill the second objective, to achieve a linear temperature gradient along the length of the column. The heater design shown in Figure 4.8 gave a nearly linear temperature gradient on the microGC. As shown in Figure 4.8, the heater was placed on a 500 µm thick silicon substrate. Three nickel plates (0.04 m x 0.03 m x 1000 µm) thick were used to mimic microGC. A heat generation of 100W was applied to model the heater coil. A natural convection boundary condition was applied to all areas of the assembly. The results of the steady-state analysis are shown in Figure 4.9 (a)-(b). The results show that the temperature is of the microGC is more where the gap between the heater elements is less. The temperature difference along the length of the microGC is 45^{o}C as shown in Figure 4.10 (b). The temperature gradient was near to linear distribution. The dimensions for the final mask patterns were adopted from the ANSYS simulations shown in Figures 4.6, and 4.8.

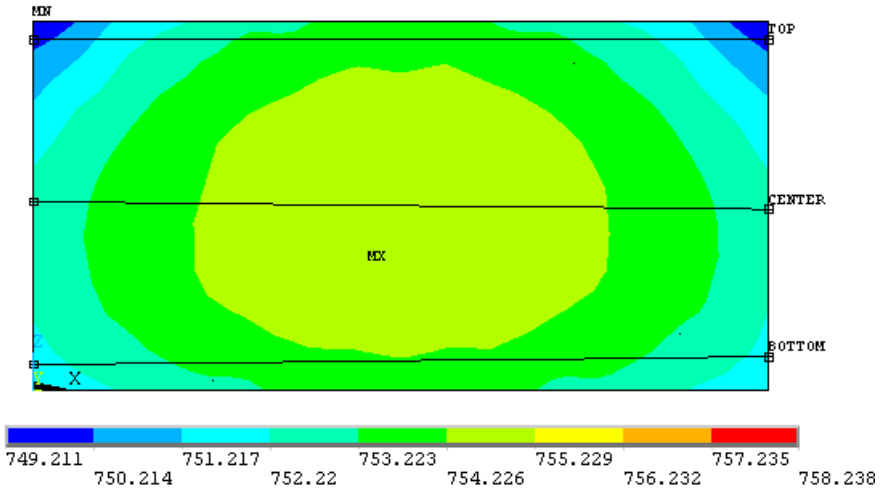

Figure 4.7(a): Temperature contour plot showing the temperature distribution (in kelvin) on the bottom of microGC.

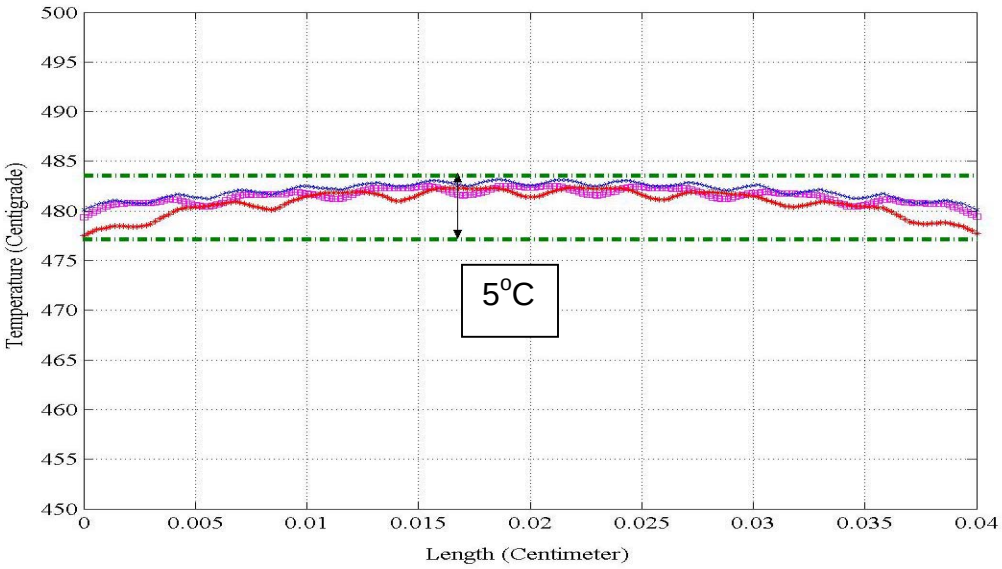

Figure 4.7(b): Temperature profile along the length of paths shown in Figure 4.7 (a).

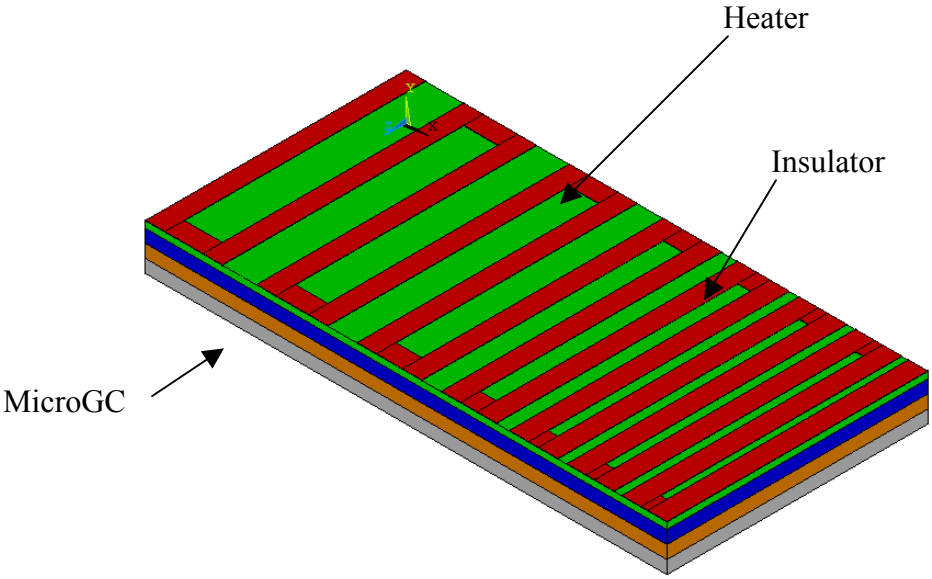

Figure 4.8: Schematic of final heater (linear heat flux) assembly.

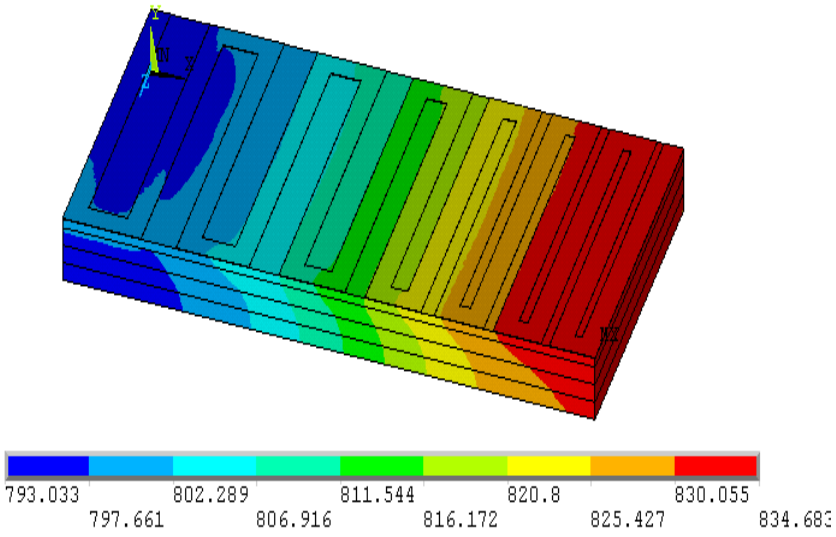

Figure 4.9(a): ANSYS simulated temperature contour plot showing the temperature distribution (in kelvin) on the microGC in an isometric view.

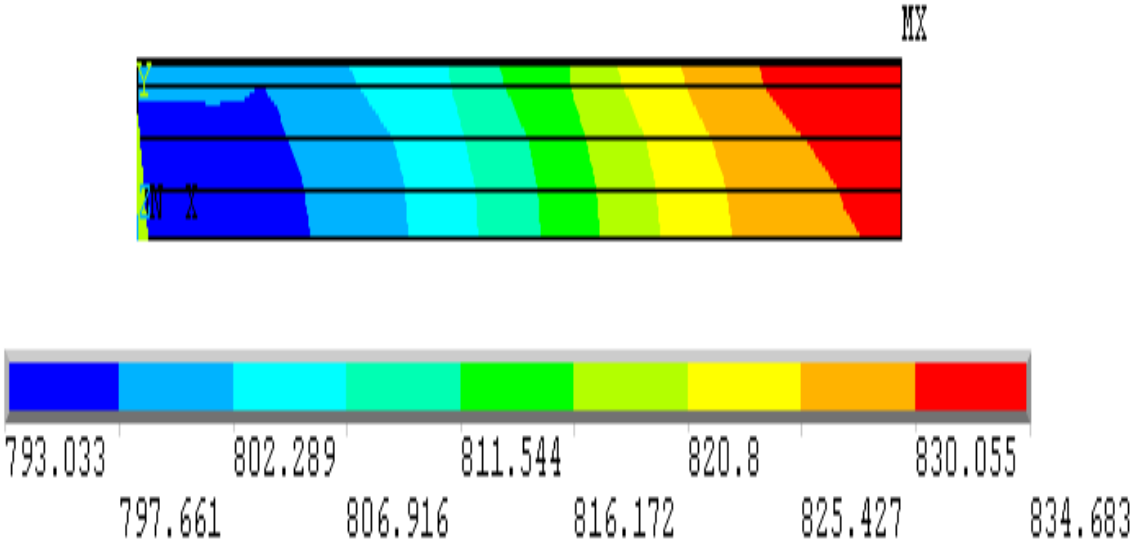

Figure 4.9(b): ANSYS simulated temperature contour plot showing the temperature distribution (in kelvin) on the microGC in front view.

4.6.1 Composition of NiCr for Final Heaters

The power supplied by the heater varies with the voltage supplied and the resistance of the heater. The relation is given by the joule's heating equation.

$$P = \frac{V^2}{R} \qquad 4.1$$

The power supply for micro gas chromatograph has limitation of voltage supply of 12 volts and 24 volts. The Figure 4.11 shows the variation of resistance for different power outputs for 12 volts and 24 volts. The resistances required for a power of 100 W were 5.76 Ω and 1.44 Ω for 24 volts for 12 volts power supplies, respectively. The width of the heater element from the ANSYS simulation was 1.481 mm and the length of the heater element was 21 cm.

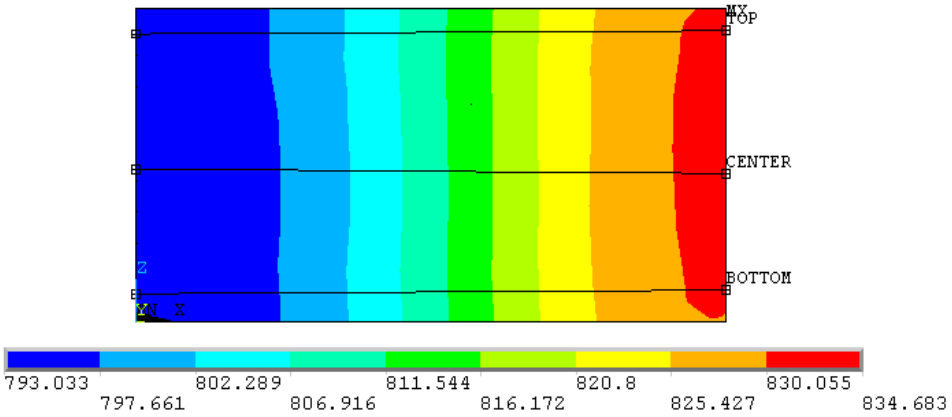

Figure 4.10(a): Temperature contour plot showing the temperature distribution on the bottom of the microGC (opposite side of heating element).

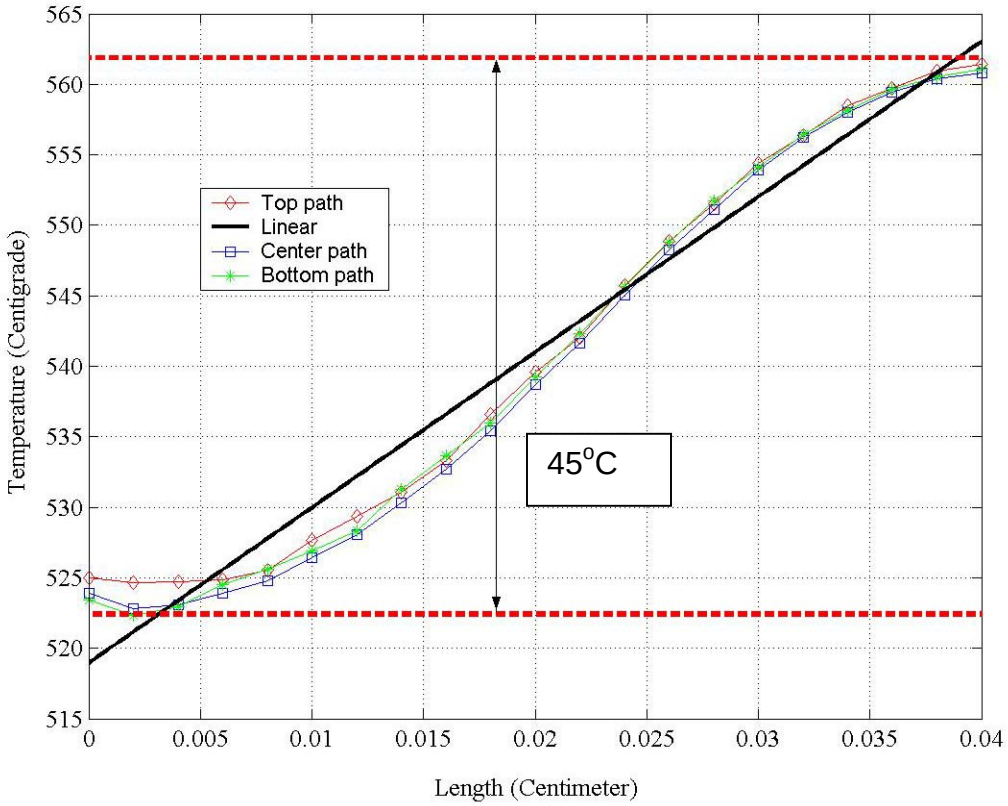

Figure 4.10 (b): Temperature profile along the paths.

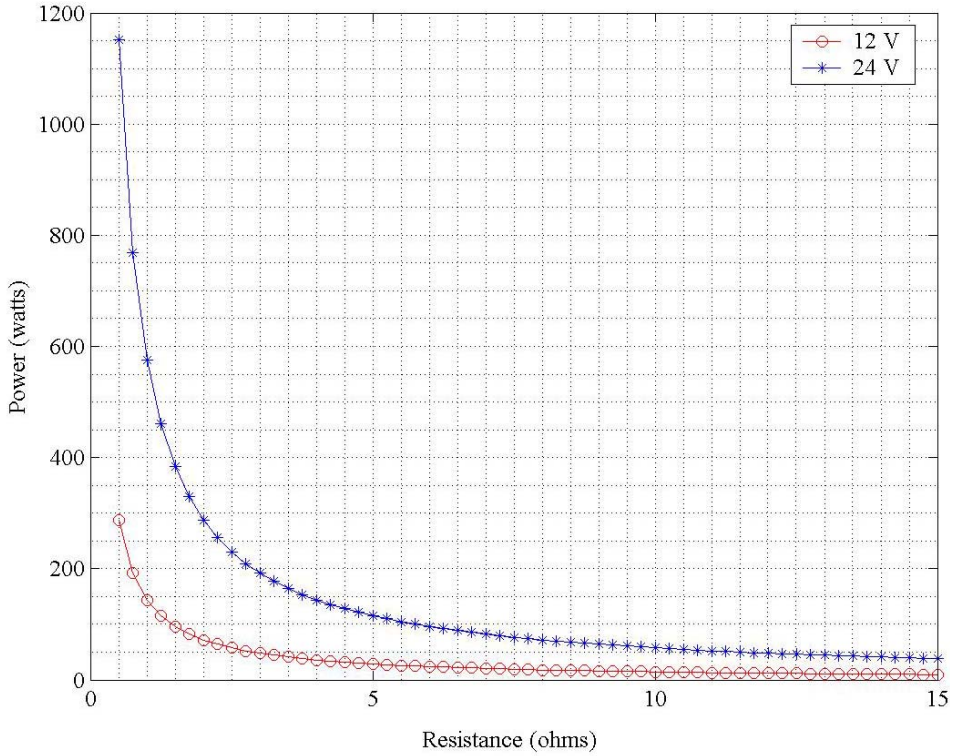

Figure 4.11: Variation of power with resistance.

The variation of resistivity of NiCr alloy with chromium composition was given in Figure 4.11. Based on equation 4.2 the thickness of the NiCr alloy to be deposited could be decided.

$$t = \frac{\rho L}{w * R} \qquad 4.2$$

Where,

R= Resistance of the electroplated metal;
L= Length of the heater element;
T= Thickness of the heater element;
W= width of the heater element;
ρ= Resistivity of the heater element.

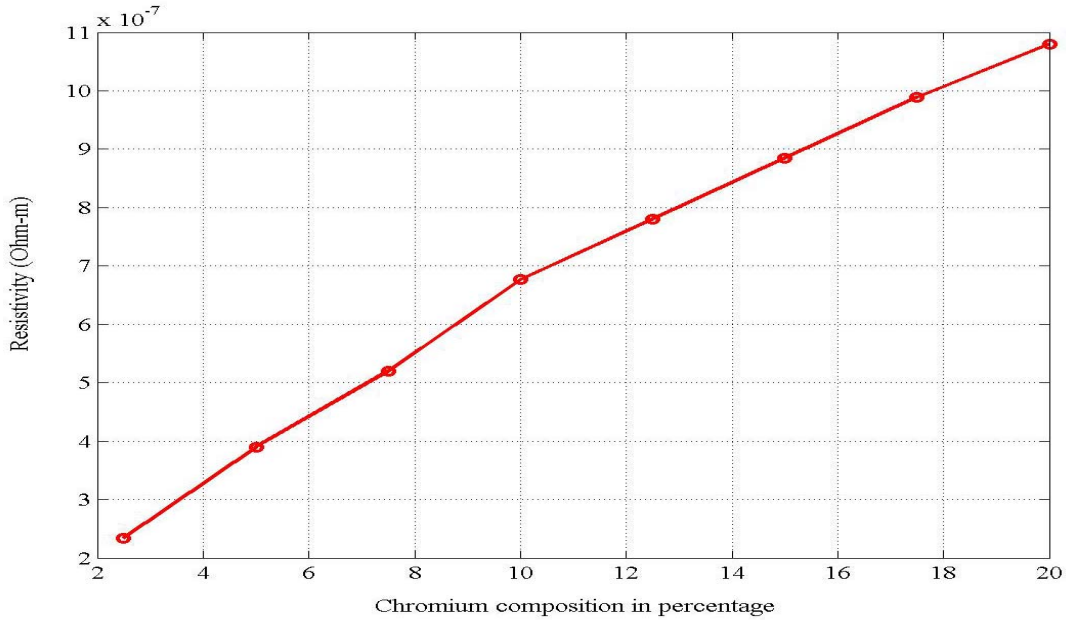

Figure 4.12: Variation of resistivity with Cr composition [18].

The thickness for different compositions of chromium percentage is given in Figure 4.13. The plating experiments showed that the thickness cannot be achieved as shown in Figure 4.13 except for chromium composition 2.5%, where the thickness required for the composition was only 5.76µm.

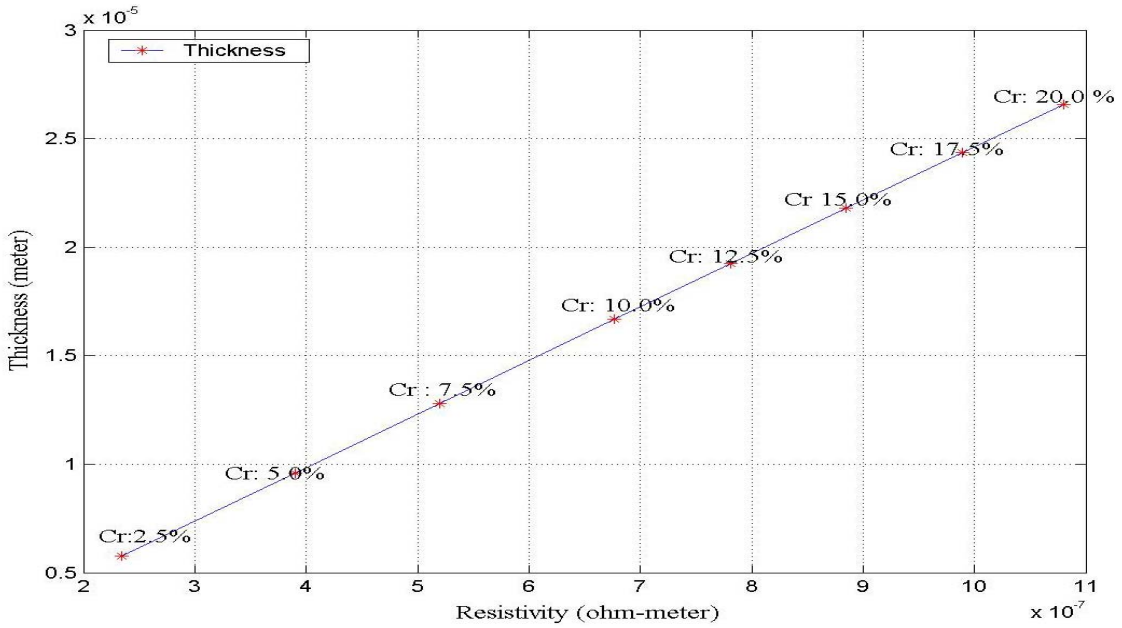

Figure 4.13: Variation of thickness with Cr composition.

4.7. Fabrication

4.7.1. Optical Lithography

Optical lithography is the first step in LIGA, where the design is transferred from paper to a physical entity in the form of an optical mask. The optical mask consists of a radiation-absorbing component laid out in a pattern based upon the device design. For ultraviolet (UV) light based optical lithography, 300 Å of chromium forms the radiation-absorbing region. Dark field regions on the mask are covered with chrome and block the UV light. Clear field regions allow the UV light to pass through and modify the photoresist. The light either polymerizes a negative resist into chains or causes molecular scissions in a positive resist. The masks where dark field regions define the pattern are called dark field masks, while those where the clear areas define the pattern are called clear field masks. Dark field and clear field masks for the same pattern have chrome on complimentary areas and are in "opposite tone" to each other [33].

4.7.2 Optical Mask Design

An optical lithography mask pattern of test micro heaters was laid out using AutoCAD 2004 (AutoDesk, San Rafael, CA). The dimensions of the pattern are shown in Figure 4.14 and the mask with three identical patterns, so that three heaters could be made in a single wafer, is shown in Figure 4.15. The dimensions of the test heater mask are chosen so that the heater element fits in the area of the test microGC. The minimum size feature on the mask was 1789 μm, which was the heating element width, and the straight heating element length was 1.0 cm. The AutoCAD drawing was saved in the .dxf file format, which was then converted to the .gds file format using DXF2GDS® (DFX, Artwork Conversion, Santa Cruz, CA) conversion software and viewed using the GDSVUE® software. After doing these conversions, both the dark and clear field images of the mask were assessed for errors. After the assessment, the industry standard chrome on soda lime glass, 0.09" thick and 5" on each side, (5" by 5"), optical masks were purchased from Advance Reproductions (North Andover, MA). The microGC and in-situ heater assembly are shown in Figure 4.16.

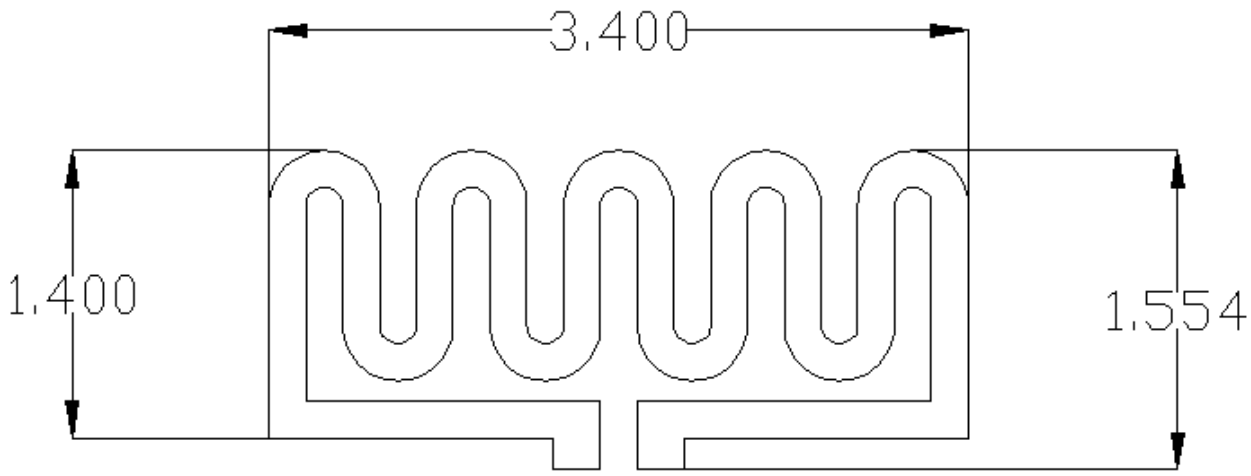

Figure 4.14: Optical mask pattern for the test heater.

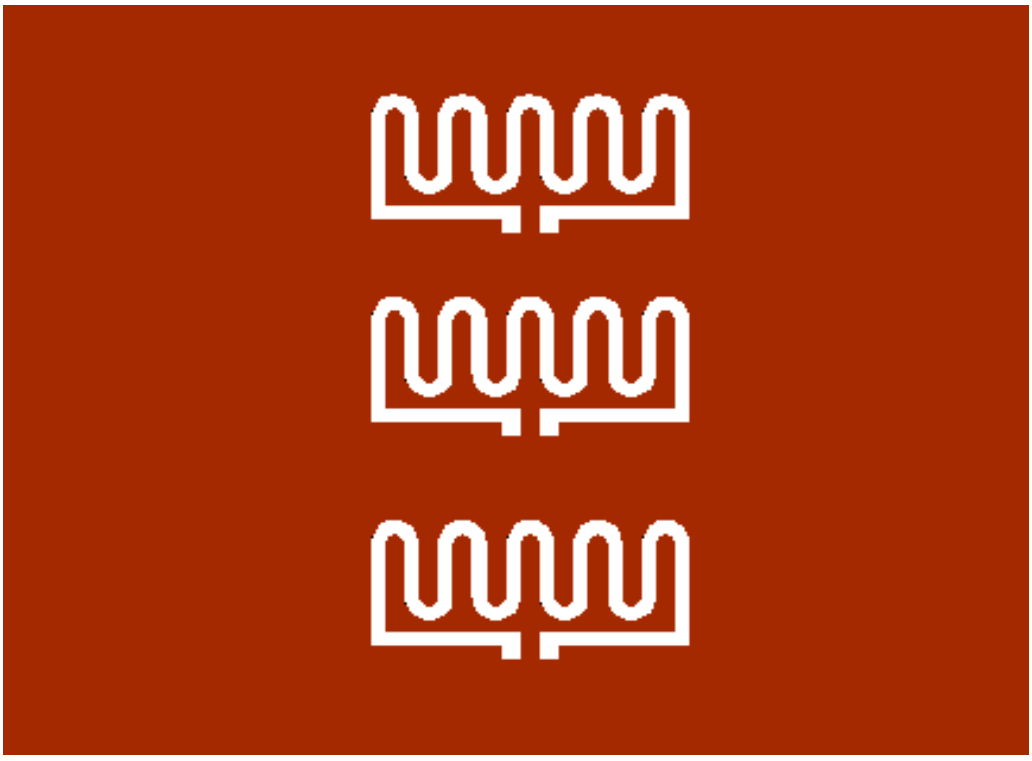

Figure.4.15: Optical mask for the test heater.

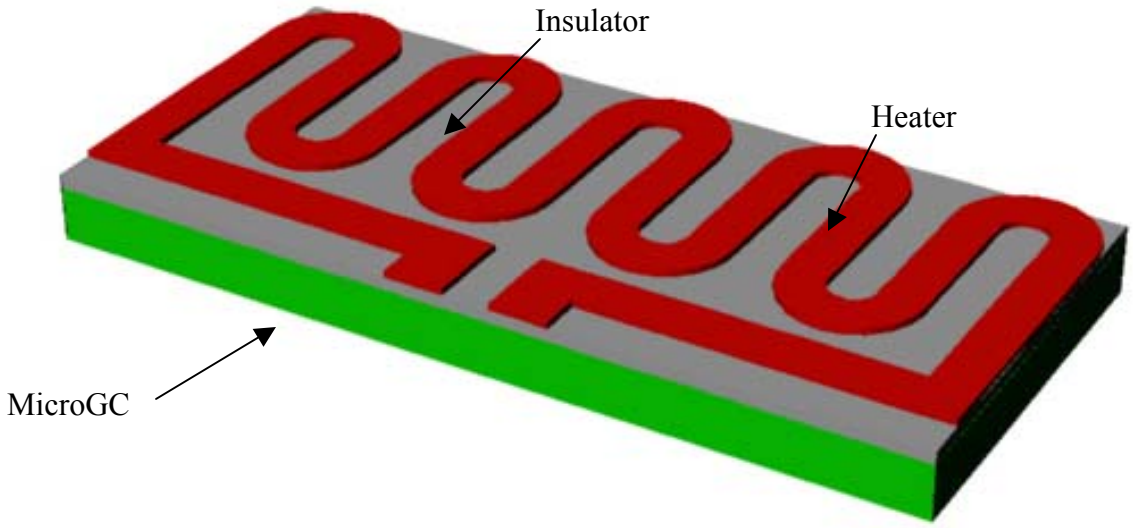

Figure.4.16: MicroGC and in situ heater assembly.

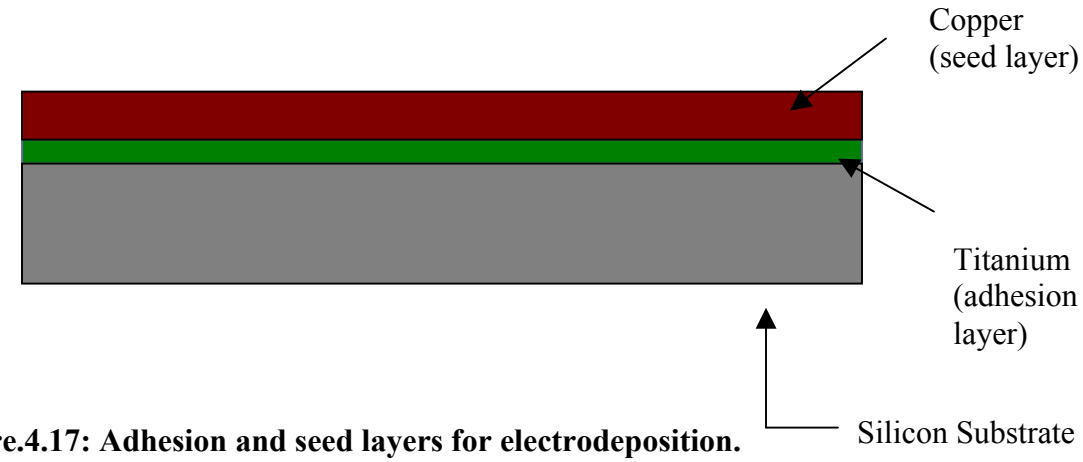

Figure.4.17: Adhesion and seed layers for electrodeposition.

4.7.3 Substrate Preparation

Silicon wafers (University Wafer, Boston, MA), 500 μm thick, were used as substrates for the test heaters. Sputtering of adhesion and seed layer was done at Center for Advanced Microstructures and Devices (CAMD). Titanium was used as an adhesion layer with, while copper was used as seed layer. The recommended thickness for adhesion and seed layers was 1000 Å and 3000 Å respectively [43].

4.7.4. Spin Coating and Pre-Bake of Resist

The silicon substrate with the titanium and copper seed layer was placed on a spin coating machine, and fixed into place using a vacuum chuck. Approximately 15 ml of AZ 4640 (MicroChem Corp., Newton, MA) positive photoresist was placed on the wafer and spun at 1500 rpm for 40 seconds to give an uniform coat of resist. A thickness of 10 μm of resist was obtained. The resist was pre-baked in a convection oven at a temperature of 100^{o}C for 30 minutes. After 30 minutes the substrate was cooled to room temperature in the oven for 50 minutes. The substrates were left at room temperature for 24 hours for stress relief.

4.7.5 UV Exposure and Development of Resist

The AZ 4620 resist coated wafers were exposed to ultraviolet light through the optical mask. The wafers were exposed to 500 mJ/cm^2 of UV light for 55 seconds, which was the required energy for exposing a 10μm thick AZ4620 resist. The patterned wafer was developed in 20% AZ 400K Developer (MicroChem Corp., Newton, MA) for 3 to 4 minutes, moving back and forth from a cleaning bath to a rinse with DI water. The appearance of a red residue indicated incomplete development of the resist. Examples of incompletely developed resist and developed resist are shown in Figure 4.18.(a) and 4.18.(b), respectively. Whenever there was any red residue, the wafers were reimmersed in the developing solution for few more seconds. After complete development they were rinsed and dried with compressed air.

4.7.6 Electroplating

Electroplating was done as explained in section 4.5.2 with pulsing parameters of 100 ms on and 100 ms off. The current density applied was 0.02 A/cm^2 Plating was done at room temperature with pH 2.2 for 6 hours with plating rate of 1 μm/hr. The chromium content in NiCr alloy was 2.5%.

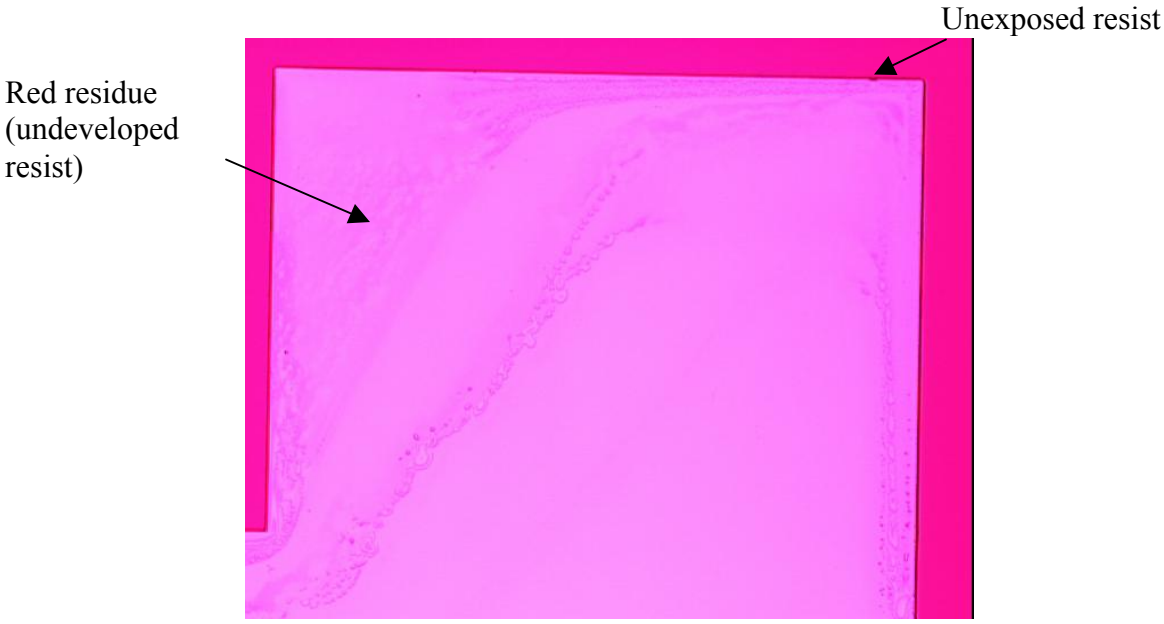

Figure 4.18: (a). Undeveloped resist

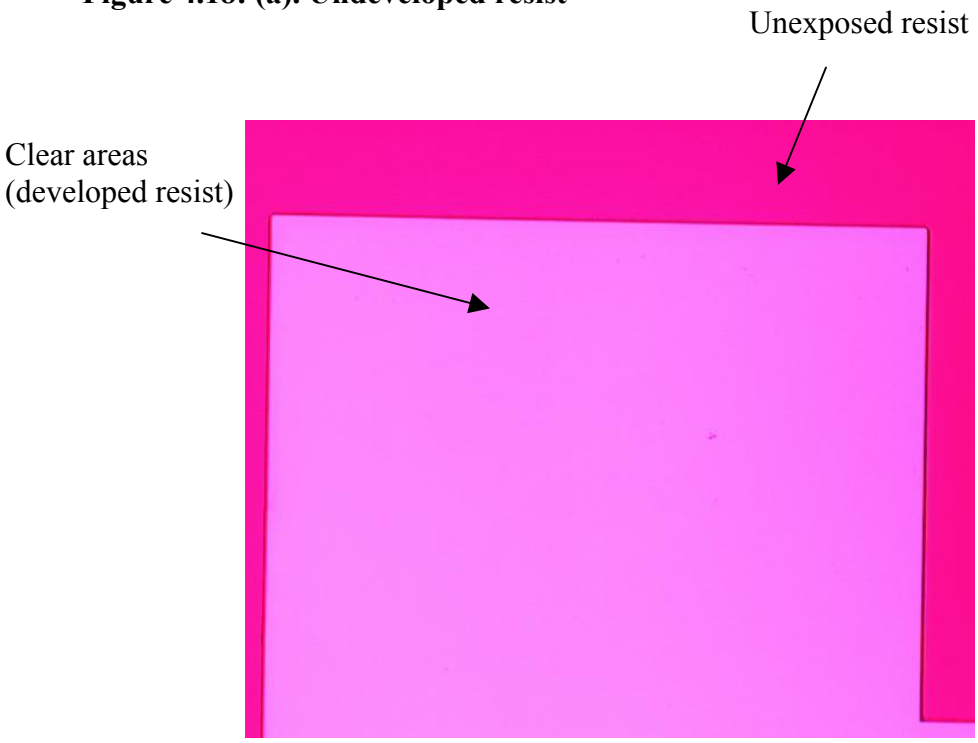

Figure 4.18. (b). Developed Resist.

4.7.7 Copper Etching

Table 4.5: Recipe for copper etchant.

Chemical	Weight in grams/liter of water
Sodium Chlorite	16
Ammonium Bicarbonate	32

The seed layer was etched after electroplating of the NiCr on the silicon substrate. The recipe for copper etchant is shown in Table 4.5. The etch rate was 10 Å/sec. The etching was carried over for 5 minutes and no significant undercutting was observed.

4.7.8 Titanium Etching

Hydrofluoric acid (5%) was used to etch the titanium layer. The etch rate was about 500 Å/sec. The reaction was exothermic and extreme care should be taken when working with hydrofluoric acid. The etch time was 5 seconds.

4.7.9 Electric Connections

Ohmex-AG (Transene Inc., Danvers, MA) thermosetting silver solder was used to make the electrical connections for the heater. Ohmex-Ag is a conductive silver preparation containing silver epoxide as a bonding constituent.

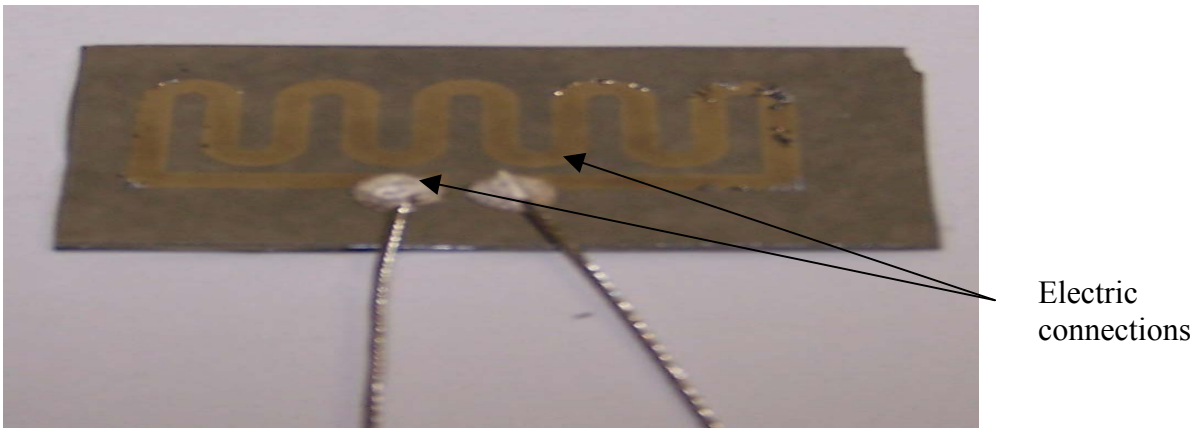

Figure.4.19: Electric connections to test heater.

It is in the form of thin paste. Ohmex-AG is a one-part system with high bond strength, low contact resistance, and low impedance. The copper wires were placed on the Ni-Cr structure on the substrate and Ohmex-AG was applied to the joint. The substrate was then placed in a convection oven at 150°C-160°C for 15 hours or one hour at 150°C, followed by 265°C for one hour. The substrate is then cooled in room temperature for 30 minutes. Figure 4.19 shows the electric connections of the test heater.

4.7.10.Resistance of Electroplated NiCr Alloy

The resistance of the heater was 6.2Ω measured using a multimeter. The resistivity of heater was estimated using Equation 4.3.

$$R = \frac{\rho L}{A} \qquad 4.3$$

where:

R = Resistance of the element (Ω)

ρ = Resistivity of the metal (Ω-m)

L = Length of the element (m)

A = Cross-sectional area (m^2)

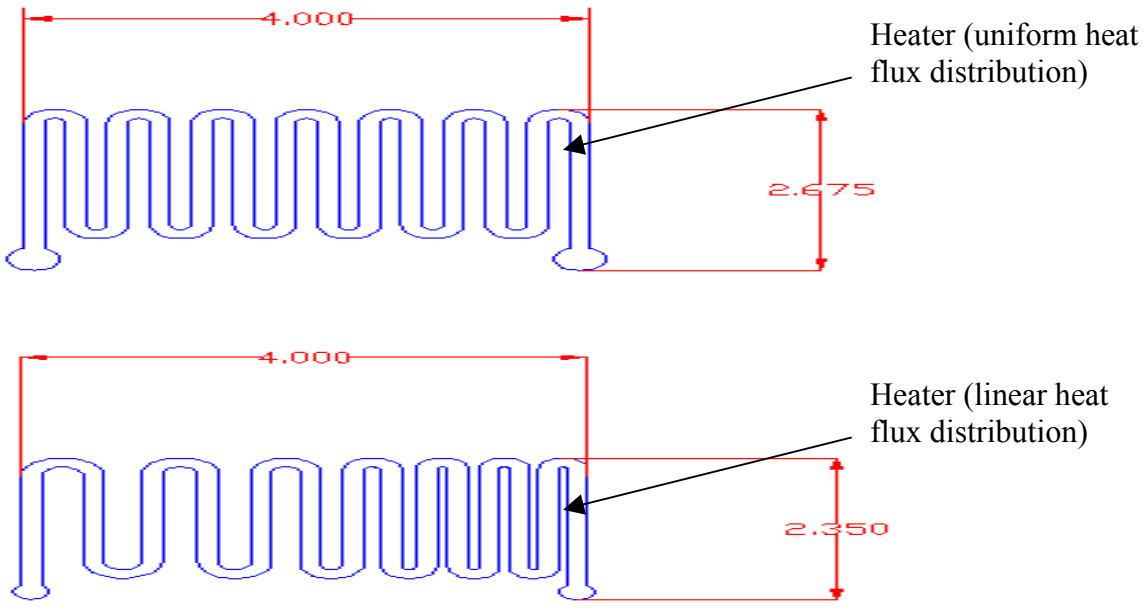

Figure 4.20: Dimensions of heaters (in cm).

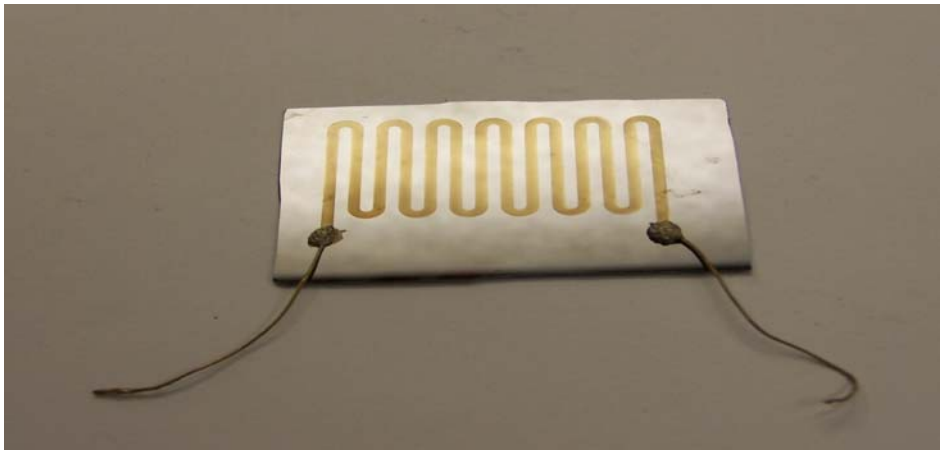

Figure.4.21: Heater with equidistant coils (uniform heat flux).

The resistivity of the electrodeposited metal was 22.64xe-08 Ω-m. The predicted resistivity was 22.924xe-08 Ω-m. The dimensions of the masks are shown in Figure 4.20. The minimum feature size of the mask was 1.481 mm, which was the width of the heater element and the maximum dimension was 1.6285 cm.

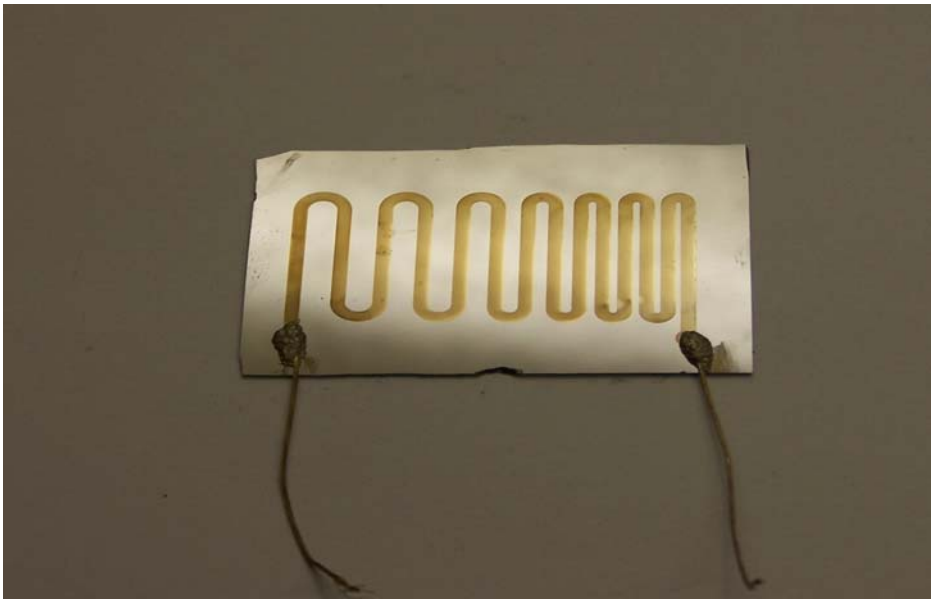

Figure.4.22: Heater with concentrated coils in one end (linear heat flux).

Figures 4.21 and 4.22 show the figures of microfabricated heaters for two designs discussed in previous section. The resistivity of the microfabricated heater is 22.64xe-08 Ω-m. The percentage of chromium in electroplated NiCr alloy heater was 2.5%.

4.8. Summary

NiCr alloy with maximum chromium composition upto 20% can be electroplated. The electrolytes for NiCr alloy plating for various chromium compositions were developed. The detailed description of experimental procedure and plating parameters were presented. The composition of chromium can be varied with change in electrolyte, and pulse parameters. Heaters, which gave uniform temperature, and linear temperature gradient, were designed and fabricated using microfabrication techniques. The development of final heater design was explained in the Appendix Heater Design. Silicon was used as a substrate, as established procedures were available for microfabrication. More study is required on the selection of substrate for heater.

CHAPTER 5
CONTROL SYSTEM

5.1. Introduction

The control system plays an important role in executing the temperature programming cycle for a gas chromatograph. Control systems are broadly classified into two categories, open loop and closed loop systems [10]. In an open loop system, as shown in Figure 5.1(a), a command is applied to the controller to generate the actuating, or the manipulating signal. There is no comparison between the actual output of the system, or controlled variable, and the desired output variable of the system.

The desired output for a given input is normally determined by calibration. The actual output obtained depends on the validity of the calibration. If the components of the system are affected by temperature, wear, or humidity, the actual output may vary from the expected output. In addition, the performance of such a system is affected by the variations of the load, external disturbances and inaccuracies in the mathematical models. The primary advantage of using open loop control is that it is simple and less expensive than the closed loop control system. In a closed loop control system or feedback control system, the output is continuously compared with the input (reference) and the difference between the two signals (error) is used as input to the controller. Figure 5.2 shows a block diagram of such a control system. Since the controller is actuated by the error signal, it will tend to drive the process to produce an output that will result in a smaller error. By the selection of the appropriate type of control law, it is possible to devise a closed loop control system that will meet given specifications [10].

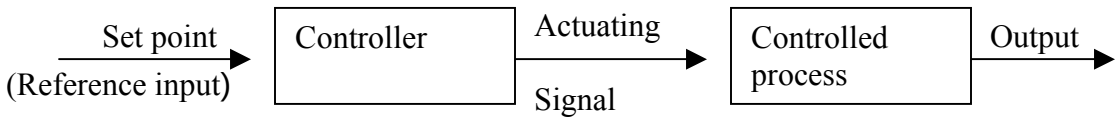

Figure 5.1: Open loop control system.

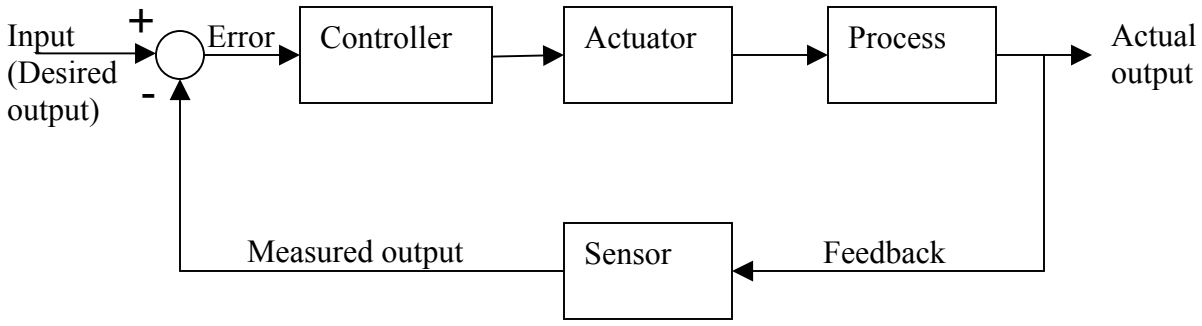

Figure 5.2: Example of a feed back control system (closed loop control system).

The algorithms used in a particular controller depend on factors such as:

1) Accuracy required;
2) Speed of response;
3) Type of the process.

For the temperature programming of the microGC a proportional plus integral plus derivative (PID) controller was selected due to its simplicity, robustness, and ease of implementation.

5.2 Controller

The temperature of the fluid in the GC column was the output of the system. To follow the desired temperature profile for temperature programming of the microGC, without operator interference, a temperature control system relies upon a controller, which accepts a temperature sensor such as a thermocouple as an input. It compares the measured temperature to the desired reference temperature, or setpoint, and provides an output to a control element. The controller is one part of the entire control system, and the whole system should be analyzed in selecting the proper controller.

5.2.1 PID Control Parameters

A PID controller uses a combination of three gains to modify the output of a system, K_P, K_I and K_D, which are referred to as the proportional, integral and the derivative gains (Ogata, 1990), respectively. The power (W) from the PID controller is given by equation 5.4.

Table 5.1: The effects of each controller gain on a closed loop system.

CLOSED LOOP RESPONSE	RISE TIME	OVERSHOOT	SETTLING TIME	STEADY-STATE ERROR
$\mathbf{K_P}$	Decrease	Increase	Small change	Decrease
$\mathbf{K_I}$	Decrease	Increase	Increase	Eliminate
$\mathbf{K_D}$	Small change	Decrease	Decrease	Small change

$$W(t) = K_P \times \left((T_S - T_O) + K_D \frac{d}{dt}(T_S - T_O) + K_I \times \int (T_S - T_O)dt \right) \qquad 5.4$$

Where, T_s and T_o are the final and initial temperature of the system, respectively. The effects of each of the controller gains on a closed-loop system are summarized in Table 5.1.

5.2.2 Control Model of LSU MicroGC

The main objective of simulating the closed loop response of microGC was to find the PID controller gains and use them to tune the PID controller in experiments. The microGC was considered as one lump, the silicon substrate was considered as a second lump, and the insulator was considered as a third lump.

Natural convection with a heat transfer coefficient of 50 W/m^{2}K [Incropera, 2002] was assumed. The model was based on the Equations 5.1. Table 5.2 shows the material thermal properties used in the system. Figure.5.3 shows the Simulink^{TM} model of the system. The gains were adjusted based on Table 5.1. For the gains K_p=1.016, K_i=0.58, and K_d=1.09, the response for the Simulink^{TM} model is shown in Figure 5.4. There was an overshoot of 1.82^{o}C in the response.

Table 5.2 Material thermal properties of materials used in model [Goodfellow, USA].

	Nickel	Silicon	Mica
Thermal conductivity (W/m-K)	60.7	130	25
Heat capacity (J/kg-K)	460	700	50
Coefficient of thermal expansion (µm /m-K)	13.1	8.6	14.68
Density (kg/m^3)	8880	230	3200

$$Q=C_1\frac{dT_1}{dt}+\frac{k_1A_1}{L_1}(T_1-T_2)+hA_{11}(T_1-T_o)$$

$$\frac{k_1A_1}{L_1}(T_1-T_2)=C_2\frac{dT_2}{dt}+\frac{k_2A_2}{L_2}(T_2-T_3)+hA_{21}(T_2-T_o) \qquad 5.1$$

$$\frac{k_2A_2}{L_2}(T_2-T_3)=C_3\frac{dT_3}{dt}+hA_{31}(T_3-T_o)$$

Where,

T_O =Ambient temperature (K);

$\{T_1, T_2, T_3\}$ =Temperatures of the lump1, lump2, and lump3 (K);

$\{C_1, C_2, C_3\}$ =Thermal capacities of lump1, lump2, and lump3 (J/kg-K);

Q =Step input (watts);

h = Heat transfer coefficient of natural convection (W/m^2-K);

$\{A_{11}, A_{21}, A_{31}\}$ =Areas subjected to natural convection (m^2);

$\{A_1, A_2\}$ =Areas subjected to conduction(area between two lumps) (m^2).

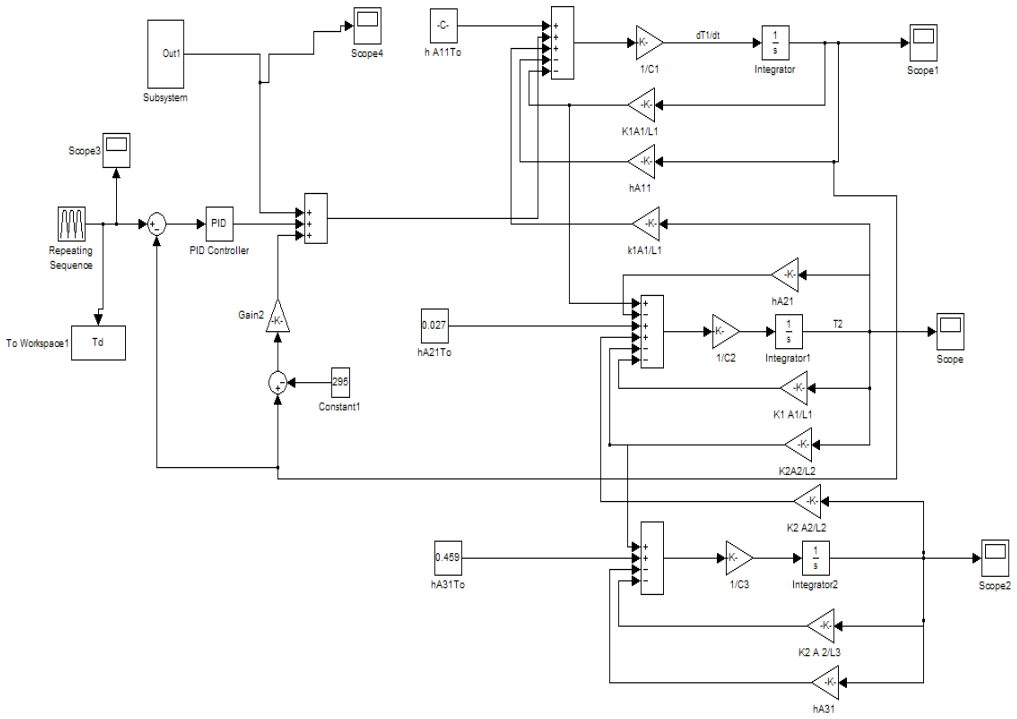

Figure 5.3: Simulink™ model to determine optimum gains for PID controller.

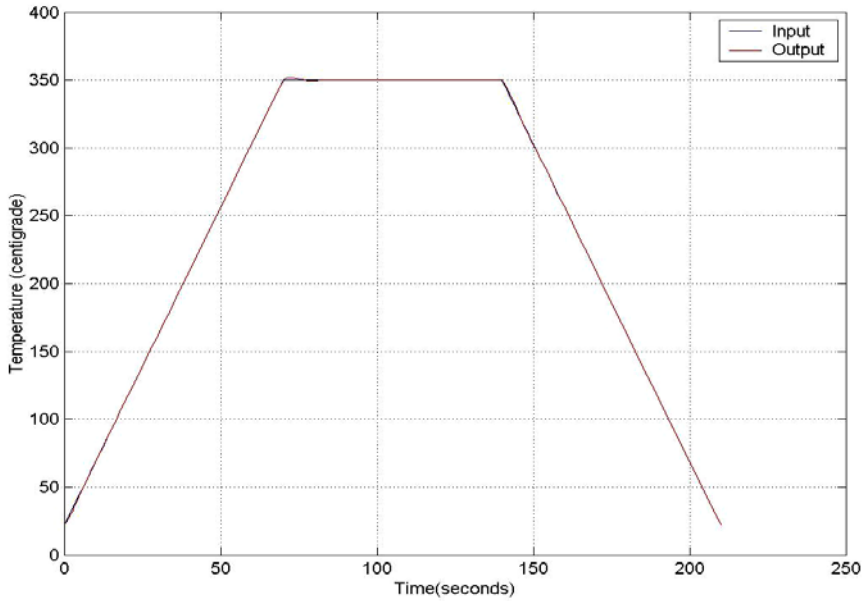

Figure 5.4: Temperature response from Simulink™ model.

5.3. MicroGC Assembly

The microGC was attached to the heater and the heater substrate using silver solder (Ohmex, Transene Inc., Rowley, MA). A mica sheet (Goodfellow Inc., Devon, PA) was used as an electrical insulator on the opposite side of the heater. A self-adhesive K-type thermocouple (SA1-K-SC, Omega Engineering Inc., Stamford, CT) was placed on the top of the test microGC to measure the temperature. The temperature of the test microGC was recorded using an OMEGAETTE^{TM} (HH306, Omega Engineering Inc., Stamford, CT) data logger thermometer with a sampling frequency of 0.5 Hz. The microGC assembly was shown in Figure 5.5.

5.3.1. Experimental Apparatus

The experimental apparatus and circuit diagram for the electrical connections are shown in Figures 5.6 and 5.7, respectively. As shown in Figure 5.7, there are two different circuits, a heating circuit and a cooling circuit. The heating circuit was comprised of a heater, a power supply (MSK 40-2.5M,Kepco, Inc., Flushing, NY), a solid-state relay (SSR-100-20A-DC1, Watlow, Winona, MN), and a controller (Series 96-AO-KK-AA-AA-RG, Watlow, Winona, MN). The cooling circuit had a fan (DC Brushless fan, CAT-273-240 (A), Radio Shack, FT.Worth, TX), a power supply (1621 A, BK Precision Corporation, Yorba Linda, CA), a solid-state relay (SSR-100-20A-DC1, Watlow, Winona, MN), and a controller (Series 96-AO-KK-AA-AA-RG, Watlow, Winona, MN). A self-adhesive K-type thermocouple (SA1-K-SC, Omega Engineering Inc., Stamford, CT) was connected to the controller and also to the temperature data-logger (OMEGAETTE^{TM}, HH306, Omega Engineering Inc., Stamford, CT). The data from data-logger were stored on a computer using Thermolog®(Omega Engineering Inc., Stamford, CT), computer-linking software.

5.3.2. Thermal Cycling

The system was turned on with proportional, integral and derivative gains from the Simulink model. It was seen that the system reached 350^{o}C in 142 seconds (ramp rate: 2.48 ^{o}C/sec) and there was 12^{o}C of overshoot. The system response was slow as compared to the desired response.

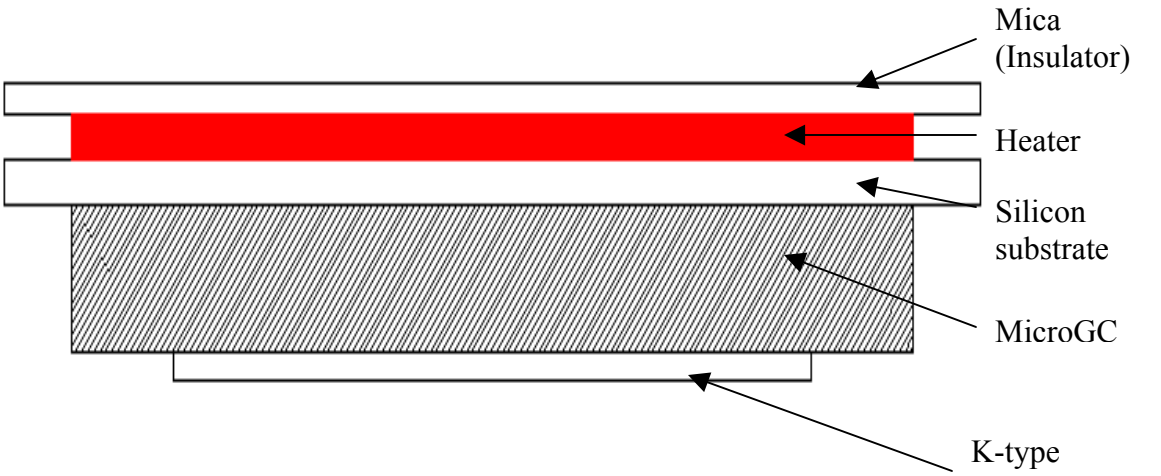

Figure.5.5: Test microGC assembly.

The commercial controller (Series 96-AO-KK-AA-AA-RG, Watlow, Winona, MN) had a limitation on ramping (3^{o}C/sec). Controller that gives higher ramp rate has to be used for ramping. The cooling of microGC was done using a fan of low volume flow rate, and had a cooling rate of 2.5 ^{o}C/sec. The fan was selected for its simplicity in use and control.

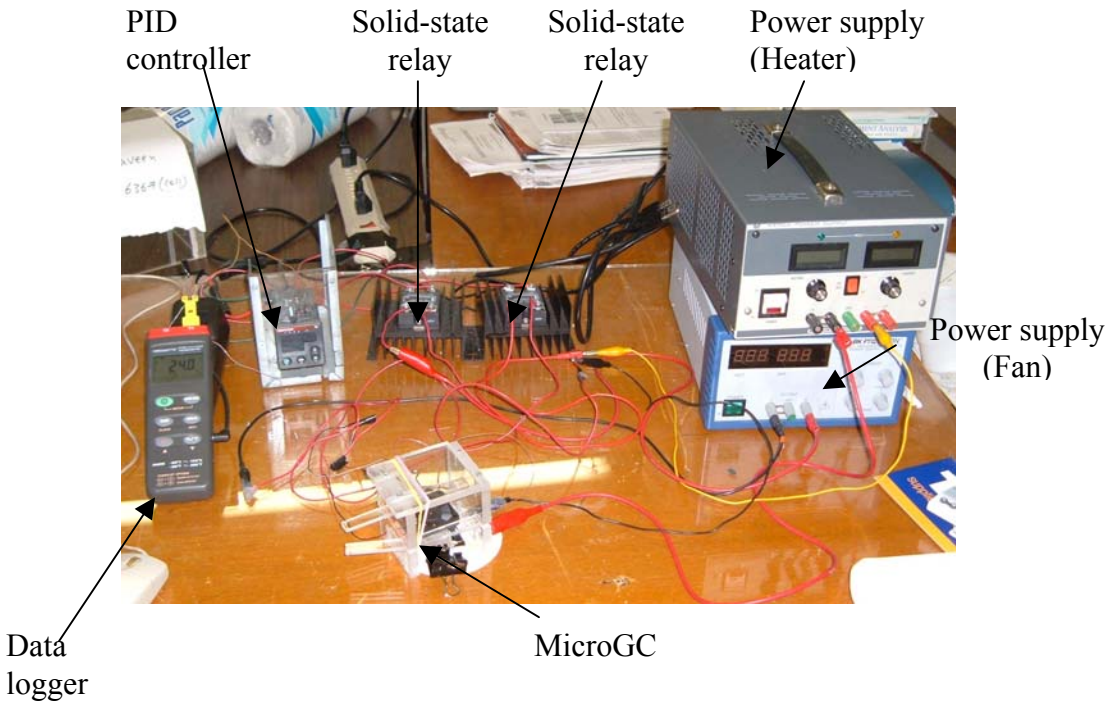

Figure 5.6: Experimental setup.

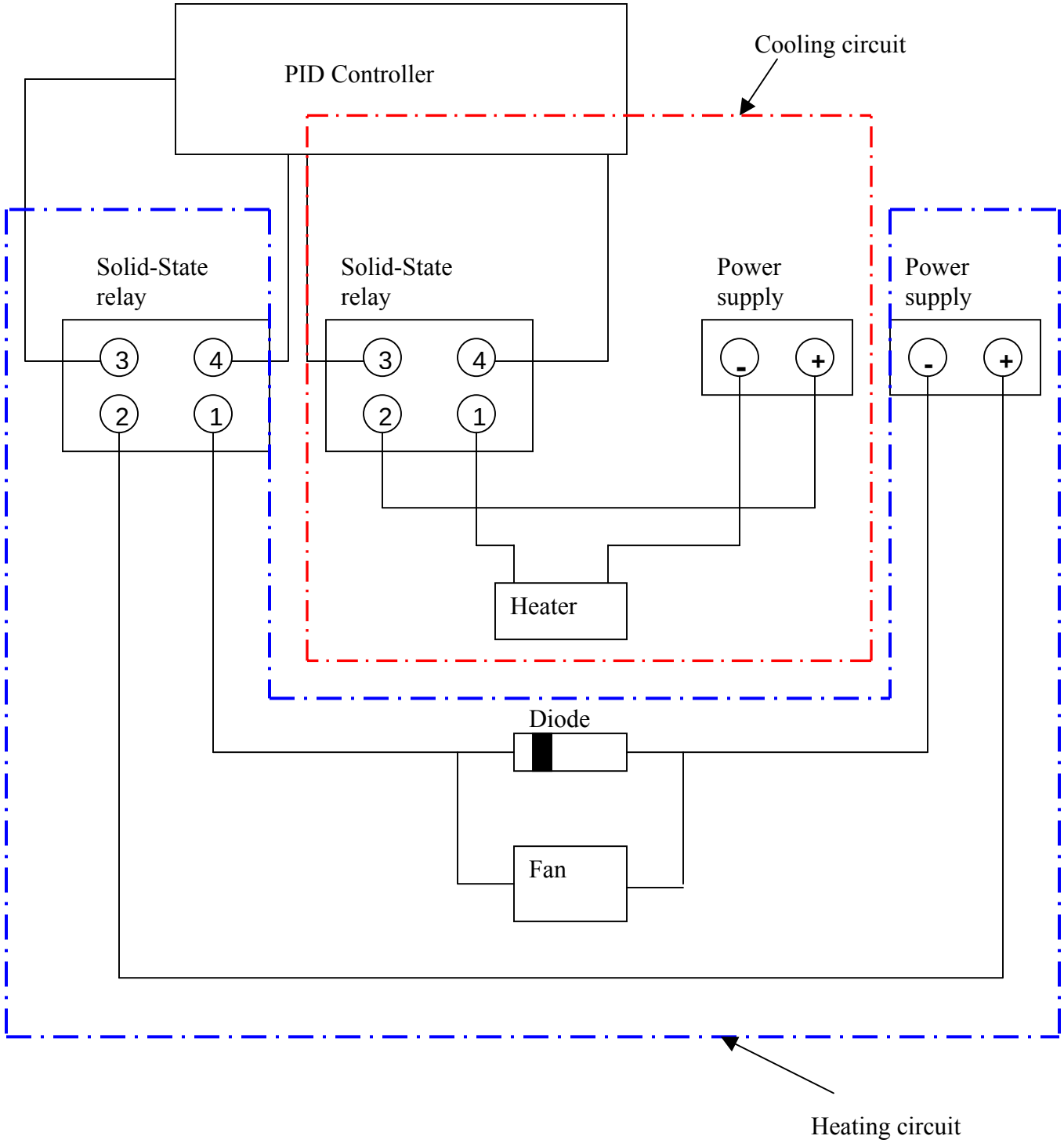

Figure 5.7: Circuit diagram of electric connections for experimental setup.

The gains were tuned according to the Table 5.1, and for the gains K_P=2, K_I=0.25 and K_D=0.15, the system performance was near to the ideal performance. The system can reach the ideal performance, but it needed further PID tuning. Figure 5.8 shows the comparison of actual system performance to ideal response.

5.4. Conclusions

A microfabricated heater was integrated with the microGC and tested for thermal cycling. The heater was able to temperature program the microGC. The desired ramping can be obtained using a controller with better ramping rate. The cooling rate can be improved using a fan, which has a higher volume flow rate. The PID tuning should be refined to remove over damping.

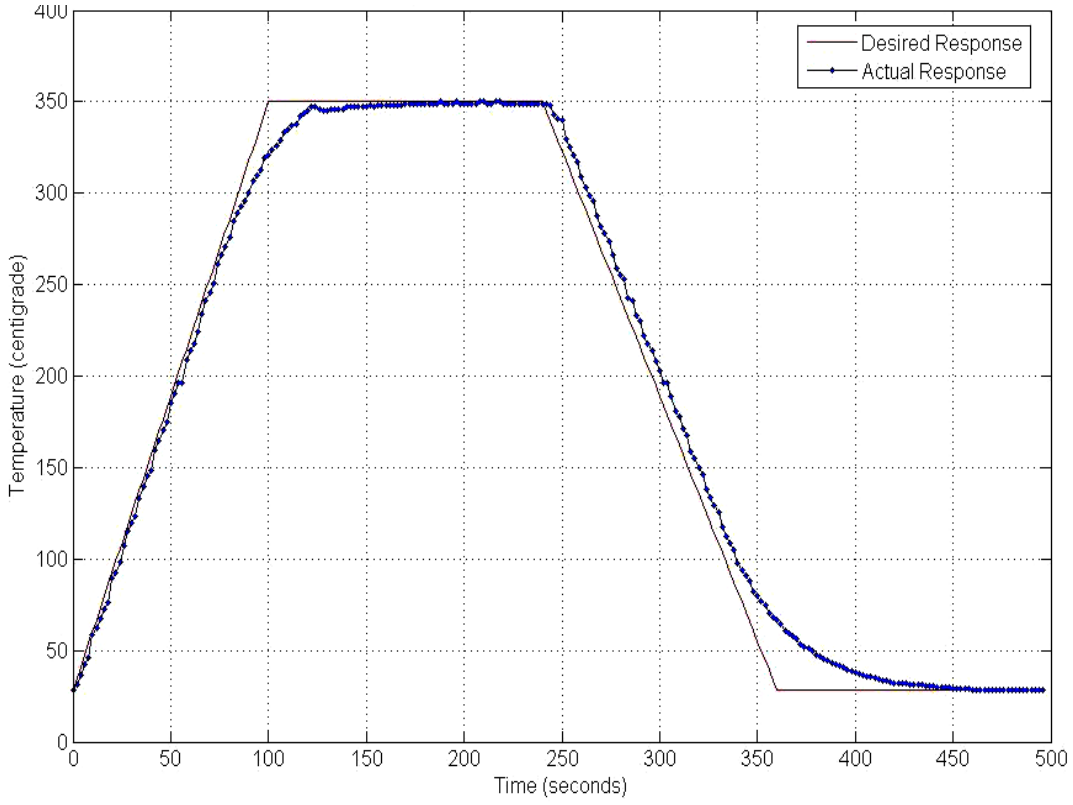

Figure 5.8: Thermal cycling with PID controller with K_P=2, K_I=0.25 and K_D=0.15.

CHAPTER 6
CONCLUSIONS AND FUTURE WORK

The focus of this work was to develop a heating and cooling scheme for temperature programming for a microGC. A high aspect ratio microGC column was developed by Bhushan [4], as a step towards a full microGC. To achieve better performance of the microGC, temperature programming had to be implemented.

To accomplish temperature programming, a heating scheme had to be developed to ramp the temperature of the microGC at a rate of 5 ^{o}C/sec or more and maintain the temperature at 350 ^{o}C for 2 minutes, and cool the system down at the same rate as heating.

6.1 Contribution to MicroGC project

The power required, to perform temperature programming for different configurations of microGC, was calculated. Heater material was selected, and a process to electroplate NiCr alloy was devised.

NiCr alloy with a maximum chromium composition upto 20% can be electroplated. The electrolytes for NiCr alloy plating for various chromium compositions were developed. The detailed description of experimental procedure and plating parameters were presented.

The composition of chromium can be varied with change in electrolyte, and pulse parameters. Heaters, which gave uniform temperature, and linear temperature gradient, were designed and fabricated using microfabrication techniques. NiCr (97.5-2.5) alloy was deposited due to design limitations as explained in Section 4.6. Silicon was used as a substrate, as established procedures were available for microfabrication. More study is required on the selection of substrate for heater. A controller was made to perform the temperature ramp, soak and ramp down, according to the temperature program. The temperature of the microGC could be ramped at the rate of 2.46 ^{o}C/sec due to limitation of commercial PID controller as explained in Section 5.3.2. Fan was used to perform the cooling of microGC for its simplicity in operation.

6.2 Recommendations for the Future Work

Low thermal capacitance of the microGC will facilitate low power, and fast and reproducible temperature programming. The insulator used to electrically insulate the heater to the microGC was a silicon substrate [500 μm thick]. Reducing the thickness of the insulator decreases the thermal capacity of the microGC system. Alternative insulating ideas may be

1) Using a thin silicon substrate (100 μm);
2) Using a thin polyimide (Hitachi Chemical Co. America, Ltd, Cupertino, CA) insulator.

Using a thin silicon insulator (100 μm) may have some practical limitations in handling the substrate while fabricating the heater, as it is very delicate. The possible solution for this problem may be providing a support of a sacrificial titanium substrate.

Using a thin polyimide layer in the place of silicon insulator can reduce the thermal capacity of the microGC system, as the polyimide is 10 times thinner than the silicon substrate. Spinning time, baking time, and other working process parameters have to be established. Comparison of heat capacity (mc_p) of both silicon and polyimide layer has to be made.

REFERENCES

1. http://www.cs.ualberta.ca/~database/MEMS/sma_mems/lab.html

2. http://www-samlab.unine.ch/Activities/Activity.html

3. http://www.lnll.gov/str/Miles.html

4. Bhushan, Fabrication of a LIGA Gas chromatograph column as a step towards a Micro-Fabricated GC, Master's thesis, LSU December 2001.

5. Kevin Robards, Paul R.Haddad, Peter E. Jackson, Principles and Practice of Modern Chromatographic Methods, Academic Press Limited, San Diego, CA.

6. Private communication with Dr.Overton.

7. Hong-seok Noh, Peter J.Hesketh, and Gregory C. Frye-Mason, Parylene Gas Chromatographic Column for Rapid Thermal Cycling. , Journal of Microelectromechanical systems, Vol. 11, No.6, December 2002.

8. From Harold M.McNair, James M.Miller, Basic Gas Chromatography., John Wiley & Sons, INC. New York, NY.

9. Vivek Jain and John B. Phillips, Fast Temperature Programming on Fused- Silica Open-Tubular Capillary Columns by Direct Resistive heating, J.Chromatography Science, vol33, Jan1995.

10. Dharmasena, A Microprocessor based Precision Thermo Electric Temperature Controller for Chemical Instrumentation, Master Thesis, LSU, May 1987.

11. M.E.Hail and R.A.Yost, Compact Gas probe for Gas Chromatography/Mass Spectrometry utilizing resistive Heater Aluminum-Clad capillary columns,1989, Analytical Chemistry, 61, 2410-2416. 84.

12. E.U.Ehrmann, H.P.Dharmasena, K.Carney, E.B.Overton, Novel Column Heater for fast Capillary Gas Chromatograph., J.Chromatogr. Sci., 34(12), 533-539, (1996).

13. http://www.llnl.gov/IPandC/technology/profile/sensor/HandHeldGasChromatograph/index.php

14. http://www-cms.llnl.gov/s-t/gas_chrom.html

15. http://pubs.acs.org/subscribe/journals/tcaw/11/i05/html/05felton.html

16. Hong-Seok Noh, Peter J. Hesketh and Gregory C. Frye-Mason, Parylene Gas Chromatographic Column for Rapid Thermal Cycling, Journal of Micro Mechanical Systems, Vol.1.1, No.6, December 2002.

17. Vivek Jain and John B. Phillips, Fast Temperature Programming on Fused-Silica Open Tubular Capillary Columns by Direct Resistive Heating, Journal of Chromatographic Science, Vol.33, January 1995.

18. Betteridge, W. Walter, Nickel and its alloys, Chichester, West Sussex, England, Ellis Horwood, New York, Halsted Press, 1984.

19. www.matweb.com

20. Private communication with Dr.David R. Wheeler and Dr.R.J. Simonson Sandia National Laboratories.

21. D.S.Lashmore, I.Weishauss, and K.Pratt, Electrodeposition of Nickel Chromium Alloys,(AESF Research Project 58), Proc. AESF Conf., Session P, American Electroplaters and Surface Finishers. Society, Orlando, FL, 1985.

22. Lin, K.L., Ho, J.K., "*Electrodeposited Ni-Cr and Ni-Cr-P alloys*"., J.Electrochem. Soc.,vol.139, no. 5, pp. 1305-1310, 1992

23. Terry Stephen Clark, A Gas Chromatography System Fabricated on a Silicon Wafer Using Integrated Circuit Technology, A Dissertation submitted to the Department of Electrical Engineering, Stanford University, 1975.

24. Larry F.Thompson, C.Grant Willson, and Murrae J.Bowden, second edition (1994), Introduction to Microlithography. American Chemical Society, Washington, DC 1994.

25. Klaus Schroder, 1983, Handbook of Electrical Resistivities of Binary Metallic Alloys, CRC Press LLC.

26. Michael B. Histand, David G. Alciatore, 1999, Introduction to Mechatronics and Measurement Systems.,Mc-Graw-Hill Companies,Inc.

27. I.J.Nagrath, M.Gopal, Third Edition (1975), Control Systems Engineering., New Age International (P) Limited.

28. Abner Brenner, Volume I &II (1963), Electrodeposition of alloys, Academic Press, New York.

29. Hostetter, Savant, Stefani, 1982, Design of Feedback Control Systems., CBS College Publishing,New York, N.Y.

30. B.E.Gatewood, 1957, Thermal Stresses with Applications to Airplanes, Missiles, Turbines, and Nuclear Reactors, McGraw-Hill Book Company, Inc.

31. Mordechay Schlesinge, Milan paunovic (2000), Modern Electroplating, John Wiley &Sons, Inc.

32. Perrin Walker, William H. Tarn, Handbook of Metal Etchants., CRC Press LLC.

33. Marc J. Madou Second Edition (2002), Fundamentals of Microfabrication- The Science of Miniaturization, CRC Press LLC.

34. Michael G. Pecht, Rakesh Agarwal, Patrick McCluskey, terrance Dishongh, Sirus Javadpour, Rahul mahajan,(1999), .Electronic packaging Materials and Their properties, CRC Press LLC.

35. Charles A. Harper (1997), Electronic packaging and Interconnection Hanbook., Mc Graw-Hill companies.

36. Jerry E.Sergent, Al Krum (1998), Thermal management Handbook for Electronic assemblies, Mc Graw-Hill companies.

37. Gordon N. Ellison, (1984), Thermal Computations for Electronic Equipment, Van Nostrand Reinhold Company Inc.

38. Charles T. Lynch, (Vol I,II,&III), (1975), .Handbook of Material Science., CRC Press LLC.

39. Georges Guiochon and Claude L. Guillemin, (1988),.Quantitative GasChromatography for laboratory analyses and on-line process control., Elsevier Science Publishing Company Inc.

40. Dr.Srinath Ekkad (Mechanical Engineering Dept, Louisiana State University), Private communication.

41. Dr.Glenn Sinclair (Mechanical Engineering Dept, Louisiana State University), Private communication.

42. Dr.De Quiroz (Mechanical Engineering Dept, Louisiana State University), Private communication.

43. Yohannes Desta (CAMD), Private communication.

44. Richard C. Dorf, Robert H. Bishop, (2001), Modern Control Systems, Prentice-Hall Inc.

45. Dean C. Karnopp, Donald L.Margolis, Ronald C. Rosenberg, (2000), System Dynamics Modelling and Simulation of Mechatronic Systems, John Wiley & Sons, I

46. Frank P. Incropera, David P. Dewitt, (2002), Fundamentals of Heat and Mass Transfer., John Wiley & Sons, Inc.

APPENDIX

HEATER DESIGN

The optimum heater design is one, which gives uniform temperature distribution (± 5 ^{o}C) across the microGC. The parameter varied is the spacing between heat generating elements. Different designs were simulated for temperature distribution, using the commercial finite element analysis package (ANSYS vs.8.0, Canonsburg, PA). The microGC, the insulation layer and heaters were considered as different blocks as shown in Figure A.1. Natural convection conditions were assumed and an ambient temperature of 25^{o}C. The heater was considered as a heat-generating element. The initial designs had alumina as an electrical insulation layer while the later designs used have silicon as an electrical insulation layer between heater and micro GC. The simulation results from the design.1 were shown in Figure A.2.

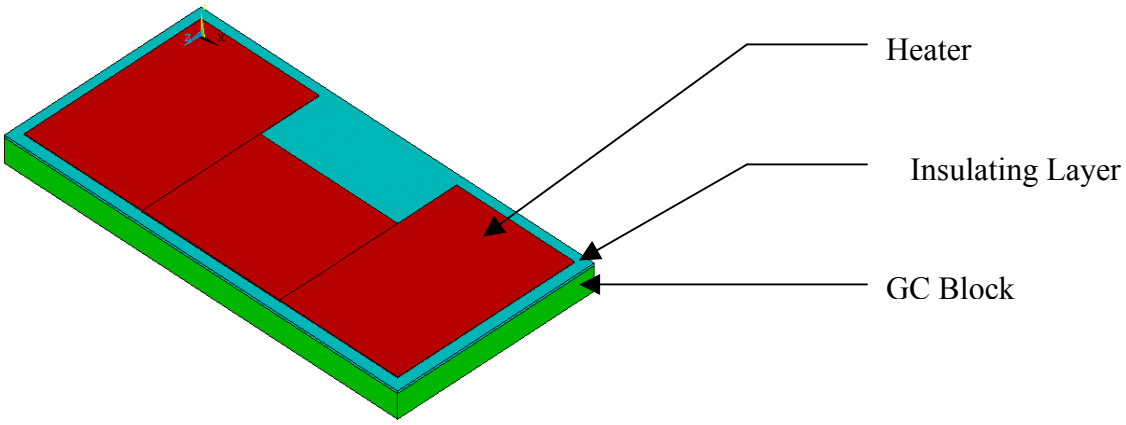

Figure.A.1: MicroGC and heater assembly.

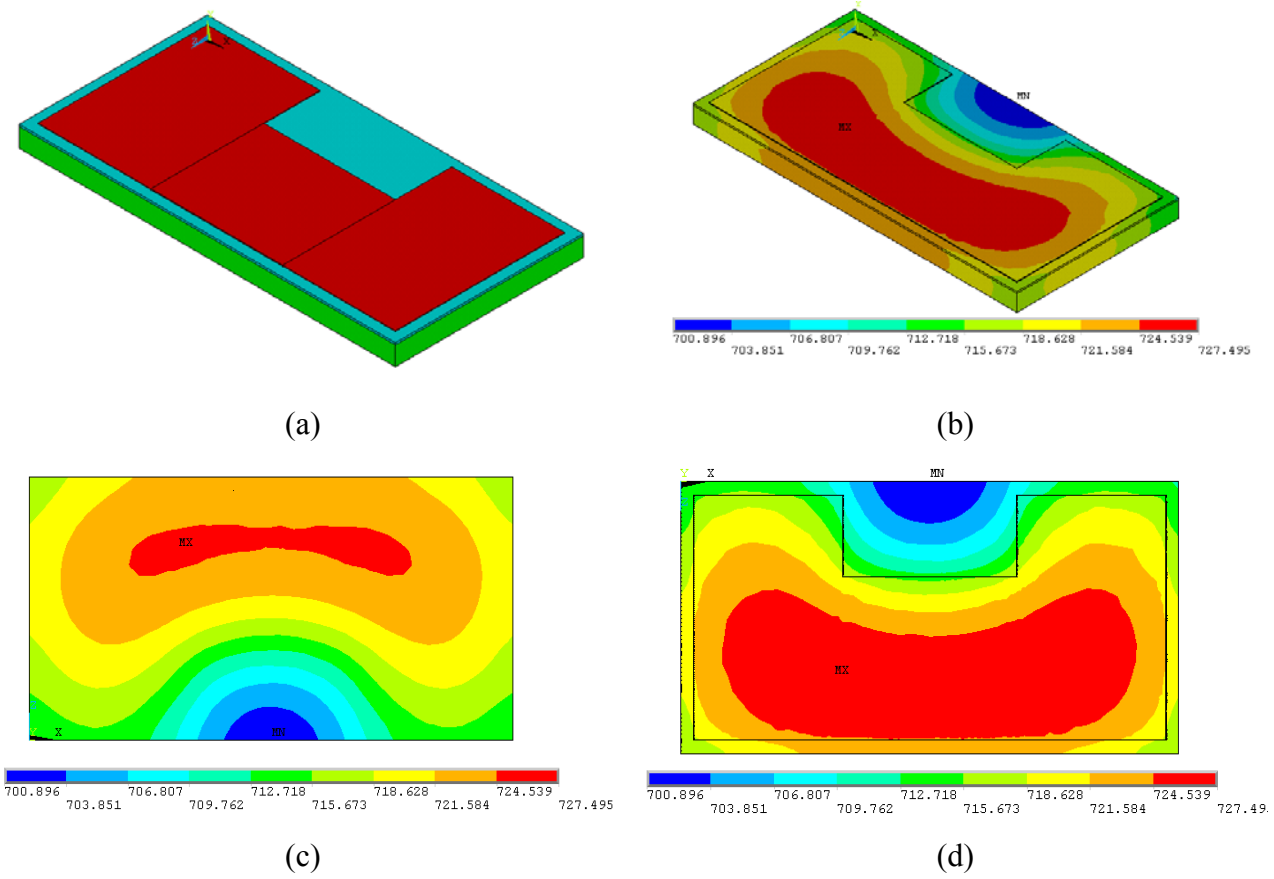

Figure A.2: (a) MicroGC assembly;

(b) Contour plot showing the temperature distribution on the microGC in an isometric view;

(c) Contour plot showing the temperature distribution on the bottom of microGC (opposite direction of heater element);

(d) Contour plot showing the temperature distribution on the top of microGC (in the direction of heater element).

The simulation results from Figure A.2 shows the non-uniform distribution of temperature on microGC. The temperature difference between the highest and lowest was 26.35 ^{o}C. The temperature difference should be around $\pm 5^{o}$C.The next iteration was to increase the number of turns and evaluate the temperature distribution. The simulation results were shown in figure A.3.

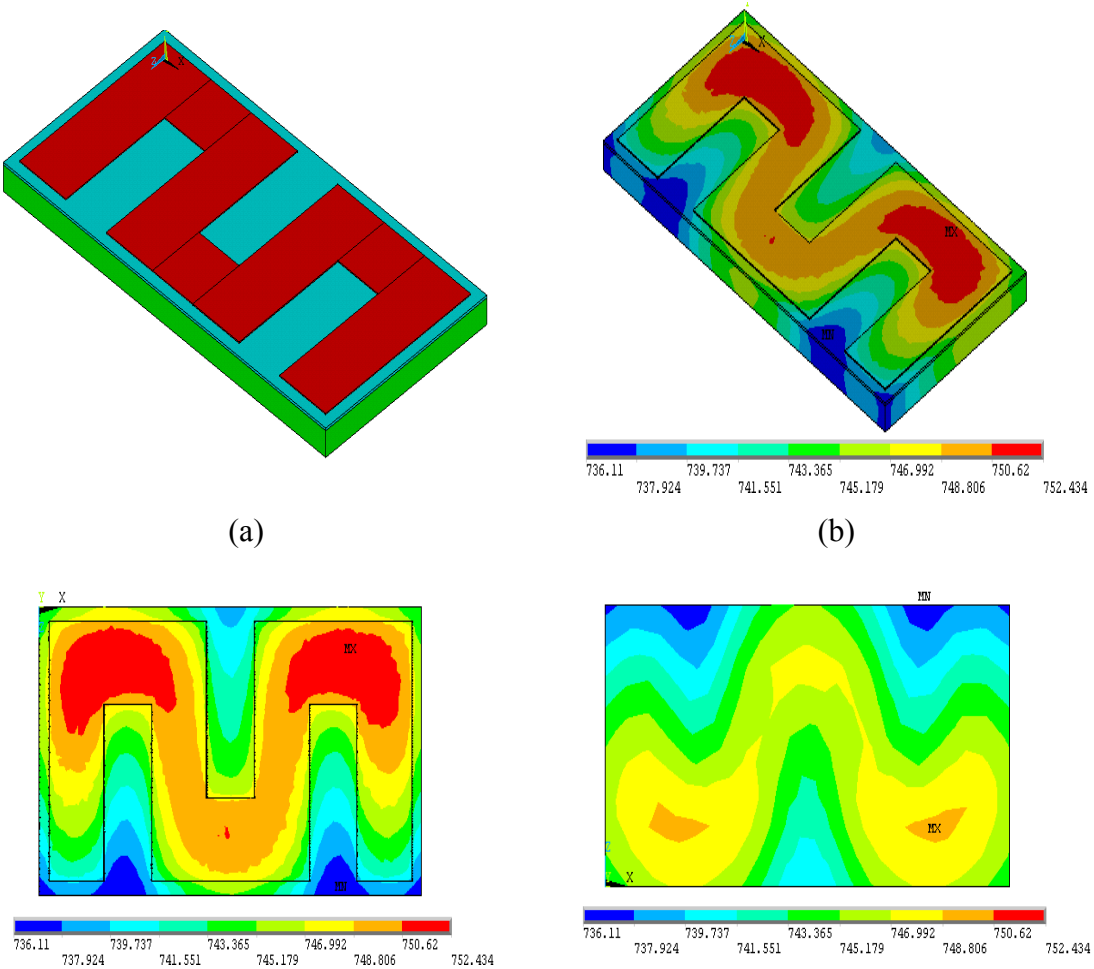

(a) (b)

(c) (d)

Figure.A.3: (a) MicroGC heater assembly;

(b) Contour plot showing the temperature distribution on the microGC in an isometric view;

(c) Contour plot showing the temperature distribution on the bottom of microGC (in the direction of heater element);

(d) Contour plot showing the temperature distribution on the top of microGC (opposite to the direction of heater element).

The design of the heater was modified by increasing the number of turns further. The simulation results were shown in Figure A.4.

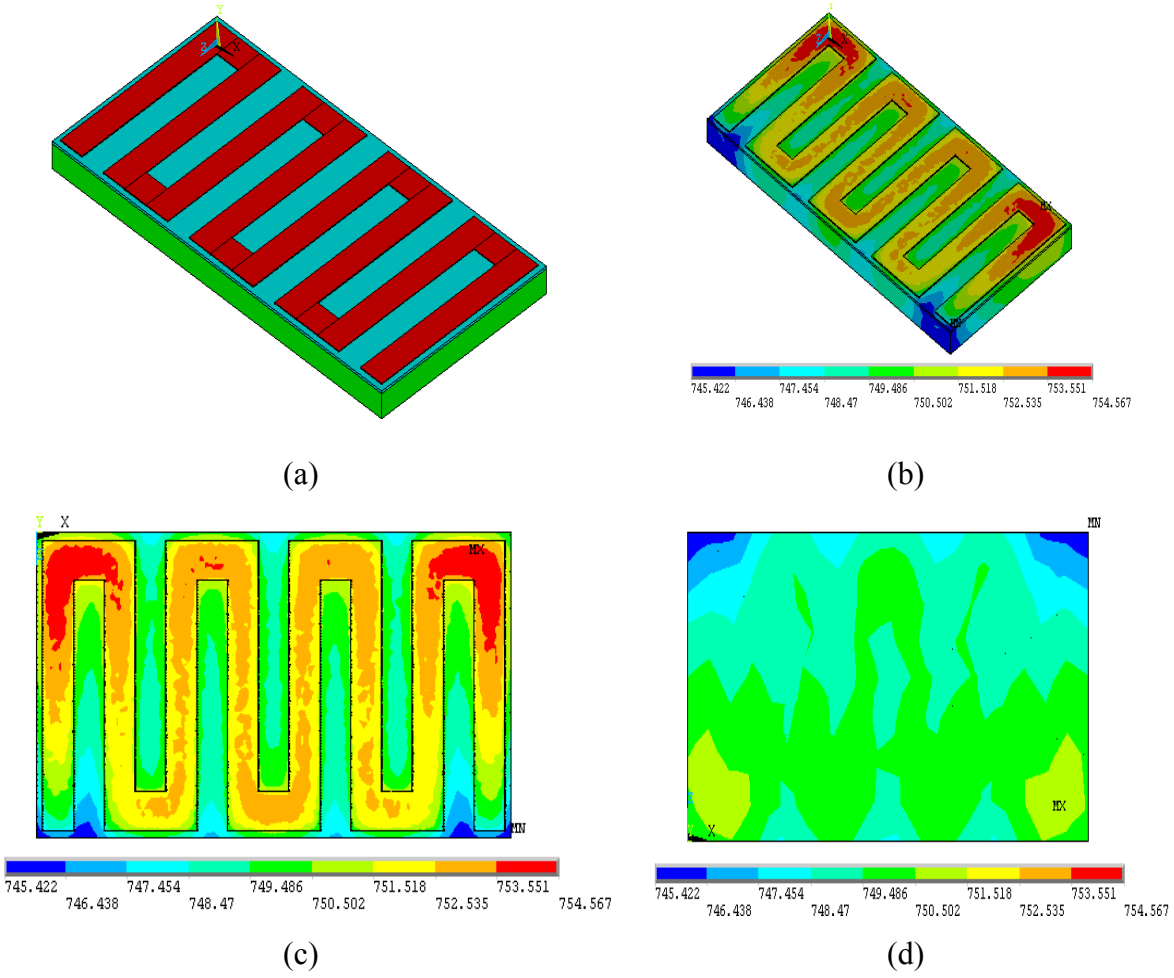

Figure.A.4: (a) MicroGC heater assembly;

(b) Contour plot showing the temperature distribution on the microGC in an isometric view;

(c) Contour plot showing the temperature distribution on the bottom of microGC (in the direction of heater element);

(d) Contour plot showing the temperature distribution on the top of microGC (opposite to the direction of heater element).

The simulation results from Figure A.4 showed non-uniform temperature distribution. The design of the heater was modified by increasing the number of turns further. The simulation results were shown in Figure A.5.

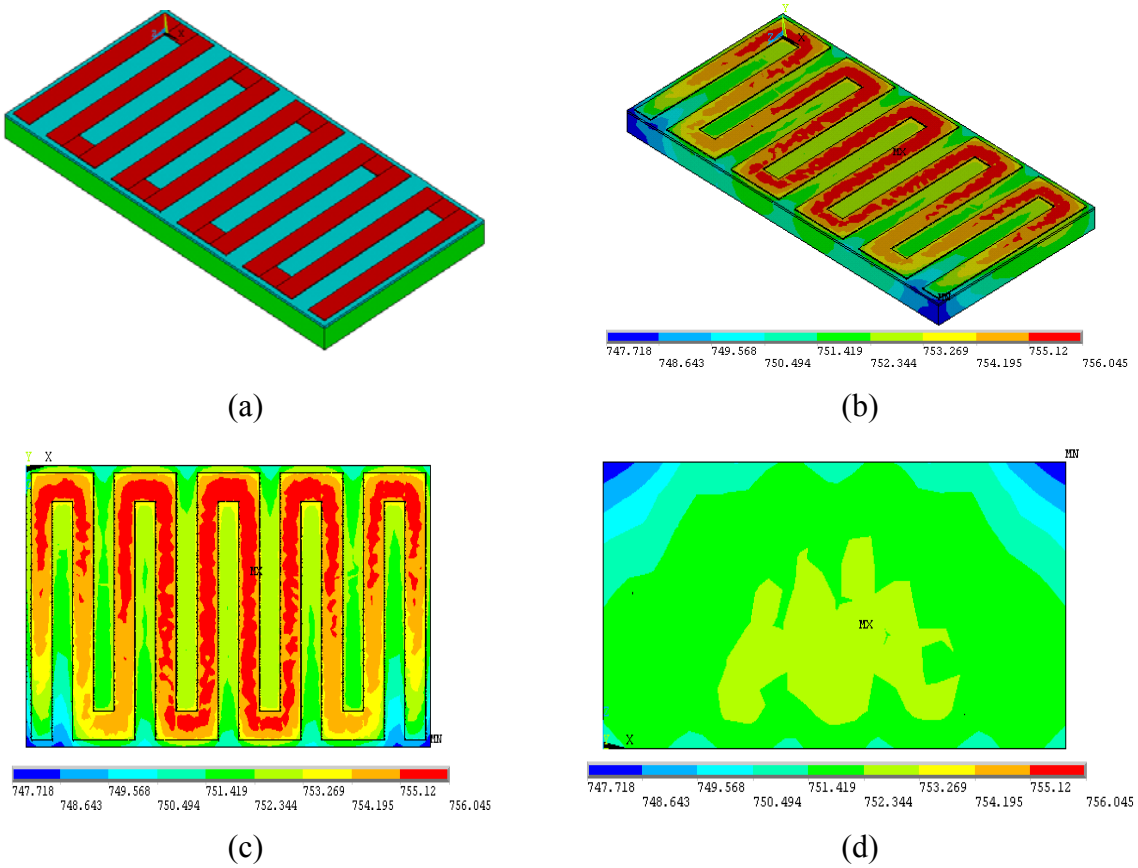

Figure.A.5: (a) MicroGC heater assembly;

(b) Contour plot showing the temperature distribution on the microGC in an isometric view;

(c) Contour plot showing the temperature distribution on the bottom of microGC (in the direction of heater element);

(d) Contour plot showing the temperature distribution on the top of microGC (opposite to the direction of heater element).

The simulation results from Figure A.5 showed non-uniform temperature distribution. The design of the heater was modified by increasing the number of turns further. The simulation results were shown in Figure A.6.

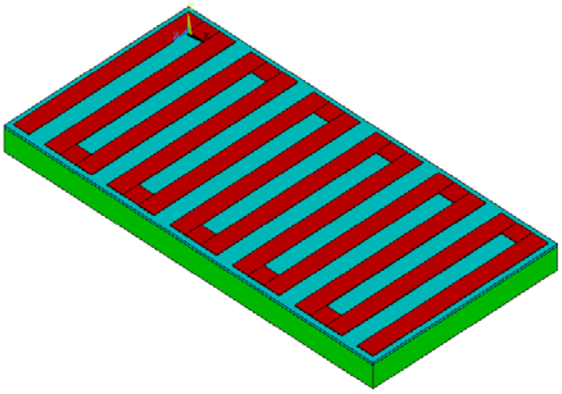

(a)

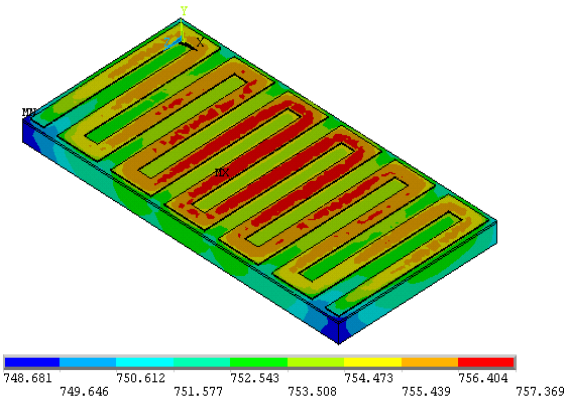

(b)

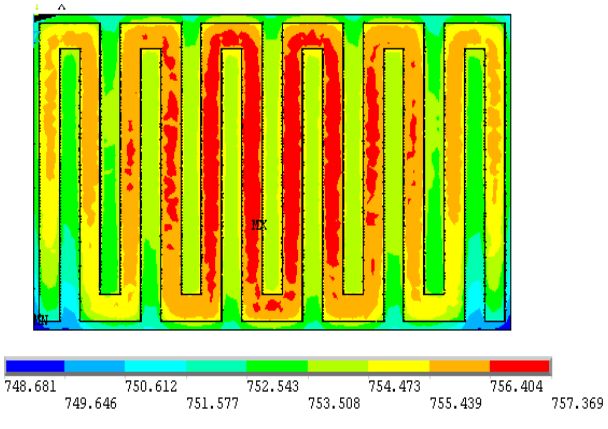

(c)

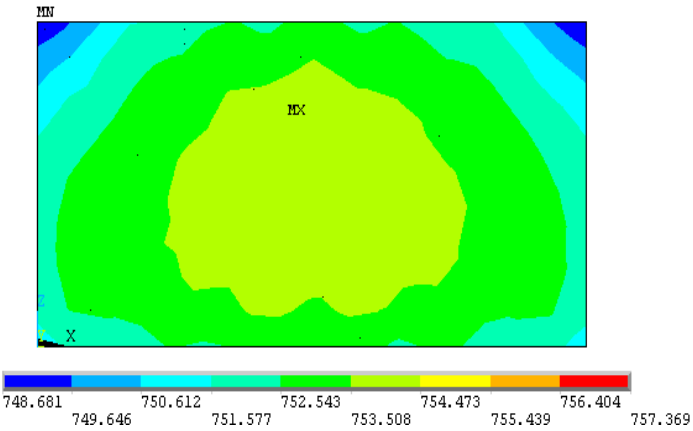

(d)

Figure.A.6: (a) MicroGC heater assembly;

(b) Contour plot showing the temperature distribution on the microGC in an isometric view;

(c) Contour plot showing the temperature distribution on the bottom of microGC (in the direction of heater element);

(d) Contour plot showing the temperature distribution on the top of microGC (opposite to the direction of heater element).

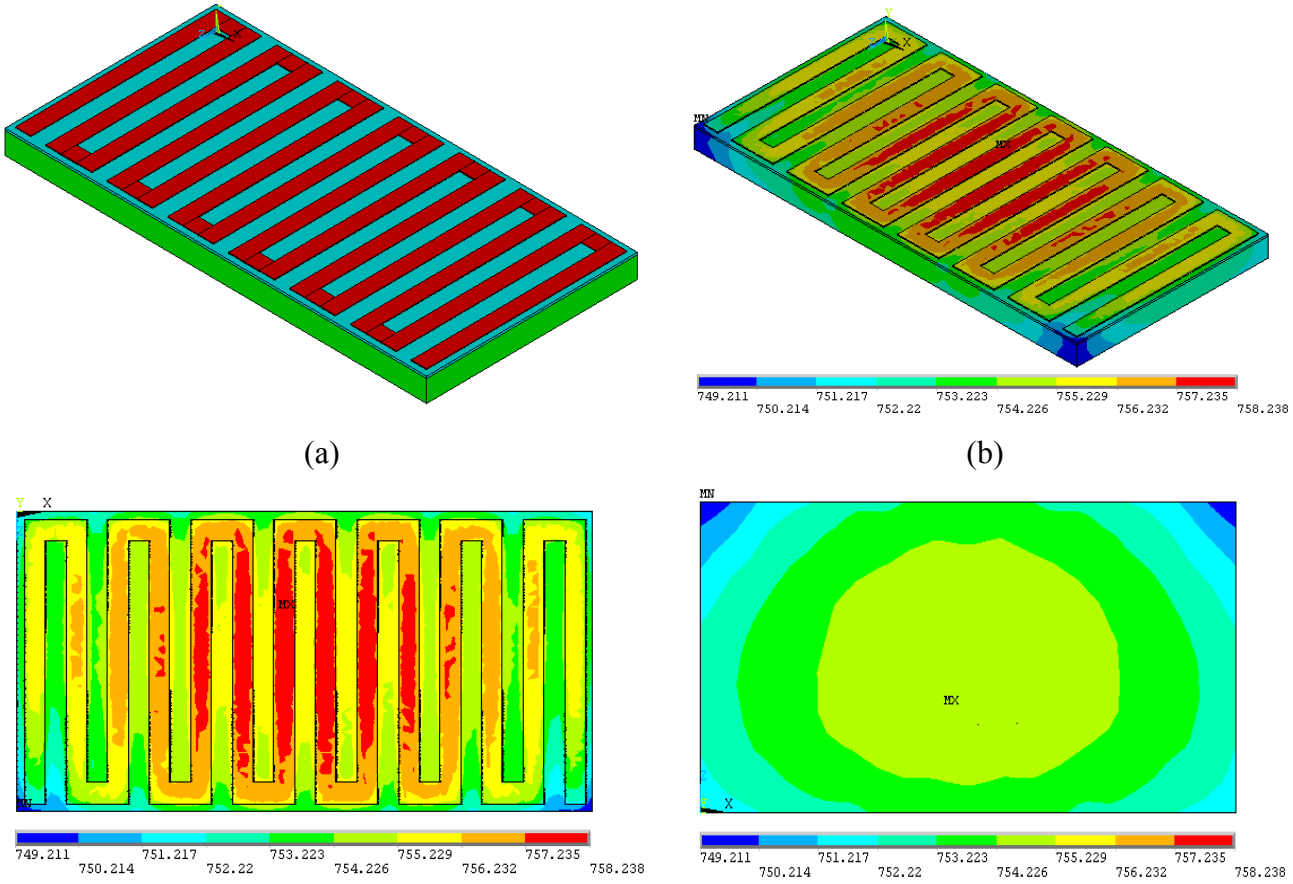

Figure.A.7: (a) MicroGC heater assembly;

(b) Contour plot showing the temperature distribution on the microGC in an isometric view;

(c) Contour plot showing the temperature distribution on the bottom of microGC (in the direction of heater element);

(d) Contour plot showing the temperature distribution on the top of microGC (opposite to the direction of heater element).

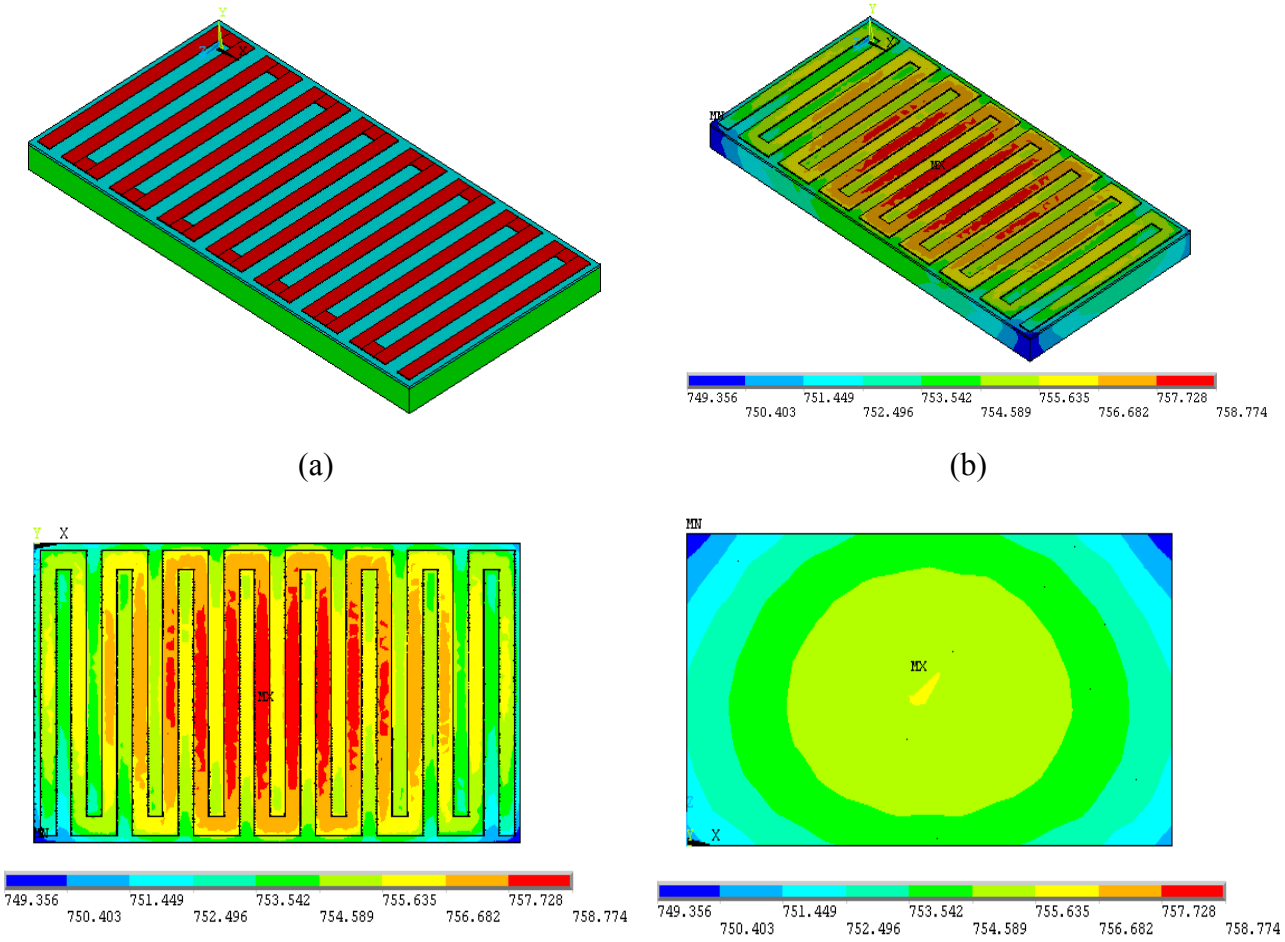

Figure.A.8: (a) MicroGC heater assembly;

(b) Contour plot showing the temperature distribution on the microGC in an isometric view;

(c) Contour plot showing the temperature distribution on the bottom of microGC (in the direction of heater element);

(d) Contour plot showing the temperature distribution on the top of microGC (opposite to the direction of heater element).

Table A.1: Comparison of properties of alumina and silicon

Properties	**Silicon**	**Alumina**
Density	2329 kg/m^3	3960 kg/m^3
Electric Resistivity	0.0001 ohm-m	1E+12ohm-m
Heat Capacity	702 J/kg-K	850 J/kg-K
CTE, 500^{o}C	4.44 μm/m-°C	8.2 μm/m-°C
Thermal Conductivity	124 W/m-K	30 W/m-K

Simulation results from Figures A.6, A.7 and A.8 shows the uniform temperature distribution with in a range of ± 10 ^{o}C. The next modification of the design is to replace the insulating layer from alumina to silicon. Comparisons of properties of silicon to alumina are described in Table A.1.

Silicon was selected for the following reasons:

- Thermal conductivity was almost three times higher than alumina;
- The seed layer for electrodeposition should be at least 3 μm for alumina, because of its surface roughness;
- The seed layer for electrodeposition on silicon can be only 3000 nm.

A 3D finite element analysis was done using the commercial finite element package ANSYS^{TM} (ANSYS vs.8.0, Canonsburg, PA).

The same designs were modeled again with silicon as the insulating layer between the heater and the microGC. The thickness of the silicon substrate was 500 μm. The microGC was assumed to be made up of three layers.

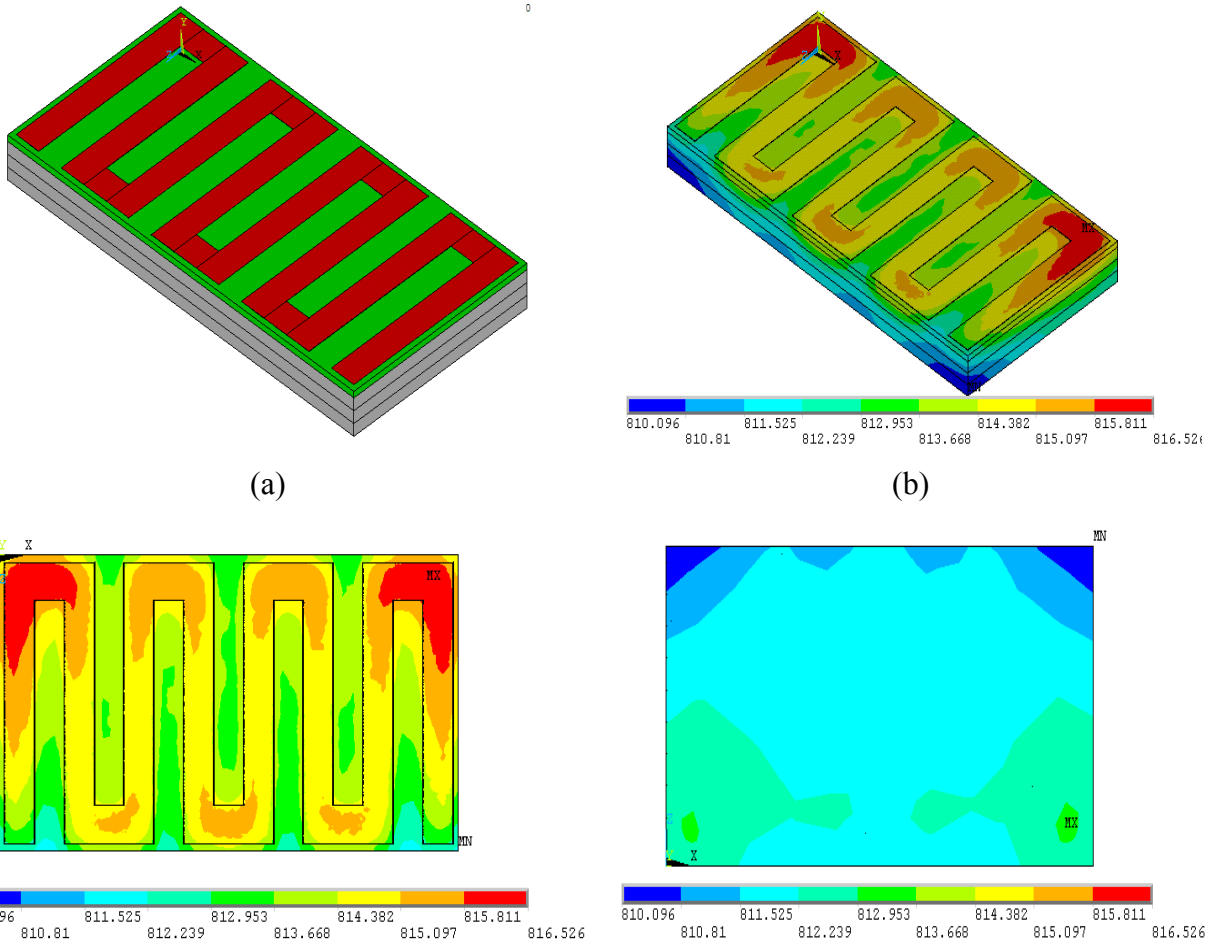

Figure.A.9: (a) MicroGC heater assembly;

(b) Contour plot showing the temperature distribution on the microGC in an isometric view;

(c) Contour plot showing the temperature distribution on the bottom of microGC (in the direction of heater element);

(d) Contour plot showing the temperature distribution on the top of microGC (opposite to the direction of heater element).

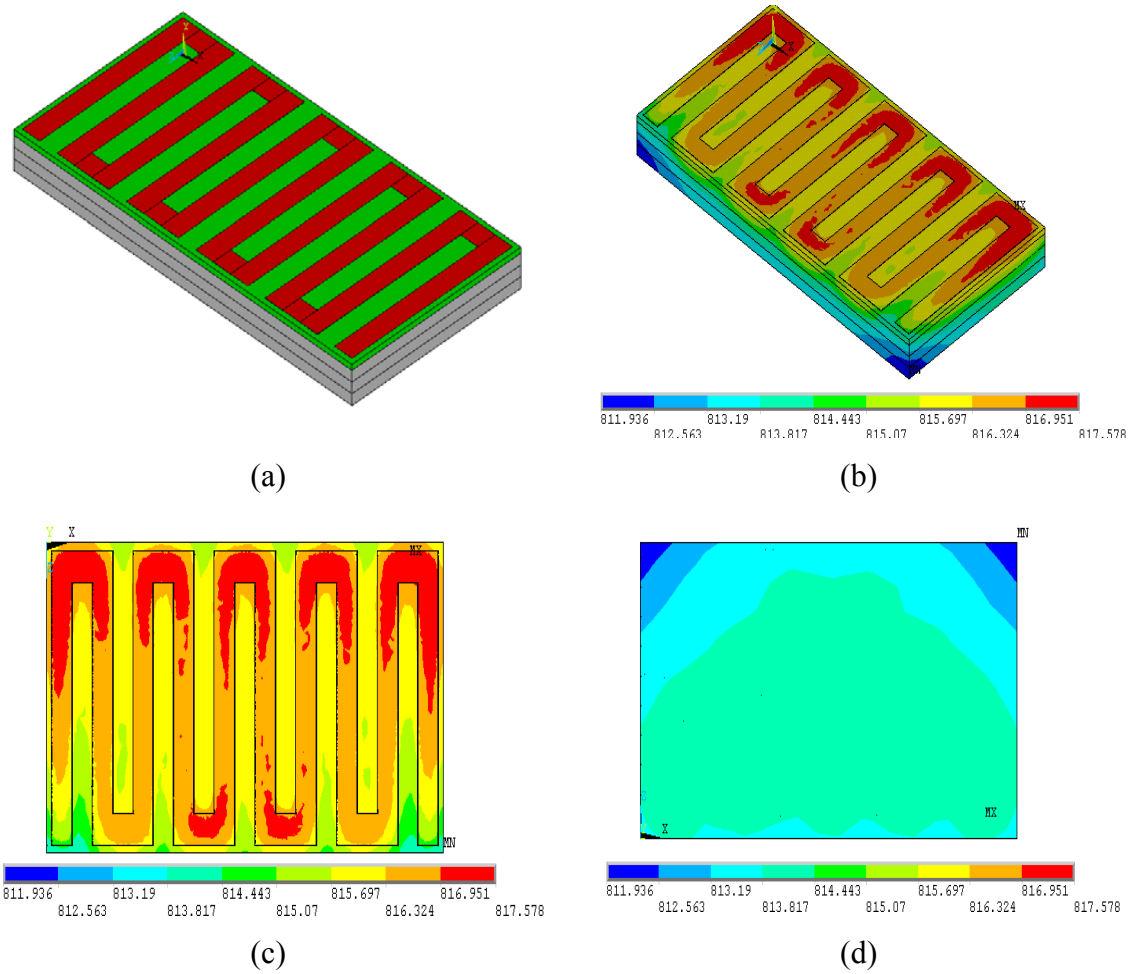

Figure.A.10: (a) MicroGC heater assembly;

(b) Contour plot showing the temperature distribution on the microGC in an isometric view;

(c) Contour plot showing the temperature distribution on the bottom of microGC (in the direction of heater element);

(d) Contour plot showing the temperature distribution on the top of microGC (opposite to the direction of heater element).

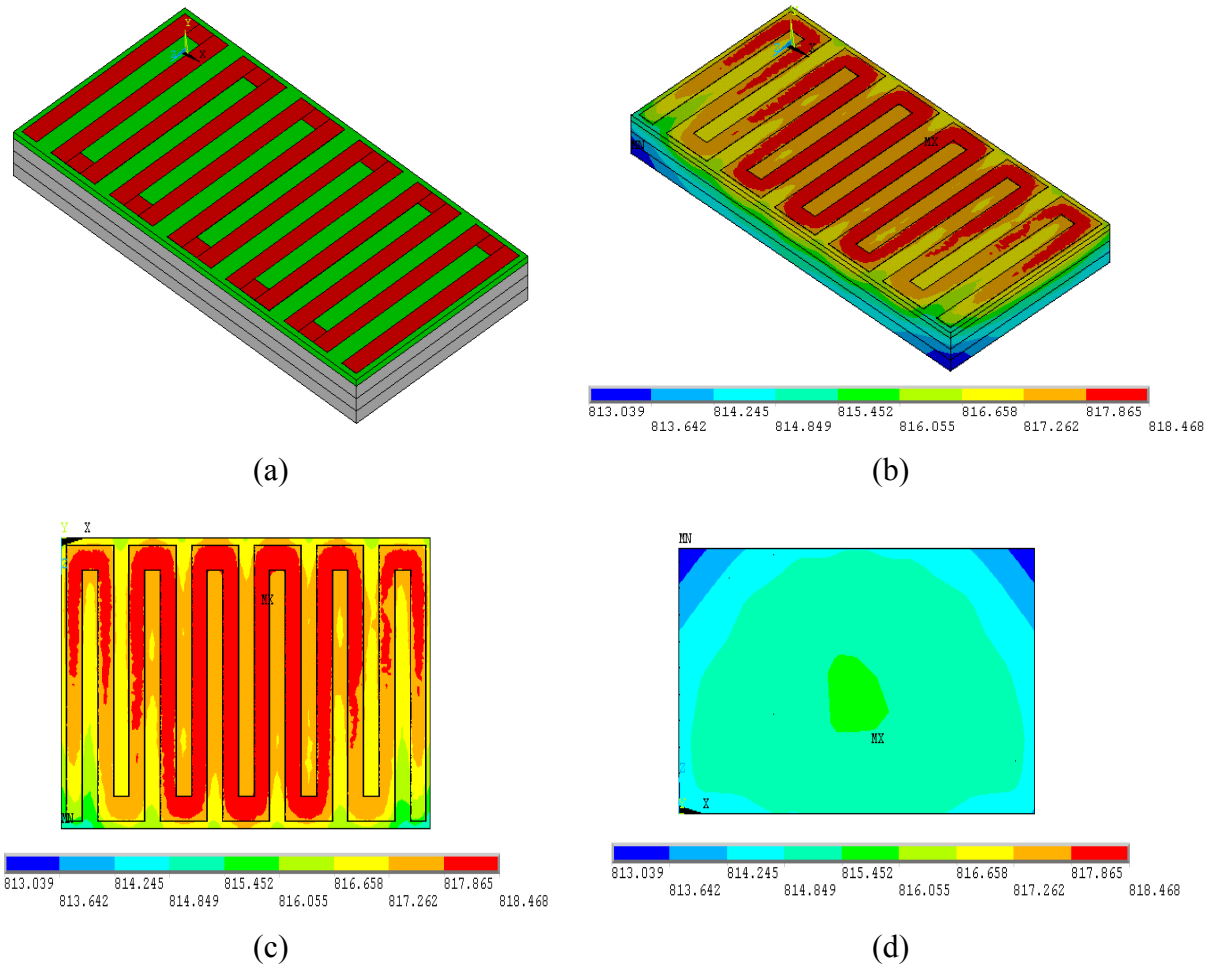

(a) (b)

(c) (d)

Figure.A.11: (a) MicroGC heater assembly;

(b) Contour plot showing the temperature distribution on the microGC in an isometric view;

(c) Contour plot showing the temperature distribution on the bottom of microGC (in the direction of heater element);

(d) Contour plot showing the temperature distribution on the top of microGC (opposite to the direction of heater element).

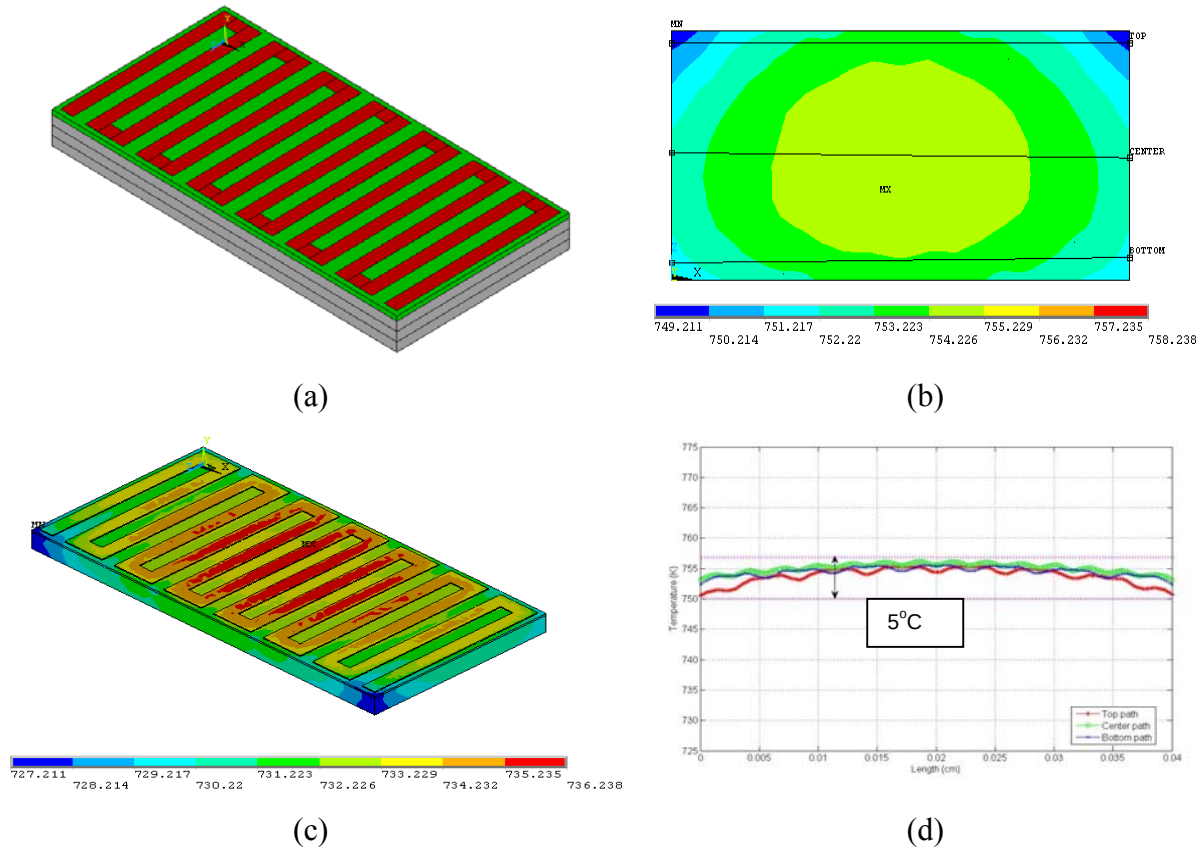

Figure.A.12: (a) MicroGC heater assembly;

(b) Contour plot showing the temperature distribution on the bottom of microGC and paths;

(c) Contour plot showing the temperature distribution in an isometric view;

(d) The temperature distribution along the paths shown in Figure A.12 (b).

The heater design in Figure A.12 gave temperature distribution within a range of ± 5 ^{o}C. The temperature distribution along the paths is shown in Figure A.12 (d). The second objective of the heater design was to device a heater that gives a temperature gradient along the length of microGC.

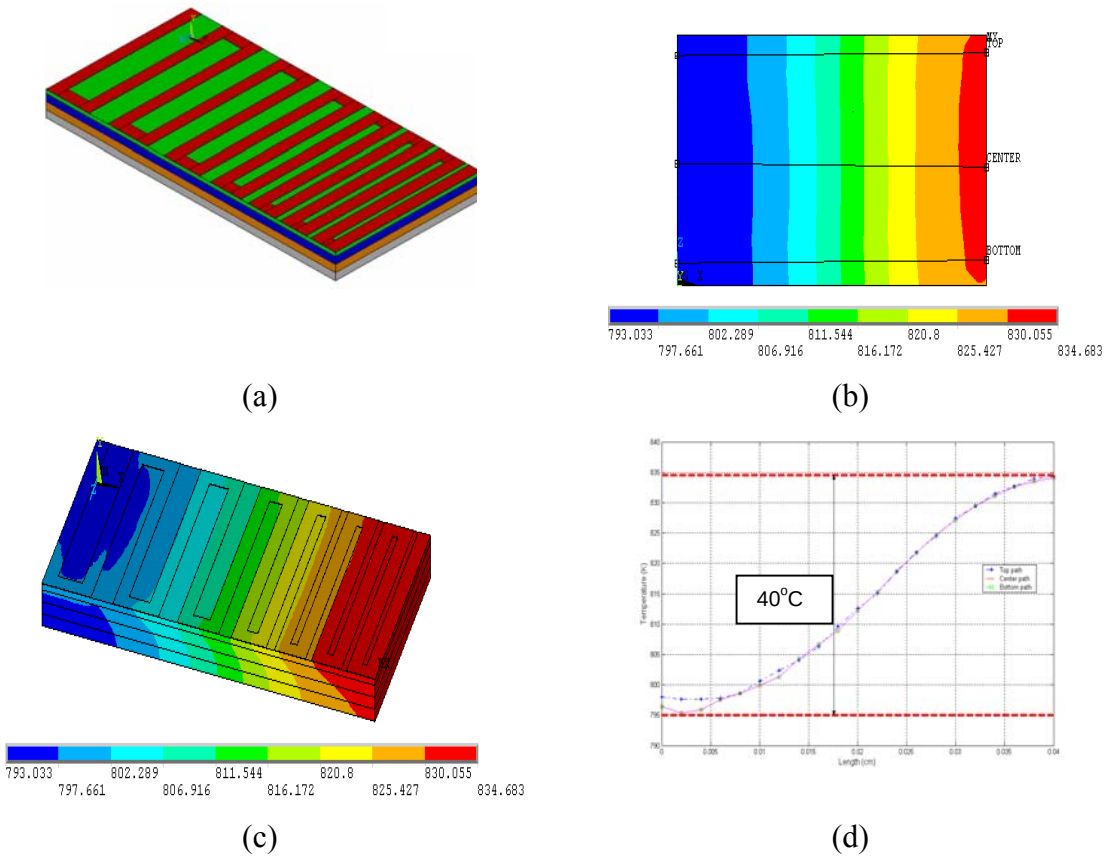

(a) (b)

(c) (d)

Figure.A.12: (a) MicroGC heater assembly;

(b) Contour plot showing the temperature distribution on the bottom of microGC (in the direction of heater element) and the paths;

(c) Contour plot showing the temperature distribution on the microGC in an isometric view;

(d) The temperature distribution along the paths shown in Figure A.13 (b).

The simulations performed on various heater designs showed that as the spacing between the heater elements increased the temperature of microGC increased. The spacing is between heater elements was increased proportionally as shown in Figure A.13 (a). The resultant simulations are shown in Figures A.13 (b) and A.13 (c). A plot of temperature distribution along the paths is shown in Figure A.13 (d).

VITA

Mr. Pasupuleti was born on June 19th, 1979, in Dornakal, India. He received the degree of Bachelor in Engineering from The Andhra University located in Vishakapatnam, India, in May of 2000. He came to United States in 2001, to pursue his masters program in mechanical engineering at LSU. Since joining the graduate program at Louisiana State University (LSU) in August of 2001, he has been a member of the Microsystems Engineering Team (μset). Currently he is a candidate for the degree of Masters of Science in Mechanical Engineering, to be awarded during the LSU commencement ceremonies in the Spring of 2005.